Modelling Surtseyan Ejecta

Emma Elizabeth Greenbank

Supervisor: Professor Mark McGuinness

VICTORIA UNIVERSITY OF WELLINGTON
Te Whare Wānanga o te Ūpoko o te Ika a Māui

School of Mathematics and Statistics
Te Kura Mātai Tatauranga

A thesis
submitted to the Victoria University of Wellington
in fulfilment of the requirements for the degree of
Doctor of Philosophy
in Mathematics.

Victoria University of Wellington
2020

Abstract

Eruptions through crater lakes or shallow sea water, known as Subaqueous or Surtseyan eruptions, are some of the most dangerous eruptions in the world. These eruptions can cause tsunamis, lahars and base surges, but the phenomenon of interest to this research is that of the Surtseyan ejecta. Surtseyan ejecta are balls of highly viscous magma containing entrained material. They occur when a slurry of previously erupted material and water washes back into the volcanic vent. This slurry is incorporated into the magma and ejected from the volcano inside a ball of lava. The large variation in temperature between the slurry and the lava causes the water in the slurry to vaporise. This results in a pressure build-up which is released by vapour either escaping through the pores of the lava or the ejectum exploding. The volcanological question of interest is under what conditions these ejecta rupture.

During this thesis the aim is to improve on the existing highly simplified model of partial differential equations that describe the transient changes in temperature and pressure in Surtseyan ejecta. This is achieved by returning to the basics and developing a model that is more soundly based on the physics and mathematics of Surtseyan ejecta behaviour. This model is developed through the systemic reduction of the coupled nonlinear partial differential equations that arise from the mass, momentum and energy conservation equations to form a fully coupled model for the behaviour of Surtseyan ejecta.

The fully coupled model has been solved numerically as well as reduced further to produce analytical solutions for temperature and pressure. The numerical solutions show a boundary layer of rapidly varying temperatures and pressures around the steam generation boundary. This allows for a boundary layer analysis to be used in both the magma and the inclusion to estimate the temperature profile at early times. The numerical solution also showed a rapid increase in pressure at the flash front that allowed for a quasi steady state approximation in

pressure to be used to form a reduced model that could be analytically solved. This produced an updated criterion for rupture and a criterion for the lower limit of permeability. The analytical and numerical results were then compared to the data from existing intact ejecta for verification.

Acknowledgements

While working on this project I have been lucky to have the support of many people. Firstly, I would like thank my supervisor Professor Mark McGuinness. Throughout my PhD Mark has been kind and supportive. Without his guidance and patient help I doubt I would have reached this point. During my studies Mark encouraged me to attend many conferences and workshops which I am extremely grateful to have had the opportunity to attend.

In 2015, Dr Ian Schipper showed me this fascinating mathematical modelling problem which would eventually become this thesis topic. I would like to firstly thank him for sharing this problem with me and secondly for his insight into Surtseyan ejecta behaviour, as well as the physical data he provided.

I am grateful to our collaborator Professor Andrew Fowler for his interest and help with the mathematical model in this thesis. I would like to thank Dr Dimitrios Mitsotakis for his help in understanding the consequences of uneven numerical meshes.

I have been extremely lucky to be a part of the School of Mathematics and Statistics at Victoria University. The School as a whole has been a pleasure to work within. I feel extremely privileged to be associated with a wonderful group of graduate students throughout my PhD and I would like to thank them for the emotional support and the life long friends I have gained.

During my PhD I have had many experiences at conferences and workshops and I am grateful to NZMS, ANZIAM and Victoria University for providing me with grants that enabled this attendance.

Finally, I would like to thank my friends and family. In particular my parents Christine and Ian, and my brothers William and Richard for their love and support throughout all my studies.

Contents

Chapter 1

Introduction

1.1 Background

The volcanic eruption that created the island of Surtsey, off the coast of Iceland, on the 14th of November 1963 is to this day the archetype for this style of marine shallow to emergent explosive volcanic eruption. This type of eruption is now more commonly known as a Surtseyan eruption. They occur when a volcanic vent is situated near the surface of a body of water. The magma and water mixing produces its characteristically violent and explosive behaviour. There are many examples of this type of eruption, including the 16th of January 2015 eruption in Tonga (which produced an island), Krakatoa in Indonesia, Taal in the Philippines and features of this eruption style can also be seen in various eruptions of Ruapehu (NZ).

During a Surtseyan eruption water containing previously erupted material can be washed back into the volcanic vent. Once inside the vent this slurry can be entrained into the magma and ejected inside balls of magma, known as Surtseyan ejecta. These ejecta contain a slurry inclusion that is significantly cooler than the surrounding magma, and as the water in the slurry boils there are competing processes occurring in the ejectum. The first is the temperature difference driving the evaporation of the water, which increases the pressure inside the ejectum. The second is the diffusion of water vapour through the pores in the magma. Whether or not an ejectum ruptures depends on the relationship between these two processes. There are plenty of examples of intact ejecta of various size

Figure 1.1: Photos of a Surtseyan ejectum taken by Mark McGuinness. In the right-hand photo an inclusion can be seen with a void space around it

classified as: ash (less than 2 mm in diameter); lapilli (between 2 - 64 mm); and bombs (greater than 64 mm).

The purpose of this thesis has been to construct a mathematical model to expand and improve upon the existing model [[20],[31]]. The aim of this research is to use a systematic reduction of the resulting coupled nonlinear partial differential equations that arise from mass, momentum and energy conservation. Then to numerically solve the resulting equations to form a better understanding of ejecta behaviour. Further aims are to validate the model with the aid of analytical solutions and to produce an updated criterion for rupture.

1.2   Literature Review

The mathematical modelling of Surtseyan ejecta is a new area of study. Most of the available literature details mechanisms of Surtseyan volcanism and magma-slurry interaction in Surtseyan eruptions. More generally, there are also existing mathematical models for magma fragmentation, as well as the behaviour of fluids in a porous medium.

The only previous model for the behaviour of Surtseyan ejecta was developed during my masters [20]. Research to date has found no other mathematical

models for this phenomena. Interest in the modelling of Surtseyan ejecta originated from Dr Ian Schipper, a volcanologist at the Victoria University. He was studying intact ejecta and wanted to understand how it was possible that they could survive an eruption without exploding.

1.2.1 Surtseyan Eruptions

Volcanic eruptions that include water often produce hazards that are not normally seen in equivalent dry land volcanoes. Mastin and Witter [28] show that subaqueous eruptions make up 8% of the world's eruptions, causing 20% of the fatalities associated with volcanic eruptions. This is because these eruptions have the ability to cause lahars, tsunamis and base surges, all of which have the potential to create devastation to people and property significant distances away from the eruption site.

There are two mechanisms, described by Mastin et al. [27], that can drive the explosive mixing of magma and water in a single vent eruption. The first is the lowering of the magma channel through the water table, which is followed by a sudden influx of water. An example of this is in the Ukinrek Maars eruption in Alaska in 1977. The second mechanism is a volcano erupting magma through a surface of water such as seawater or a crater lake. This mechanism also includes craters with water seeping through their porous walls. It is this second mechanism that describes Surtsey, where the eruption occurred through shallow sea water.

Surtseyan volcanism is characterised by intermittent, almost silent, jets or a continuous up-rush of tephra along with a large amount of steam. This behaviour has been observed by Thorarinsson [46], at Surtsey:

```
''After each explosion a tephra-laden mass rushes up,
and out of it shoot numerous lumps of liquid or plastic lava,
called bombs, each with a black tail of tephra.
Within a few seconds these black tails turn greyish white
and furry as the superheated vapour ... cools and condenses."
```

He also added that this behaviour continued for as long as the water had access to the vent. Water can gain access to the vent by either flooding across the top or seeping through the volcanic pile.

Kokelaar's model for Surtseyan eruption processes is an explanation for the observed characteristics ([23] [24]). He proposes that there is a funnel-shaped vent filled with a mixture of water and previously erupted material. This vent is surrounded by a ring of previous erupted material which, as the eruption continues, will slip back into the vent. As the volcano erupts the slurry is continuously incorporated into the magma and then is replenished as more slurry is washed from the pile into the vent. Pockets of relatively cool liquid water enclosed in the magma cause violent and continuous expansion, producing the characteristic jets seen in Surtseyan eruptions and described by Thorarinsson. If there is a higher rate of magma supply, a continuous up-rush of tephra is the result, instead of the intermittent jets. When the water can no longer be replenished, the slurry in the vent, gradually dries and the eruptive style changes to Hawaiian fountaining of incandescent magma.

The fragmentation and magma mixing processes described by Kokelaar are difficult to observe directly. In order to quantitatively determine the mechanisms causing magma mixing and fragmentation, a textural study of the pyroclasts is needed. Zimanowski et al. [50] study the differences in the pyroclasts between those produced by decompression and by a molten fuel-coolant interaction.

A textural study of scoria bombs conducted by Schipper et al. [39] shows that entrained material has a crystalline structure when magnified, which is not seen in the surrounding rock. This structure is caused by the reheating of the inclusion inside the bomb. The slurry inclusions are also surrounded by a void space, which is consistent with the presence of water at the time of entrainment. The postulated presence of wet slurry can explain Thorarinsson's observation that ejecta tails turn from black to white in mid-flight. This phenomenon can be attributed to the escaping water vapour. This textual study supports Kokelaar's model of Surtseyan jets and columns being driven by a magma-slurry mingling in a flooded vent.

1.2.2 Previous Modelling

A previous mathematical model for the behaviour of Surtseyan ejecta [[20], [31]] considers the transient heating of a single inclusion placed at the centre of a spherical ball of magma. Both the magma and the inclusion are treated as porous media and the inclusion is assumed to be solely heated by conduction of heat from the surrounding magma. The model considers small inclusions where the temperature in the surrounding magma does not reduce significantly. The water in the inclusion vaporises to form a flashing front that propagates inwards at a rate determined by a heat balance. Pressure build up forces the resulting vapour through the pores, thus reducing pressure. The pressure model is inspired by the modelling of the injection of geothermal waste seen in Pruess [34], although Pruess's work relies in part on relatively small pressure changes, whereas large pressure changes are anticipated here.

The temperature equation in this model [[20], [31]] is determined by considering an estimate for the rate of heat flow into the inclusion and matching this to the rate of change of internal energy of the inclusion:

$$\frac{4}{3}\pi R_1^3 \rho c_p \frac{\partial T}{\partial t} = 4\pi K R_1^2 \frac{\partial T_m}{\partial r} \tag{1.1}$$

where R_1 is the size of the inclusion, ρ is the effective density of the inclusion, c_p is the effective heat capacity of the inclusion, K is the thermal conductivity of the hot magma and T_m is the temperature of the magma (Please refer to the Glossary of terms in Appendix H). Then, using a crude approximation of $\frac{\partial T_m}{\partial r} = \left(\frac{T_m - T}{0.3R_1}\right)$ where the length-scale for the radial distance was estimated by considering the amount of heat energy required to vapourise the water in the inclusion and the amount of magma surrounding the inclusion required to provide this heat, equation 1.1 can be solved to give the temperature (T) at the surface of the inclusion with T_0 as the initial inclusion temperature:

$$T = T_m - (T_m - T_0)e^{-\alpha t} \tag{1.2}$$

$$\alpha = \frac{10K}{\rho c_p R_1^2} \tag{1.3}$$

The temperature equation is completely decoupled from the pressure model (p). The pressure model arises from the conservation of vapour mass in the

surrounding hot magma along with Darcy's law for fluid flow in a porous medium, giving:

$$\frac{\partial(\phi_m \rho_v)}{\partial t} = -\nabla \cdot \mathbf{F}_v \tag{1.4}$$

$$\mathbf{F}_v = -k\frac{\rho_v}{\mu_v}\nabla p \tag{1.5}$$

where ϕ_m is the magma porosity, ρ_v is the vapour density, $\mathbf{F}_v$ is the mass flux, k is the permeability of the magma and μ_v is the dynamic viscosity which is taken to be constant. Then, using the ideal gas law and neglecting changes in magma temperature, the density of the vapour can be converted to pressure to obtain

$$\frac{\partial p}{\partial t} = \frac{k}{\mu_v \phi_m}\nabla \cdot (p\nabla p). \tag{1.6}$$

Using the ideal gas law is a common assumption for water vapour in geothermal modelling however this assumption can become invalid at very high pressures because of the interactions between the water molecules that have been forced closer together. Neglecting the changes in magma temperature is a valid assumption because, in this model, it is assumed that there is a small inclusion inside a large magma ball. With this assumption it can be assumed that the temperature drop will not propagate a significant distance into the magma, leaving the majority of the magma at a constant temperature.

In models for the injection of geothermal waste, equation 1.6 would be linearised by using an average pressure in the magma. However in the Surtseyan ejecta model there are large pressure variations and an average pressure cannot be assumed. At the time of entrainment and at the outermost boundary of the ejectum the partial pressure of water in the vesicular magma is considered negligible.

Another boundary starts at the surface of the inclusion: the flashing front. This front is propagating into the inclusion at a rate governed by a heat balance between the conducted heat into the inclusion and the latent heat required to move the flashing front some distance into the inclusion. The amount of heat provided by conduction when the flash front is located at $s(t)$ after some time Δt

is:

$$4\pi s^2 K \frac{dT}{dr} \Delta t, \tag{1.7}$$

where $\frac{dT}{dr} \approx \frac{(T_m - T_0)e^{-\alpha t}}{0.3R_1}$ with the length scale estimated by calculating the amount of magma needed to vaporise that amount of water assuming that in the time Δt the flashing front moves Δs towards the centre of the inclusion. The heat required to vaporise this thin spherical shell of water is:

$$4\pi s^2 \Delta s \rho_l \phi h_{vl}, \tag{1.8}$$

where h_{vl} is the latent heat of vaporisation of water. Then, using equations 1.7 and 1.8 and taking the limit as Δt tends to zero, noting that $\dot{s} = \lim_{\Delta t \to 0} \frac{\Delta s}{\Delta t}$, an expression for the speed of the flash front is obtained:

$$\dot{s} = -\frac{K(T_m - T_0)e^{-\alpha t}}{0.3\rho_l \phi h_{vl} R_1}. \tag{1.9}$$

If the flash front at the time of entrainment is at distance R_1 from the centre of the ejecta, this gives an equation for s and the critical time (t_0), i.e., the time it takes for the water to be depleted and the distance of the steam generation boundary from the centre of the ejecta to equal zero:

$$s(t) = B(e^{-\alpha t} - 1) + R_1 \tag{1.10}$$

$$B = \frac{(T_m - T_0)\rho c_p R_1}{3\rho_l \phi h_{vl}} \tag{1.11}$$

$$t_0 = -\frac{1}{\alpha} \ln\left(1 - \frac{R_1}{B}\right). \tag{1.12}$$

The boundary condition is set by the vapour mass flux across this flash front. To calculate this the mass of vapour produced per second over the entire flash front is equated with the total flow rate of vapour that is flowing away from the flashing front in to the magma:

$$-\phi \rho_l 4\pi s^2 \dot{s} = -4\pi s^2 \frac{k\rho_v}{\mu_v} \nabla p. \tag{1.13}$$

Then by applying the ideal gas law (with R as the gas constant and M the molar mass of water) to convert the density to pressure and considering the flux to be

zero after the water is depleted (i.e., when the critical time t_0 is reached) gives:

$$\left(\frac{k}{\phi_m \mu_v}\right) p \nabla p = \begin{cases} \frac{RT_m \phi \rho_l \dot{s}}{M\phi_m} & : t < t_c \\ 0 & : t \geqslant t_c \end{cases} \quad , \quad r = s(t) \qquad (1.14)$$

The system is re-scaled on the time it takes for the water to be depleted (t_c), the pressure when the magma ruptures (p_c), the temperature of the magma (T_m) and the radius of the magma (R_2) to form the following equations:

$$\frac{\partial \tilde{p}}{\partial \tilde{t}} = \frac{1}{\tilde{r}^2}\frac{\partial}{\partial \tilde{r}}\left[\tilde{D}\tilde{r}^2\frac{\partial \tilde{p}^2}{\partial \tilde{r}}\right] \qquad (1.15)$$

$$\tilde{p}(\tilde{r},0) = 0, \ \tilde{p}(1,\tilde{t}) = 0 \qquad (1.16)$$

$$\tilde{D}\frac{\partial \tilde{p}^2}{\partial \tilde{r}} = \begin{cases} C\dot{s} & : \tilde{t} < 1 \\ 0 & : \tilde{t} \geqslant 1 \end{cases} \quad , \quad \tilde{r} = \frac{s(t)}{R_2} \qquad (1.17)$$

$$\dot{s} = -\frac{K(T_m - T_0)e^{-\alpha t_c \tilde{t}}}{\rho_l \phi h_{vl} \times 0.28 R_1} \qquad (1.18)$$

$$C = \frac{t_c RT_m \phi \rho_l}{R_2 p_c M \phi_m} \qquad (1.19)$$

$$\tilde{D} = \frac{t_c p_c k}{2\phi_m \mu_v R_2{}^2}. \qquad (1.20)$$

This system of equations can be solved numerically using the PDEPE command in Matlab (which solves initial-boundary value problems for systems of parabolic and elliptic partial differential equations with a single space dimension and time). At first, the flashing front was fixed at the surface of the inclusion and delivered vapour at this point for the time t_0 (the time it would have taken for the boundary to reach the centre of the inclusion). This results in a larger amount of vapour than the moving boundary model would, as it does not take into account the reducing area of the flashing surface.

By fixing the boundary and setting the vapour flux to the maximum possible value (seen at initial times as it has largest flashing surface and therefore the most liquid flashed to vapour at the boundary at one time), for the time t_0 this will produce an upper limit on the maximum pressure that can be obtained with a

moving boundary model. It is an upper limit because the pressure is only affected by two processes: the production of vapour and the time it takes for this vapour to escape through the pores of the magma. If the vapour production is maximal then this will produce an upper limit on the pressure, as the time it takes for the vapour to escape the pores of the magma is not affected by fixing the boundary. These moving boundary pressures can be simulated by updating the fixed boundary positions at regular time intervals.
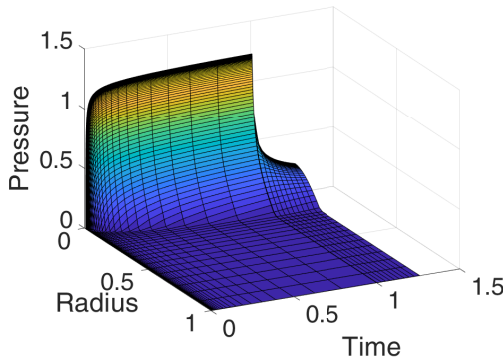

Figure 1.2: Numerical solution for a 1mm inclusion with a fixed boundary
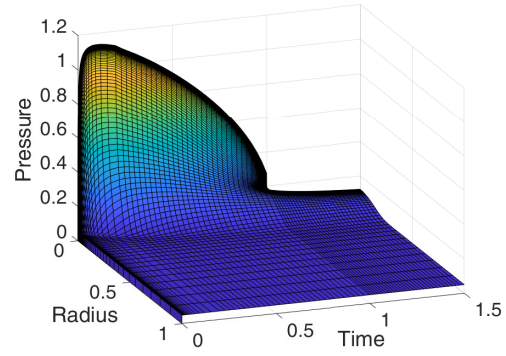
Figure 1.3: Numerical solution for a 1mm inclusion with a moving boundary

The rapid stabilisation of pressure at the surface of the inclusion indicates that the maximum pressure can be approximated by a steady-state solution for pressure with a constant and persistent flow of vapour at the surface of the inclusion. Using this steady-state approximation, a formula for the criterion for rupture of a spherical ejectum containing a small centred spherical inclusion can be derived:

$$p_{max} = \sqrt{\frac{7RT_m K(T_m - T_0)\mu_v}{M p_c^2 h_{vl} k}\left(1 - \frac{R_1}{R_2}\right)}. \tag{1.21}$$

This approximation produces results that are consistent with the numerical simulations from the model. From equation 1.21 a critical permeability is found for typical values of other parameters for ejected rock, $k_c = 3 \times 10^{-14}$. Intact ejecta permeability measured by Schipper et al. [38] ranges from 10^{-10} to 10^{-13} m^2. This suggests the true critical permeability is lower that these values and this is consistent with the critical permeability calculated from the fragmentation criterion.

1.2.3   Magma Fragmentation

Magma fragmentation in high energy eruptions, such as Vulcanian, Plinian and Ultra-Plinian, is caused by rapid decompression of the volcanic vent. This decompression can be the result of either the dislodging of a blockage in the volcanic vent or the collapsing of the dome [[18], [1], [41]]. This fragmentation may be able to provide insight into how pressure build-up will effect the magma in Surtseyan ejecta.

Magma fragmentation occurs inside the volcanic vent and various analogue materials have been studied to shed light on this process. Alidibirov [1] used porous volcanic rock for this analogue, which he justified by considering that the magma, at the time-scale of the experiment, would act like a brittle solid. Alidibirov also designed a vertical shock tube to simulate the depressurisation process. The apparatus had rock glued into a sample holder and then this was placed inside an autoclave. The autoclave is attached to a large chamber, held at atmospheric pressure, with a diaphragm to separate it. It is slowly pressurised and rapid decompression is triggered and a high speed camera is used to capture the results. This experiment has since been modified to investigate a variety of different problems, such as Spieler's [44] research on the fragmentation threshold of pyroclastic rocks.

There are many different proposed fragmentation mechanisms and they can be categorised into groups depending on the viscosity or temperature of the magma. A proposed low magma viscosity mechanism is bubble formation. This was first suggested by Verhoogen [48] and later modified by McBirney and Murase [30]. The mechanism proposes that decompression causes bubbles to be formed by the enclosed gases in the porous magma. The enclosed gas, after decompression, is at a higher pressure than the surface. The pressure difference causes deformation in the low viscosity magma and expands the pores to form bubbles. If the volume ratio of bubbles to magma becomes too large then fragmentation of the magma occurs. Sparks proposed that explosive fragmentation is the result of these bubbles bursting [42].

If the magma has a higher viscosity, then a larger force will be required to deform it. The trapped gases cannot expand the pores to release the pressure

resulting in an over-pressure. There is some debate over the cause of fragmentation in this case. Bennet [8] proposed that the mechanism relies on expansion waves and that it can be studied using one dimensional shock tube experiments. Another theory (Sparks [42]) argues that the bubbles in the magma would create their own expansion and compression waves and every bubble would act as its own diaphragm.

Explosive fragmentation of vesicular magma was mathematically modelled by Fowler et al. [18]. The fragmentation mechanism in this model is controlled by the gas pore pressure exceeding the yield stress, the lowest stress needed for the rock to rupture, of the porous rock. At the time of rapid decompression the decreasing pressure at the surface causes an over-pressure in the pores of the rock. This creates a pressure difference between the pores and the surface that will cause fragmentation if it exceeds the yield stress. The Surtseyan ejecta problem can also be considered as an over-pressure between the entrained slurry and the magma surface, which may cause the ejectum to fragment. Therefore, some of the methods used in this model, particularly the momentum and stress equations, could be used to inform the Surtseyan ejecta model. However, unlike the explosive fragmentation model, the pressure build-up inside Surtseyan ejecta is driven by a temperature difference, not a rapid decompression, and therefore the temperature analysis also needs to be considered.

1.2.3.1 Fluid flow in a porous medium

Porous rock can be used as an analogue for vesicular magma hence fluid flow through a uniformly constant porous media is of interest. The equations describing fluid flow in a porous medium were developed in the petroleum, groundwater and soil science literature and were applied to geothermal reservoirs by Grant et al. [19]. If the porous medium is not uniform then averaging is needed to determine the fraction of liquid, vapour or a mixture of both states in the pores of the medium. This averaging is detailed by both Drew and Wood [15] and Fowler [17].

Conservation equations for mass, momentum and energy apply separately to each phase, but they can be combined to obtain a single equation for the two phase flow. The mass conservation equation for a single phase fluid flow through

a medium with uniform porosity (ϕ) is:

$$\phi\frac{\partial \rho_x}{\partial t} + \nabla \cdot (\mathbf{u}_x) = 0, \tag{1.22}$$

where $\mathbf{u}_x$ is the mass flux density and ρ_x is the density of the fluid.

The conservation of mass equation for a two-phase flow is a combination of the single phase vapour and liquid flows. If the porous media is saturated with a mixture of liquid and vapour, a fraction of the pore space is filled with each phase. The fraction of the pore space containing liquid is denoted S_l and as the pore space is saturated with fluid the fraction containing vapour is $1 - S_l = S_v$. The conservation of mass equation for a two phase flow is:

$$\phi\frac{\partial (\rho_l S_l + \rho_v S_v)}{\partial t} + \nabla \cdot (\mathbf{u}_v + \mathbf{u}_l) = 0. \tag{1.23}$$

The pore space in the momentum and energy conservation equations can be split between liquid and vapour sections in the same way.

Jacob Bear in his book 'Modeling Phenomena of Flow and Transport in Porous Media' [5], details in a similar manner to Drew and Wood [15] and Fowler [17] the continuum approach to porous media and the use of relative elementary volume (REV). By definition these REV are of a size such that wherever they are placed in the porous media they contain both solid and fluid material, in averaging over the porous media. Bear's book also contains details of the Non-Darcy flux laws, like the Forchheimer equation, and also describes under what conditions Darcy's laws can be used. In order to use Darcy's law the Reynolds number of a system must not exceed one. The Reynolds number is defined as:

$$R_e = \frac{qd}{\gamma},$$

where q is the flow speed, d is the pore size and γ is the kinematic viscosity.

Bear [5] also details four different mechanisms for thermal energy transport in a porous medium (assuming that radiation plays no rule in the energy transport). These mechanisms are:

- Advection: the movement of fluid(s) in the pore space

- Conduction in both the solid and the fluid

- Mass diffusion in the fluid

- Thermal dispersion in the fluid.

He notes that due to the advection, the movement of fluid in the pore space carrying thermal energy, any complete heat transport model must by made up of a coupled heat and mass transport model. The fluid mass transport models in non-porous media assume that the solid is impervious to mass or heat transport. Bear states that in a porous medium this is not the case and the condition between the fluid in the pore space and the surrounding solid will cause their temperatures to equalise over time.

The text [5] also details the use of advective and diffusive fluxes to produce the total energy flux need in the conservation of mass equation. He notes that the total energy flux is made up of total advective energy flux and three diffusive energy fluxes:

- Diffusive flux of internal energy, expressed by Fourier's law

- Diffusive flux of kinetic energy, which is calculated using the stress and the velocity vectors and represents the work done by surface forces

- Diffusive flux of potential energy, which is calculated considering the work done by the diffusive mass fluxes against the conservative forces, for example gravity.

The advective and diffusive fluxes are used in Bear's book to derive the point-wise energy equation that is averaged over to find the energy in the solid and fluid regions.

1.2.4 Summary

In summary, this thesis expands upon the previous model for the behaviour of Surtseyan ejecta [[20], [31]]. To achieve this, ideas from the magma fragmentation literature are used to provide an understanding of how changes in pressure can cause the fragmentation of magma. Of particular interest is the

explosive fragmentation of vesicular magma mathematical model by Fowler et al. [18]. The rapid decompression in this model creates an over-pressure in the pores of the rock. This pressure difference between the pores and the surface will cause fragmentation if it exceeds the yield stress. This information is highly relevant in the modelling of Surtseyan ejecta as it is similar to the pressure build-up in the ejectum at the flash front, which in the ejecta model is driven by a temperature difference instead of a rapid decompression. In both cases the over-pressure may cause the ejectum or the magma to fragment if the yield stress is exceeded. Therefore, some of the methods used in this model, particularly the momentum and stress equations, are useful to inform the Surtseyan ejecta model.

The other area of interest in the literature review is fluid and heat flow in porous media. The averaging techniques using a relative elementary volume over a porous media are required to simplify the mass, momentum and energy conservation equations for a fluid in a porous media. The derivation of the pointwise energy conservation equation [[5],[16]] also helps with the construction of the energy conservation equation in the Surtseyan ejecta model. The derivation and the explanation covering the purpose of each term helped with the simplification of the Surtseyan model as both Bear's and Fowler's books [[5],[16]] contained information which helped with the discussion concerning neglecting the diffusive flux of potential energy, viscous dissipation and the deviatoric stress tensor.

Lastly, the literature review provides general background about Surteyan ejecta and eruptions. This includes Kokelaar's model of the eruption at Surtsey [[23], [24]]. The information in this section of the literature review along with conversations with Ian Schipper [40] helped with keeping the assumptions and typical parameters in the Surtseyan ejecta model realistic. Also, the observations of Thorarinsson [46] detailing magma bombs with black tails that turn white in mid-flight is evidence that in reality water vapour is escaping the Surtseyan ejecta and the approach of modelling the water vapour escaping through the magma in flight is valid.

1.3 Overview of thesis

This thesis focuses on developing a rigorous numerical model for the temperature and pressure behaviour in Surtseyan ejecta. The new model uses the conservation of mass, momentum and energy equations to describe the fluid flow through the porous magma of the Surtseyan ejecta. Porous rock is used as a analogue for the magma in the ejecta. The resulting equations are solved numerically using the method of lines for typical parameter values.

In chapter 5 the consequences of the infinite gradients at the flash front on the maximum pressure are considered. This includes a study on the convergence of the numerical solutions for the maximum pressure and the time it takes for this maximum pressure to be reached.

The temperature diffusion equations, derived in chapter 2, have thermal diffusivities that when compared to the pressure diffusivity suggest a thermal boundary layer near the flash front. In chapter 3 asympototic methods from Bender and Orszag [7] are used to form temperature profiles in the inclusion and the magma. These temperature profiles apply for early times before the movement of the steam generation boundary can significantly affect the temperatures.

In chapter 6, a theoretical upper-bound on the maximum pressure at the flash front in a Surtseyan ejectum is produced. This chapter also produces a theoretical lower-bound for the time it takes for this pressure to be reached. This is achieved by estimating the early time pressure behaviour and equating it to the pressure null surface. This theoretical upper-bound on the maximum pressure at the flash front can be directly compared with the criterion for rupture from the previous model. It is clear that the theoretical upper-bound on the maximum pressure at the flash front and the criterion for rupture from the previous model are close to identical except for a factor comprised of some constants and the ramp distance used over the step function.

The numerical simulations are compared with the temperature profiles calculated in chapter 3 and the theoretical upper-bound on the maximum pressure at the flash front from chapter 5. The temperature profiles provide a close match to the

numerical simulations for typical parameter values in both the inclusion and the magma regions. The theoretical upper-bound on the maximum pressure at the flash front is about 5 times that of the simulated value for the typical parameter values.

Finally, the maximum pressure from the numerical simulations and the upper-bound on the maximum pressure at the steam generation boundary are compared with the permeability and porosity data for existing intact Surtseyan ejecta.

Chapter 2

Fully Coupled Model

Previous work modelling Surtseyan ejecta [[20],[31]] contained many shortcomings. Firstly, in the model it was assumed that the temperature and the pressure were uncoupled and the inclusion heated in a uniform manner. This is an issue as one of the justifications for the ejectum remaining intact is that the liquid in the inclusion evaporates gradually and this can only occur if the boiling point of the liquid is affected by the pressure. The second shortcoming is the treatment of the steam generation boundary and the assumed temperature gradient at that point in the magma. This temperature gradient was estimated using a length scale determined by the amount of magma needed to vaporise the liquid in the inclusion. This length scale is likely to be larger than the true length scale and thus produces a lower temperature gradient in the magma at the steam generation boundary.

In order to combat the shortcomings found in the previous model this work will return to basics and develop a model that is more soundly based on the physics and mathematics of the Surtseyan ejecta behaviour. This will include a systematic reduction of the coupled nonlinear partial differential equations that arise from the mass, momentum and energy conservation equations to form a fully-coupled model for the behaviour of Surtseyan ejecta.

2.1   Dimensional Model

This model considers the boiling of water within a single slurry inclusion, enclosed by a ball of vesicular magma, and how the generated vapour diffuses through the magma. The ejectum is taken to consist of two concentric spheres of slurry and magma [1] .

The centre sphere is the slurry, which is comprised of previously erupted and cooled vesicular magma that has been washed back into the volcanic vent. As the vesicular magma cools it forms a porous rock and therefore it can be assumed that the slurry is made up of porous rock with liquid water in the pores. After the water has evaporated the slurry centre becomes a rock-like material, with a similar make up to the surrounding cooled magma, that is typically fused into one piece and surrounded by a void space.
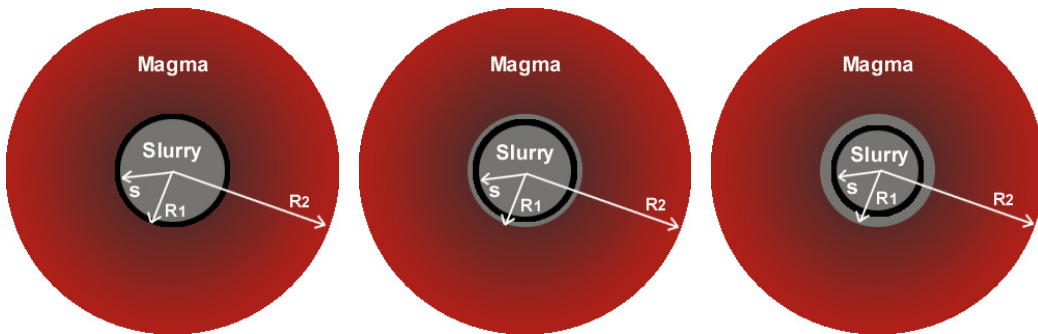
Figure 2.1: Diagram showing a slurry inclusion, of radius R_1, entrained in a magma ejectum, of radius R_2. The diagram (left to right) shows the motion of the steam generation boundary, s, as it moves towards the centre of the slurry inclusion.

For the outer sphere a common analogue for magma, at the timescales in this model, is to treat it as a porous medium [2]. The medium will only contain water in vapour form within its pores. This model is concerned with the first few seconds of existence for this ejecta. In this time period they erupt from the volcanic vent

---

[1]   The validity of using two concentric spheres of slurry and magma in this model is discussed in section 7.3.1

[2]   This is a common assumption first made by Alidibirov [1]; see section 1.2.3

and travel though the air in free fall. Initially the temperature of the magma is about 1200 K. At this temperature all the magma components are completely molten. The starting temperature of the slurry is taken to be 300 K, which is approximately the temperature of sea water. This model set-up allows spherical symmetry to be applied in order to simplify the problem to one dimension.

The model derivation begins with the pointwise conservation of energy equation for fluid, in liquid or vapour phase. In terms of pressure and temperature this is:

$$\rho c_p \left(\frac{\partial T}{\partial t} + \mathbf{v} \cdot \nabla T \right) - \beta T \left(\frac{\partial p}{\partial t} + \mathbf{v} \cdot \nabla p \right) = \nabla \cdot (K \nabla T). \qquad (2.1)$$

This equation is derived using the pointwise enthalpy conservation equation, as detailed in appendix A.

2.1.1 The Magma Region

The magma region is that which is situated between the steam generation boundary, at distance s from the centre of the inclusion, and surface of the ejectum, at distance R_2 from the inclusion centre. For the conservation of energy within the porous rock analogue (denoted with subscript m) it is assumed that the rock is competent (rock that is able to sustain openings/pores without structural support), stationary (in the ejecta's reference frame) and has negligible compressibility [3]. The porosity of the analogue in the magma region is also taken to be constant. It is assumed that the representative elementary volume, used in the averaging detailed in [22] and [17], is small with no local temperature variation at the interfaces between the rock and vapour. After averaging over a volume with porosity ϕ, the conservation of energy equation for the rock is:

$$(1 - \phi)\rho_m c_{pm} \frac{\partial T}{\partial t} = (1 - \phi)\nabla \cdot (K_m \nabla T), \qquad (2.2)$$

where c_{pm} is the specific heat of the magma. This equation contains only the energy transfer due to conduction, and this is a consequence of the stationary and compressibility assumptions.

---

[3] These assumptions are made to aid in the averaging of the energy conservation equation. The assumption that the rock is competent is also standard when used as a magma analogue.

Now consider the conservation of energy in the water vapour (denoted with subscript v) in the pores of the magma region. It is assumed that the water vapour is the sole presence in the pores and that it can be approximated as an ideal gas. With Batchelor's [4] approximation $\beta T \approx 1$, equation 2.1 can be written as:

$$\rho_v c_{pv} \left(\frac{\partial T}{\partial t} + \mathbf{v} \cdot \nabla T \right) - \left(\frac{\partial p}{\partial t} + \mathbf{v} \cdot \nabla p \right) = \nabla \cdot (K_v \nabla T). \qquad (2.3)$$

However, this is still a pointwise equation and averaging [[22],[17]] over a representative elementary volume of porous magma containing flowing vapour gives the energy conservation equation for this moving pore fluid as:

$$\phi \rho_v c_{pv} \left(\frac{\partial T}{\partial t} + \mathbf{v} \cdot \nabla T \right) - \phi \left(\frac{\partial p}{\partial t} + \mathbf{v} \cdot \nabla p \right) = \phi \nabla \cdot (K_v \nabla T), \qquad (2.4)$$

where ϕ is the fraction of the magma volume occupied by the escaping steam (which in this case is equivalent to the porosity). Also, like the magma energy conservation equation, the temperature variation at the interfaces has been neglected.

The combined averaged conservation of energy equation for the magma and the vapour is, using equations 2.2 and 2.4:

$$c_{pe} \rho_e \frac{\partial T}{\partial t} + \rho_v c_{pv} \mathbf{u} \cdot \nabla T - \phi \frac{\partial p}{\partial t} - \mathbf{u} \cdot \nabla p = K_e \nabla^2 T, \qquad (2.5)$$

where $\mathbf{u} = \phi \mathbf{v}$ represents the Darcy velocity of the vapour, $c_{pe} \rho_e = (1 - \phi) \rho_m c_{pm} + \phi \rho_v c_{pv}$ is the combined heat capacity for the rock and vapour and $K_e = (1 - \phi) K_m + \phi K_v$ is the effective thermal conductivity of the pore space. The variation in the $c_{pe} \rho_e$ term (in the range of temperatures, 300K to 1300K, and pressure, from atmospheric to that of fragmentation at about 2 MPa) is less than 0.5%, see figure 2.2, and is dominated by the thermal capacity of the rock and this will therefore be taken to be constant.

In this magma region, the conservation of vapour mass and momentum need to be considered. The conservation of vapour mass equation is:

$$\phi \frac{\partial \rho_v}{\partial t} + \nabla \cdot (\rho_v \mathbf{u}) = 0, \qquad (2.6)$$
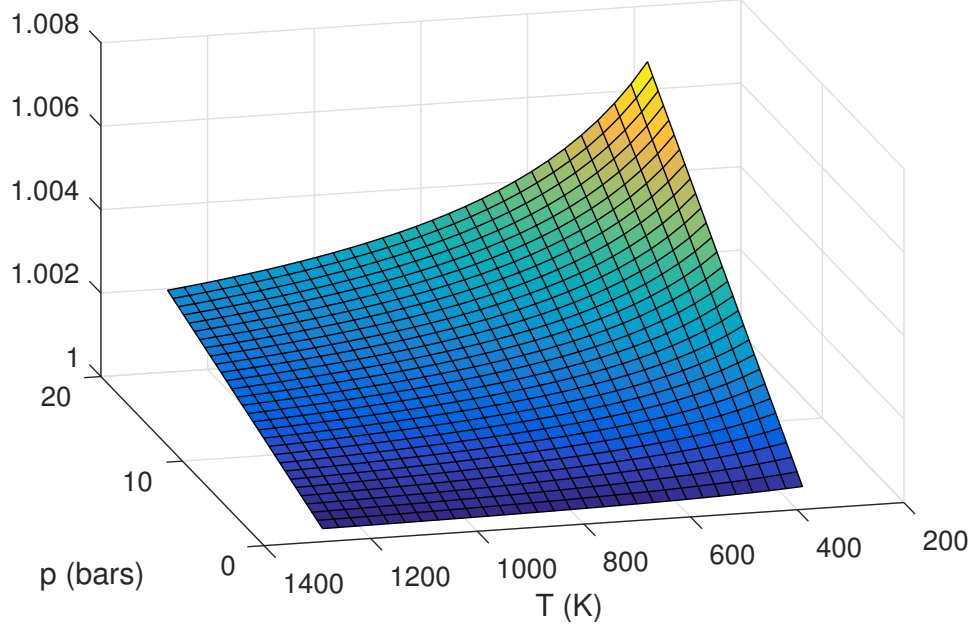
Figure 2.2: A graph showing the variation in $\frac{c_{pe}\rho_e}{(1-\phi)\rho_m c_{pm}}$ of water vapour in the temperature's and pressure's of interest.

and conservation of vapour momentum is given by Darcy's Law, which describes a fluid flow in a porous medium,

$$\mathbf{u} = -\frac{k}{\mu_v}\nabla p, \tag{2.7}$$

where k is the permeability of the magma and μ_v is the viscosity of the vapour.

Assuming that the vapour in this region is an ideal gas [4] this allows for the temperature, pressure and density when $r > s(t)$ to be related by:

$$\rho_v = \frac{pM}{R_g T}, \tag{2.8}$$

where M is the molar mass of water and R_g is the universal gas constant.

---

[4]   Water vapour is not an ideal gas because it is a polar molecule. However, at lower pressures this is a common assumption, and it is not expected to significantly alter the modelling results.

2.1.2   The Inclusion Region

In the inclusion region between the origin at the centre of the ejectum and the steam front at distance s, conservation of energy, mass and momentum equations are used in a similar manner to the magma region. Starting with the pointwise conservation of energy equation 2.1 consider the rock (denoted with subscript m), and liquid (denoted with subscript l) in a similar way to how the magma and vapour were treated. After averaging, the combined rock and liquid water energy conservation equation is:

$$c_{pi}\rho_i \frac{\partial T}{\partial t} + \rho_l c_{pl} \mathbf{u}_l \cdot \nabla T - \phi \beta T \frac{\partial p}{\partial t} - \beta T \mathbf{u}_l \cdot \nabla p = K_i \nabla^2 T \qquad (2.9)$$

where $c_{pi}\rho_i = (1-\phi)\rho_m c_{pm} + \phi\rho_l c_{pl}$, $\mathbf{u}_l = \phi \mathbf{v}_l$ is the Darcy velocity for liquid water and the combined thermal conductivity is $K_i = (1-\phi)K_m + \phi K_l$ (note the subscript i to denote the inclusion). As the slurry is made up of previously erupted material from the volcano it is assumed that the slurry and the magma will have similar properties. This allows for the porosity in both regions to be considered to be equal.

In the inclusion region conservation of liquid water mass,

$$\phi \frac{\partial \rho_l}{\partial t} + \nabla \cdot (\rho_l \mathbf{u}_l) = 0, \qquad (2.10)$$

and conservation of the liquid water momentum given by Darcy's law,

$$\mathbf{u}_l = -\frac{k}{\mu_l}\nabla p, \qquad (2.11)$$

must be applied. In addition, as the liquid water is considered to be a compressible fluid in this model (due to the large fluctuations in pressure and temperature), an expression for water density is required. By fitting specific volume data from [37] between the pressures of 1 and 100 bar and temperatures between saturation and the critical point an expression for density is deduced:

$$\rho_l = \rho_{0l} + \beta_e(p - p_0) - \alpha(T - T_R). \qquad (2.12)$$

In equation 2.12 the reference parameters ρ_{0l}, p_0 and T_R are set to 1000 kg/m^3 , atmospheric pressure and 300 K respectively (these are the initial temperature,

pressure and density values in the inclusion). The compressiblity factor of liquid water is $\beta_e = 4.6 \times 10^{-10}$ kg/m^3/Pa and the thermal expansion is $\alpha = 0.5$ kg/m^3/K. This equation gives a fit that is within 10% of [5] the specific volume data within the ranges stated [37].

2.1.3 The Steam Generation Boundary

The final region considered is the steam generation boundary located at $r = s(t)$, separating the vapour and the liquid regions. The evaporating liquid in this region causes an increase in inclusion pressure and this results in the inclusion temperatures staying at or below boiling point. This leaves a small two-phase or a boiling region at the edge of the inclusion that can increase or decrease in size depending on the pressure behaviour. This boiling region is the steam generation boundary. In section 2.2 this is shown to be a thin region.

Using the conservation of enthalpy and mass equations, averaged over a small representative volume for both the inclusion and magma regions, the boundary behaviour can be found by integrating over the steam generation boundary as detailed in appendix B. This results in:

$$\phi \rho_v h_{vl}(v_v - \dot{s}) = \phi \rho_l h_{vl}(v_l - \dot{s}) = [K \nabla T]_-^+ + \phi(v_v - v_l)p, \qquad (2.13)$$

where the subscript v denotes the water vapour.

In this region it is assumed that the temperature and the pressure are at saturation [6] and are therefore related by the Clausius-Clapeyron equation:

$$p = p_R e^{\frac{Mh_{vl}}{R_g T_R}\left[\frac{T - T_R}{T}\right]} \qquad (2.14)$$

where p_R and T_R are reference pressure and temperature.

---

[5] This linear model is sufficient for the current model. Water is normally treated as an incompressible liquid and this model is an improvement on that assumption.

[6] This is a reasonable assumption if the temperature at the boundary remains below the critical temperature, as is assumed in this model. However in a later model it would be interesting to take a look at this.

Equations 2.5 to 2.14 form the equations for the dimensional model. The
boundary conditions are that the pressure at the surface of the ejectum is at
atmospheric pressure, $p(R_2) = p_a$, and there is no flow of fluid or heat at the
centre of the inclusion:

$$\left.\frac{\partial p}{\partial r}\right|_{r=0} = 0$$

$$\left.\frac{\partial T}{\partial r}\right|_{r=0} = 0$$

The temperature and pressure are assumed to be continuous across the steam
generation boundary. The initial conditions are that at time $t = 0$ the magma
temperature is T_m, the inclusion temperature is at boiling for atmospheric
pressure and the pressure is taken to be atmospheric pressure throughout the
ejectum[7].

2.2   Non-Dimensional Model

To reduce the complexity of the coupled equations, rescalings are chosen to
non-dimensionalise the model. After rescaling, the small terms determined by
the parameters in table 2.1, are neglected in the model. The rescalings used in
this model are:

$$r = \tilde{r}R_2, \quad s = \tilde{s}R_2, \quad T = \tilde{T}T_m, \quad p = \tilde{p}p_a, \quad t = \tilde{t}t_0,$$

$$v_l = v_{0l}\tilde{v}_l, \quad v_v = v_{0v}\tilde{v}_v, \quad \rho_l = \rho_{0l}\tilde{\rho}_l, \quad \rho_v = \rho_{0v}\tilde{\rho}_v.$$

In this chapter the rescalings are applied to Equations 2.5 to 2.14 (details in
Appendix C) and then the tildes are dropped.

The time rescaling (t_0) is the time taken for the liquid in the inclusion to flash to
steam. This process is the driving force behind the build-up of pressure. Another
possible choice of scaling is the time taken for the vapour to escape through the

---

[7]   The pressures inside a volcanic vent would be significant higher than this. However, this
       mixing occurs at the surface of the vent, which is at atmospheric pressure.

pores of the ejectum. However as the maximum pressures occur at early times, this scaling misses important behaviour. The t_0 rescaling can be estimated by balancing the energy required to flash the liquid in the inclusion to vapour and the conduction of heat across the surface of the slurry (using the variables in table 2.2), giving:

$$t_0 = \frac{\phi \rho_{0l} h_{vl} R_1^2}{3 K_e (T_m - T_i)} \approx 17. \tag{2.15}$$

Using the ideal gas law we can choose

$$\rho_{0v} = \frac{p_a M}{R_g T_m} \tag{2.16}$$

and since the vapour is produced at the steam generation boundary, balancing the amount of liquid flashing to steam with the amount of vapour crossing the boundary gives

$$v_{v0} = \frac{R_2 \rho_{l0}}{t_0 \rho_{s0}}. \tag{2.17}$$

2.2.1 The Steam Generation Boundary

Dropping the tildes on the dimensionless variables on equation 2.13 gives the mass balance:

$$\dot{s}(\rho_l - f_1 \rho_s) = f_2 \rho_l v_l - \rho_s v_v, \tag{2.18}$$

where the parameters f_1 and f_2 are defined in table 2.1. As $K_e \approx K_i$ the difference is neglected. The energy balance, equation 2.13, across the steam generation boundary is given by:

$$\rho_s (v_v - f_1 \dot{s}) = \frac{1}{f_3} [\nabla T]_-^+ + f_4 (v_v - f_5 v_l) p, \tag{2.19}$$

with the ratios f_4, f_3 and f_5 defined in table 2.1. The full details of this derivation and those of the inclusion and magma equations can be found in appendix C.

The Clausius Clapeyron equation in dimensionless terms is:

$$p = e^{H\left[\frac{T - T_n}{T}\right]}, \tag{2.20}$$

where the reference pressure is set to atmospheric pressure and the reference

temperature to the boiling point of water at atmospheric pressure.

2.2.2   In the Inclusion

In the inclusion, the equation of state ,equation 2.12, non-dimensionalises to:

$$\rho_l = 1 + f_6(p - 1) - f_7(T - T_n), \tag{2.21}$$

where the parameter values can be found in table 2.1. The only mechanisms that can cause the liquid in the inclusion to move are expansion and contraction. This is due to the spherical assumption and that the ejectum is in free fall and, so gravitational effects do not apply. Also in this model rotations are not considered. If the ejecta was rotating, this would push the water vapour towards the edge of the bomb, decreasing the pressure at the steam generation boundary. Therefore this model will still provide an upper limit for the maximum pressure produced. In table 2.1 it is clear that f_6 is relatively small and can therefore be ignored. The implication of this is that thermal expansion dominates changes in density in the inclusion.

An estimate for the rescaling of the liquid velocity is obtained by calculating the change in dimensional radius due to the density decrease when the inclusion is heated to near-critical temperature. The time taken for the inclusion to heat to critical temperature is also required to estimate the liquid velocity (details in appendix C.2). The resulting over-estimate for the liquid velocity is:

$$v_{l0} \approx \frac{\alpha K_i(T_{crit} - T_0)}{3R_1((1 - \phi)\rho_m c_{pm} + \phi \rho_v c_{pv})(\rho_l - \alpha(T_{crit} - T_0))}. \tag{2.22}$$

The conservation of mass in the inclusion becomes:

$$\phi \frac{\partial \rho_l}{\partial t} + f_2 \nabla \cdot (\rho_l \mathbf{u}_l) = 0. \tag{2.23}$$

As f_2 is very small (table 2.1), the density of the liquid can be considered as a constant and therefore the velocity of the liquid (v_{l0}) which is caused buy the expansion or contraction of the liquid is considered negligible. This is consistent with the estimate for the velocity of the liquid in Appendix C, which also

indicated that there was very little change in the radius of the inclusion. It follows that the pressures in the inclusion do not vary appreciably with the radius and therefore can be taken to be equal to the time-varying pressure at the flash front. Another consequence of the liquid density being treated as a constant is that $c_i\rho_i$ can be treated as a parameter. Lastly, the boundary condition can also be reduced due to the small sizes of f_1 and f_5 (see table 2.1) to:

$$\rho_v v_v = -\dot{s} = \frac{1}{f_3}[\nabla T]_-^+ + f_4 v_v p. \tag{2.24}$$

The energy equation in the inclusion can also be reduced by neglecting the liquid velocity and removing the small pressure work term (details in appendix C.2):

$$\frac{\partial T}{\partial t} = \frac{f_9}{r^2}\frac{\partial}{\partial r}\left(r^2\frac{\partial T}{\partial r}\right). \tag{2.25}$$

The small term f_9 is retained so that the thermal boundary layer that forms near the flash front can be resolved.

2.2.3 In the Magma

The ideal gas law and Darcy's law become, respectively, (see derivation in appendix C.3):

$$p = \rho_v T \tag{2.26}$$
$$v_v = -f_{10}\nabla p. \tag{2.27}$$

When these are substituted into the boundary equations the pressure work term can be neglected, due to a very small coefficient, resulting in the equations being reduced to:

$$\rho_v v_v = -\dot{s} = \frac{1}{f_3}[\nabla T]_-^+. \tag{2.28}$$

The mass conservation equation is re-scaled to:

$$\frac{\partial \rho_v}{\partial t} = \frac{f_{11}}{r^2}\frac{\partial}{\partial r}\left(\rho_v r^2\frac{\partial p}{\partial r}\right) \tag{2.29}$$

and the energy conservation equation takes the form:

$$\frac{\partial T}{\partial t} - f_{12}\rho_v \frac{\partial p}{\partial r}\frac{\partial T}{\partial r} - f_{13}\frac{\partial p}{\partial t} + f_{14}\left(\frac{\partial p}{\partial r}\right) = \frac{f_{15}}{r^2}\frac{\partial}{\partial r}\left(r^2\frac{\partial T}{\partial r}\right). \qquad (2.30)$$

The smallest terms f_{12}, f_{13} and f_{14} in equation 2.30 are neglected (see table 2.2). f_{15} is retained so that it can be used to analysis the thermal boundary layer at the flash front. With these simplifications equation 2.30 is reduced to:

$$\frac{\partial T}{\partial t} = \frac{f_{15}}{r^2}\frac{\partial}{\partial r}\left(r^2\frac{\partial T}{\partial r}\right). \qquad (2.31)$$

2.2.4   Summary and Table of Parameters

To summarise, the non-dimensional equations that describe the reduced model are:

$$\frac{\partial T}{\partial t} = \frac{f_9}{r^2}\frac{\partial}{\partial r}\left(r^2\frac{\partial T}{\partial r}\right), \qquad\qquad r < s(t) \qquad (2.32)$$

$$\rho_s v_v = -\dot{s} = \frac{1}{f_3}[\nabla T]_-^+, \qquad\qquad r = s(t) \qquad (2.33)$$

$$p = e^{H\left[\frac{T-T_n}{T}\right]}, \qquad\qquad r = s(t) \qquad (2.34)$$

$$v_v = -f_{10}\nabla p, \qquad\qquad r \geq s(t) \qquad (2.35)$$

$$\frac{\partial T}{\partial t} = \frac{f_{15}}{r^2}\frac{\partial}{\partial r}\left(r^2\frac{\partial T}{\partial r}\right), \qquad\qquad r > s(t) \qquad (2.36)$$

$$p = \rho_v T, \qquad\qquad r > s(t) \qquad (2.37)$$

$$\frac{\partial \rho_v}{\partial t} = \frac{f_{11}}{r^2}\frac{\partial}{\partial r}\left(\rho_v r^2\frac{\partial p}{\partial r}\right), \qquad\qquad r > s(t). \qquad (2.38)$$

The outer boundary of the ejecta at $r = 1$ is fixed at the non-dimensional initial temperature of the fluid, $T = T_0$, and at non-dimensional atmospheric pressure, $p = 1$. Symmetry applies such that there is no temperature flux at the centre of the inclusion, $\frac{\partial T}{\partial r} = 0$. The initial temperature inside the inclusion is non-dimensional giving $T = T_0$ and inside the magma to give $T = 1$ with an initial pressure of non-dimensional atmospheric pressure, $p = 1$. Lastly, the initial position of the steam generation boundary is at the non-dimensional distance $\frac{R_1}{R_2}$. The pressures in the slurry are assumed to be equal to those at the steam generation boundary. A further reduction of this model, assuming that the

temperature diffusion in the inclusion is relatively slow, and taking the temperatures in the inclusion to be equal to T_0, will recover the temperature equations seen in the model described in section 1.2 [20].

---

[8]   We will be taking 373K as the initial temperature, which is the boiling temperature of water. This value is taken instead of 300 for the ease of calculation as 373K is the boiling point of water at one atmosphere. Due to the large temperature difference between the magma and the inclusion (about 1000K) a difference of 73K in the initial temperature will not change the result significantly.

Physical Constants			
Constant	Name	Typical Value	Units
c_{pl}	specific heat of liquid water	4200	$J.kg^{-1}.K^{-1}$
c_m	specific heat of magma	840	$J.kg^{-1}.K^{-1}$
c_{pv}	specific heat of water vapour	2000	$J.kg^{-1}.K^{-1}$
h_{vl}	specific heat of vaporisation	2.3×10^6	$J.kg^{-1}$
k	permeability	10^{-14}	m^2
K_e	thermal conductivity	2	$W.m^{-1}.K^{-1}$
K_i	thermal conductivity	3	$W.m^{-1}.K^{-1}$
M	molar mass of water	18×10^{-3}	$kg.mol^{-1}$
p_a	atmospheric pressure	10^5	Pa
R_g	universal gas constant	8.314	$J.K^{-1}.mol^{-1}$
R_1	inclusion radius	0.01	m
R_2	magma radius	0.1	m
T_i	initial inclusion temperature [8]	373	K
T_m	initial magma temperature	1300	K
T_{crit}	critical temperature of water	647	K
T_R	reference temp, T_i		
α	thermal expansion coefficient of water	0.5	$kg.m^{-3}.K^{-1}$
β_e	isothermal compressibility of water	4.6×10^{-10}	$kg.m^{-3}.Pa^{-1}$
μ_v	dynamic viscosity	3×10^{-5}	Pa.s
ϕ	porosity	0.4	
ρ_m	density of basalt	2750	$kg.m^{-3}$
$\rho_e c_{pe}$	$(1-\phi)\rho_m c_m + \phi \rho_v c_{pv}$	1.4×10^6	$J.m^{-3}.K^{-1}$
$\rho_i c_{pi}$	$(1-\phi)\rho_m c_m + \phi \rho_l c_{pl}$	3×10^6	$J.m^{-3}.K^{-1}$
T_0	$\frac{T_i}{T_m}$	0.29	
ρ_{v0}	$\frac{p_a M}{R_g T_m}$	0.17	kgm^{-3}
v_{v0}	$\frac{R_2 \rho_{l0}}{t_0 \rho_{v0}}$	34.6	ms^{-1}

Table 2.1: This table contains of typical physical constants that are used in the dimensional and reduced models. These constants are taken from the steam tables [6], the previous model [20] and through conversations with Ian Schipper [40]
.

Typical Values		
Parameter	**Value**	**Typical Value**
f_1	$\dfrac{\rho_{v0}}{\rho_{l0}}$	1.7×10^{-4}
f_2	$\dfrac{v_{l0}t_0}{R_2}$	2×10^{-3}
f_3	$\dfrac{v_{v0}R_2\phi\rho_{v0}h_{vl}}{K_eT_m}$	212
f_4	$\dfrac{p_a}{\rho_{v0}h_{vl}}$	0.26
f_5	$\dfrac{v_{l0}}{v_{v0}}$	4×10^{-7}
f_6	$\dfrac{\beta_e p_a}{\rho_{l0}}$	4.6×10^{-8}
f_7	$\dfrac{\alpha T_m}{\rho_{l0}}$	0.6
f_8	$\dfrac{\phi\beta p_a}{\rho_i c_i}$	6×10^{-12}
f_9	$\dfrac{K_i t_0}{R_2^2\rho_i c_i}$	0.002
f_{10}	$\dfrac{kp_0}{\mu_v R_2\phi v_{v0}}$	7×10^{-5}
f_{11}	$\dfrac{t_0 kp_0}{\phi\mu_v R_2^2}$	0.14
f_{12}	$\dfrac{t_0\rho_{v0}c_{pv}kp_0}{\rho_e c_e\mu_v R_2^2}$	4.2×10^{-5}
f_{13}	$\dfrac{\phi p_0}{\rho_e c_e T_m}$	2.3×10^{-5}
f_{14}	$\dfrac{kt_0 p_0^2}{\rho_e c_e T_m R_2^2\mu_v}$	9.1×10^{-6}
f_{15}	$\dfrac{K_e t_0}{R_2^2\rho_e c_e}$	0.0025
t_0	$\dfrac{\phi\rho_{l0}h_{vl}R_1^2}{3K_e(T_m-T_i)}$	17
H	$\dfrac{Mh_{vl}}{R_g T_0}$	13

Table 2.2: This table contains typical dimensionless parameter values for the reduced model using the typical values of the physical constants in table 2.1

Chapter 3

Asymptotic Temperature Solutions

The non-dimensional model described in equations 2.32 to 2.38 in chapter 2.2.4 contains small parameter values for the thermal diffusivity in both the inclusion and magma diffusion equations. The thermal diffusivity is of order 10^{-3} for typical parameter values (table 2.1). This is much smaller than the pressure diffusivity, which is given by $\frac{f_{11}p}{T}$, which is of order 10^{-1}. The differences in the thermal and pressure diffusivity suggests that the temperature changes will propagate at a much slower rate than the pressure changes. This slow propagation implies the existence of thermal boundary layers in both the magma and inclusion sides of the steam generation boundary. This boundary layer is driven by the infinite temperature gradients at the flash front and consists of an area of rapidly varying temperature.

The temperature boundary layers in the magma and the inclusion are areas of rapid temperature variation. Outside of these boundary layers the temperature variation is on a significantly slower time scale. The temperature equation representing the region of slow temperature variation can be approximated by setting the temperature variation to zero.

In order to model the behaviour of the temperature in the boundary layer a coordinate rescaling is required. The rescaling is chosen so that all terms in the temperature diffusion equations have the same order. As temperature is continuous across the magma and inclusion regions the approximate temperature equation in the boundary layer must tend towards the temperature in the outer region. Using asymptotic methods from Bender and Orszag's book on

Asymptotic Methods and Perturbution ([7]) asymptotic solutions for the temperature equations in the magma and inclusion regions as well as an asymptotic equation for temperature gradients at the flash front can be determined.

3.1 Asymptotic temperature solution in the magma region

The diffusion equation for temperature in the magma region is:

$$\frac{\partial T}{\partial t} = \frac{f_{15}}{r^2} \frac{\partial}{\partial r} \left(r^2 \frac{\partial T}{\partial r} \right). \tag{3.1}$$

This contains a small parameter f_{15}. Therefore the first derivative with respect to time of temperature is the dominant term in the equation when the radius r is greater that $2 \times f_{15}$. If only the dominant terms in the thermal diffusion equation are considered the equation can be simplified to:

$$\frac{\partial T}{\partial t} = 0. \tag{3.2}$$

This equation is an approximation for the behaviour of the temperature in the outer region at times that are early enough that the magma has not been significantly cooled near the outer boundary (at the surface of the ejecta), nor been affected by the movement of the flashing front. Using the initial condition for the magma temperature, $T = 1$, the asymptotic solution in the outer magma region can be taken as constant, set to 1, at these early times.

The thermal boundary layer is driven by the infinite temperature gradients at the boundary of the magma and inclusion. In the magma region close to the infinite temperature gradients (at the flashing front) the rate of change of temperature with time is no longer dominant. The region can be described using the radial coordinate σ given by $r = \varepsilon + \delta_m \sigma$, where $\delta_m = \sqrt{f_{15}}$. This radial coordinate σ describes the region close to the steam generation boundary $s(t = 0) = \varepsilon$ and is the area of rapid temperature variation in the magma at times early enough that the movement of the steam generation boundary can be reasonably be ignored.

The temperature equation for the areas of rapid variation in the magma becomes:

$$\frac{\partial T}{\partial t} = \frac{1}{(\varepsilon + \delta_m \sigma)^2} \frac{\partial}{\partial \sigma}\left((\varepsilon + \delta_m \sigma)^2 \frac{\partial T}{\partial \sigma} \right).$$ (3.3)

Then, by considering the limit as δ_m tends to zero, thus taking the solution for the rapidly varying region to only be valid when $\varepsilon >> \delta_m \sigma$, the thermal equation describing the rapidly varying temperature behaviour becomes:

$$\frac{\partial T}{\partial t} = \frac{\partial}{\partial \sigma}\left(\frac{\partial T}{\partial \sigma} \right)$$ (3.4)

with the boundary conditions $T(0,t) = T_f$ and T tending to 1, the temperature in the outer region, as $\sigma \to \infty$. T_f represents the temperature at the flash front. This temperature is coupled, through the Clausius Clapeyron equation, to the pressure at the flash front. As the pressure at the flash front fluctuates so will the temperature at the flash front. The temperature at the flash front can be estimated using the Clausius Clapeyron equation. If the non-dimensional pressures at the boundary range between 1 and 100 the non-dimensional flash temperatures would vary between 0.29 and 0.45 , see figure 3.1. Therefore 0.4 can be taken as an approximation for the temperature at the flash front. The variation in the temperature at the flash front can be ignored because it is small compared to the temperature variation between the approximate flash front temperature and the outer solution, $T = 1$.
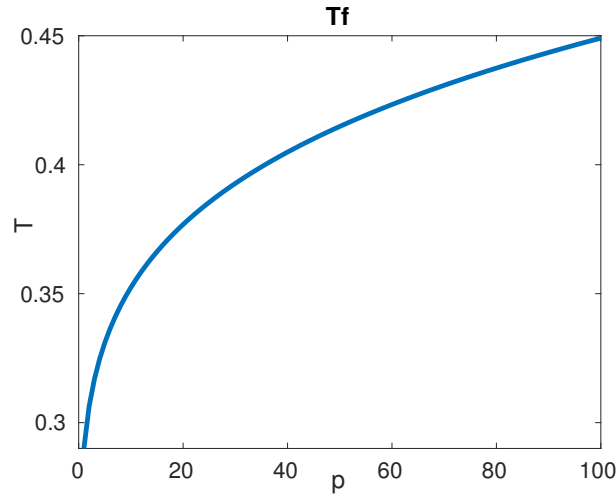

Figure 3.1: Temperature values at the flash front compared with possible pressure values

Using the similarity solution $\eta = \frac{t}{\sigma^2}$, detailed in Appendix D.1, the behaviour in the rapidly varying region in the magma can be modelled as:

$$T = (T_f - 1)\left(1 - \text{erf}(\frac{\sigma}{2\sqrt{t}})\right) + 1. \tag{3.5}$$

This inner solution provides the following temperature gradient in the inner magma region:

$$\frac{\partial T}{\partial r} = \frac{1}{\delta_m}\frac{\partial T}{\partial \sigma} = \frac{(1 - T_f)e^{(\frac{\sigma^2}{4t})}}{\delta_m \sqrt{\pi t}}. \tag{3.6}$$

The magma temperature profile, equation 3.5, derived in this chapter will be compared with the numerical simulations for the temperature in the magma in chapter 7.

3.2   Asymptotic Temperature Solution in the Inclusion

The asymptotic temperature equation in the inclusion is calculated using the same method as the asymptotic temperature equation in the magma. The diffusion equation for temperature in the inclusion:

$$\frac{\partial T}{\partial t} = \frac{f_9}{r^2}\frac{\partial}{\partial r}\left(r^2\frac{\partial T}{\partial r}\right) \tag{3.7}$$

is used and this contains a small parameter f_9. In the outer region the limit of f_9 tending to zero is taken to produce:

$$\frac{\partial T}{\partial t} = 0. \tag{3.8}$$

By considering the initial non-dimensional temperature in the inclusion, $T = T_0$, the asymptotic solution in the slowly varying region can be taken as constant, T_0.

The rapidly varying region in the slurry is driven by the large temperature gradients at the boundary of the inclusion. Therefore the outer region (the region with slow temperature variation) is at the centre of the inclusion.

The rapidly varying region is a thermal boundary layer described by the radial coordinate ψ given by $r = \varepsilon - \delta_i \psi$, where $\delta_i = \sqrt{f_9}$. This region, like the thermal boundary layer in the magma, is a region near to the steam generation boundary $s(t = 0) = \varepsilon$ at times early enough that the movement of the steam generation boundary can be reasonably be ignored. The temperature equation for the areas of rapid variation in the inclusion becomes:

$$\frac{\partial T}{\partial t} = \frac{1}{(\varepsilon - \delta_i \psi)^2} \frac{\partial}{\partial \psi} \left((\varepsilon - \delta_i \psi)^2 \frac{\partial T}{\partial \psi} \right). \tag{3.9}$$

Then by considering the limit as δ_i tends to zero and taking the solution for the rapidly varying region to only be valid when $\varepsilon >> \delta_i \psi$ the thermal equation describing the rapidly varying temperature behaviour becomes:

$$\frac{\partial T}{\partial t} = \frac{\partial}{\partial \psi} \left(\frac{\partial T}{\partial \psi} \right) \tag{3.10}$$

with the boundary conditions $T(0,t) = T_f$ and T tending to the T_0, the temperature solution in the region of slow variation, as $\psi \to \infty$.

Using the similarity solution $\eta = \frac{t}{\psi^2}$, detailed in Appendix D.2, the behaviour in the rapidly varying region in the inclusion can be modelled as:

$$T = (T_f - T_0)(1 - \text{erf}(\frac{\psi}{2\sqrt{t}})) + T_0. \tag{3.11}$$

The temperature gradient in the thermal boundary layer in the inclusion can be estimated, using equation 3.11, to be:

$$\frac{\partial T}{\partial r} = \frac{1}{\delta_i} \frac{\partial T}{\partial \psi} = \frac{(T_f - T_0)e^{(\frac{\psi^2}{4t})}}{\delta_i \sqrt{\pi t}}. \tag{3.12}$$

As with the magma temperature, the inclusion temperature profile (equation 3.11) will be compared with the numerical simulations for the temperature in the inclusion in chapter 7.

3.3   Estimates for the gradients at the flashing front

Estimates for the temperature gradients at the flash front in the magma and in the inclusion can be found using equations 3.6 and 3.12 and setting σ and ψ to zero. This gives a temperature gradient of:

$$\left.\frac{\partial T}{\partial r}\right|_{\sigma=0} = \frac{(1-T_f)}{\delta_m\sqrt{\pi t}}. \tag{3.13}$$

in the magma at the flash front and:

$$\left.\frac{\partial T}{\partial r}\right|_{\psi=0} = \frac{(T_f-T_0)}{\delta_i\sqrt{\pi t}}. \tag{3.14}$$

in the inclusion.

Noting that $\delta_i \approx \delta_m$ the contributions for the temperature gradients in the magma and the inclusion can be compared. If the temperature at the flashing front is taken to be 0.4 the magma temperature gradient at the steam generation boundary is approximately:

$$\left.\frac{\partial T}{\partial r}\right|_{\sigma=0} \approx \frac{0.6}{\delta_m\sqrt{\pi t}} \tag{3.15}$$

with a temperature gradient in the inclusion and also at the steam generation boundary being approximately:

$$\left.\frac{\partial T}{\partial r}\right|_{\psi=0} \approx \frac{0.04}{\delta_i\sqrt{\pi t}}. \tag{3.16}$$

This shows that the contribution to the temperature gradient from the inclusion is about a fifteenth of the contribution from the magma. This is due to the similar thermal diffusivities and the larger temperature difference between the flash front and the magma when compared to the flash front and the inclusion. The temperature difference between the flash front and the magma is approximately 0.6, using the non-dimensional temperatures, and the difference between the flash front and the inclusions is approximately 0.2.

In the upper bound on the maximum pressure calculations in chapter 6 these approximations are used to justify ignoring the contribution of the heat flow into the inclusion in the boundary equation at the flash front.

Chapter 4

Numerical Method

In this chapter the focus is on numerically solving the reduced model (equations 2.32 to 2.38). This model consists of a set of coupled partial differential equations with a moving front, the steam generation boundary, travelling towards the centre of the inclusion over time.

4.1 Freezing the moving boundary

To aid in numerically solving the model, a coordinate transformation is used to freeze the steam generation boundary between the magma and the inclusion. To freeze the moving boundary, two Landau transformations [[26],[13]] are required, one in the inclusion and the other in the magma.

In the inclusion a new radial coordinate ζ is defined, where:

$$\zeta = \frac{\varepsilon r}{s(t)},$$

(4.1)

freezing the moving boundary at ε, which is the initial position at time zero of the steam generation boundary. The new coordinate system ζ, ranges from 0 to ε and the chain rule gives:

$$\frac{\partial f(r,t)}{\partial t} = \frac{\partial f(\zeta,t)}{\partial t} + \left(\frac{-\zeta}{s}\dot{s}\right)\frac{\partial f(\zeta,t)}{\partial \zeta}$$

while the radial derivatives become:

$$\frac{\partial f(r,t)}{\partial r} = \left(\frac{\varepsilon}{s}\right)\frac{\partial f(\zeta,t)}{\partial \zeta}$$

$$\frac{\partial^2 f(r,t)}{\partial r^2} = \left(\frac{\varepsilon^2}{s^2}\right)\frac{\partial^2 f(\zeta,t)}{\partial \zeta^2}.$$

In the magma section of the model we define a new radial coordinate, ξ, where:

$$\xi = \left(\frac{1-\varepsilon}{1-s(t)}\right)r + \left(\frac{\varepsilon - s(t)}{1-s(t)}\right) \tag{4.2}$$

and ranges from ε to 1. The chain rule gives the new temporal derivative:

$$\frac{\partial f(r,t)}{\partial t} = \frac{\partial f(\xi,t)}{\partial t} + \frac{\partial f(\xi,t)}{\partial \xi}\left(\frac{\xi - 1}{1-s}\right)\dot{s}$$

and the radial derivatives as:

$$\frac{\partial f(r,t)}{\partial r} = \left(\frac{1-\varepsilon}{1-s}\right)\frac{\partial f(\xi,t)}{\partial \xi}$$

$$\frac{\partial^2 f(r,t)}{\partial r^2} = \left(\frac{1-\varepsilon}{1-s}\right)^2\frac{\partial^2 f(\xi,t)}{\partial \xi^2}.$$

The model in the new coordinate system becomes:

$$\frac{\partial T}{\partial t} = \left[\frac{2f_9\varepsilon^2}{s^2\zeta} + \frac{\zeta\dot{s}}{s}\right]\frac{\partial T}{\partial \zeta} + \frac{f_9\varepsilon^2}{s^2}\frac{\partial^2 T}{\partial \zeta^2}, \qquad \zeta = [0,\varepsilon] \tag{4.3}$$

$$\rho_v v_v = -\dot{s} = \frac{1}{f_3}\left[\left(\frac{1-\varepsilon}{1-s}\right)\frac{\partial T}{\partial \xi} - \frac{\varepsilon}{s}\frac{\partial T}{\partial \zeta}\right], \qquad \zeta = \xi = \varepsilon \tag{4.4}$$

$$v_v = -f_{10}\left(\frac{1-\varepsilon}{1-s}\right)\frac{\partial p}{\partial \xi}, \qquad \xi \geq \varepsilon \tag{4.5}$$

$$p = e^{H\left[\frac{T-T_n}{T}\right]}, \qquad \zeta = \xi = \varepsilon \tag{4.6}$$

$$\frac{\partial T}{\partial t} = \left[\frac{2f_{15}}{g(\xi,t)}\left(\frac{1-\varepsilon}{1-s}\right) - \frac{\xi - 1}{1-s}\dot{s}\right]\frac{\partial T}{\partial \xi}$$

$$+ f_{15}\left(\frac{1-\varepsilon}{1-s}\right)^2\frac{\partial^2 T}{\partial \xi^2}, \qquad \xi = [\varepsilon,1] \tag{4.7}$$

$$p = \rho_v T, \qquad \xi = [\varepsilon,1] \tag{4.8}$$

$$\frac{\partial \rho_v}{\partial t} = \left[f_{11}\left(\frac{1-\varepsilon}{1-s}\right)^2\frac{\partial p}{\partial \xi} - \frac{\xi - 1}{1-s}\dot{s}\right]\frac{\partial \rho_v}{\partial \xi} + \frac{2\rho_v f_{11}}{g(\xi,t)}\left(\frac{1-\varepsilon}{1-s}\right)\frac{\partial p}{\partial \xi}$$

$$+ f_{11}\rho_v \left(\frac{1-\varepsilon}{1-s}\right)^2 \frac{\partial^2 p}{\partial \xi^2} \qquad\qquad \xi = [\varepsilon, 1] \qquad\qquad (4.9)$$

$$g(\xi, t) = \frac{(1-s)\xi + (s-\varepsilon)}{1-\varepsilon} \qquad\qquad\qquad (4.10)$$

with the boundary conditions:

$$p = 1, \quad \xi = 1; \quad \frac{\partial T}{\partial r} = 0, \quad \zeta = 0; \quad T = T_0, \quad \xi = 1;$$

and the initial conditions:

$$T = T_0, \quad \zeta = [0, \varepsilon]; \quad T = 1, \quad \xi = [\varepsilon, 1]; \quad p = 1.$$

4.2 Numerical Method

The equations 4.3 to 4.9 are solved using the method of lines. The method of lines, appendix F, is used to discretise the spatial terms leaving a system of temporal ordinary differential equations. Matlab can solve differential equations in the form of $y' = f(t, y)$ where y and f are vector-valued functions. The Matlab program must be provided with a function that will return a vector value for f, given t and y. From this, Matlab can find a solution numerically within specified tolerances. In this model the y variables are made up of the spatially discretised temperatures in both the inclusion and magma, the spatially discretised magma density, and the location of the steam generation boundary.

The temperature at the steam generation boundary is calculated using the nonlinear solver fsolve. This is only possible if there is a unique solution in the ranges of temperatures being considered. Appendix E shows that there is a unique solution in this range and the use of fsolve is valid. At the steam generation boundary there is a step function and the model initially produces infinite temperature gradients. These infinite temperature gradients result in the temperature at the steam generation boundary varying substantially when the step size adjacent to the flash front in the spatial discretisation is refined. This in turn results in maximum pressure being dependent on this step size. At the steam generation boundary the smallest length scale for the discretisation is the pore size of the magma. Below this size the porous medium approximation breaks

down. As pore size is the maximum refinement that can be used in this model
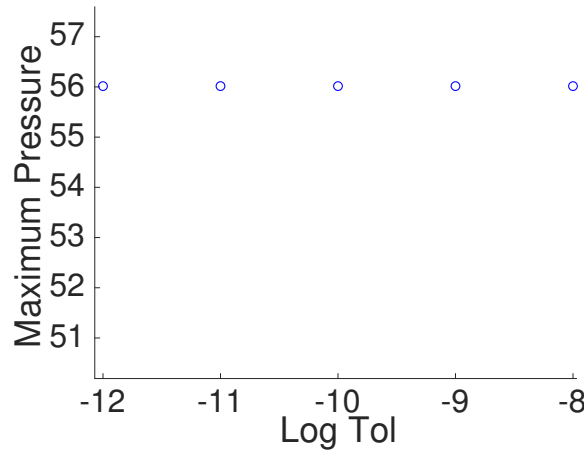this step size will be used at the steam generation boundary.

Figure 4.1: The circles represent the maximum pressure produced when using
different tolerances in the numerical solutions. These numerical solutions use the
typical parameters from table 2.1 and a minimum step size of 10 microns. The
mesh used is the log-based mesh with 200 mesh points in the inclusion and 800 in
the magma.

The method of lines requires spatial discretisation of magma and inclusion
regions. The area of interest, the flashing front, in the Surtseyan ejecta model has
rapidly varying temperatures and pressure that require a fine mesh to prevent
averaging effects lowering the maximum pressure. A uniform mesh is not as
efficient as the flashing front requires a fine mesh with a dimensional spacing of
10 microns, which is the approximate pore size of the magma, but the outer
region of the magma does not require this precision. Furthermore, the use of a
uniform mesh with 10 micron spacing is computationally expensive and takes a
very long time to conduct on a single computer.

To improve the computational workload involved in numerically solving this
model two different meshes were originally considered; the first was a log-based
mesh focusing on the flashing front. In this mesh the first step in both the
inclusion and magma regions are set to be equal; the second mesh used is a
coordinate transform, this transformation is chosen such that the required spacing
at the steam generation boundary is achieved while also producing a mesh that is

a uniform mesh of this new coordinate system. The coordinate transform we used is an arc tan transformation, as detailed in Appendix F.3.

The log-based mesh is an example of an uneven mesh. Uneven meshes require the use of Taylor expansion methods to determine the second and first order derivatives. The Taylor expansion methods in this case are first-order accurate. This is most apparent in the magma density equation which, when using this method, relies on a first-order derivative to determine the second-order derivative in pressure. However, with the co-ordinate transformed mesh, a uniform mesh is used after transforming co-ordinates, and this allows for a more accurate treatment of the second-order derivatives, making the result more accurate than the uneven log-based mesh. Therefore, as the co-ordinate transformed mesh has more refined approximations, it is used to find the numerical solutions for this model.

The arc tan transformed mesh is set up for each variable. In the magma there are two variables, temperature and pressure, this region also has two boundary points and contains n mesh points. In the inclusion the number of mesh points is set to m. The numbers m and n are the number of spatial variables to be solved for each variable. The total number of coupled differential equations to be solved simultaneously is $2n + m + 1$. This includes n equations for each of the temperature and pressure variables in the magma, m for the temperature variable in the model plus an equation at the location of the steam generation boundary.

The initial conditions in the model have a step change in temperature and pressure at the steam generation boundary. When solving this numerically the maximum pressure is therefore expected to be sensitive to the mesh size adjacent to the infinite gradients at the steam generation boundary. The initial temperature gradients at the flash front are unbounded as the mesh size decreases, due to the numerical value of the gradient being calculated by taking the change in temperature divided by the mesh size. The pressure at the flash front depends on the amount of water vapour produced and this is driven by the temperature gradients. In the computer code this step function is replaced by a ramp function. The steepness of this ramp function is dependent on the smallest mesh size. In the limit as the mesh size reduces to zero the temperature gradient tends towards the theoretical step function. The dimensional value of a typical pore size is

approximately 10 microns, which will be taken as the smallest possible computational mesh step. If the computational step size was smaller that the typical pore size this would break the porous media assumptions.

In Matlab there are multiple solvers for ordinary differential equations. A Runge Kutta solver of order 4-5 (ODE45) is the most commonly-used solver. However, in this case due to the complex nature of the multiple timescales in the system it was extremely computationally expensive. The method of lines is known to typically produce stiff systems of equations. The boundary layers in temperature and pressure have variables that fluctuate much more rapidly than the outer region, thus producing a stiff system. Therefore using a variable step solver, ODE15s, allows for the step size to be reduced in the boundary layer to increase accuracy, but to remain broad in the outer region, thus decreasing the computation time compared to the 4-5 Runge Kutta solver.

Matlab requires specified tolerances to calculate y. The tighter the tolerance used the more computationally expensive the solver is. Figure 4.1 shows that in this model when using tolerances below 10^{-8} there is no change in the maximum pressure value. This maximum pressure is the value of interest for this research and decreasing the tolerance below 10^{-8} does not affect the value. This allows for all further results to use 10^{-8} as the specified tolerance ensuring a quicker running time than using the tighter tolerances.

A sample of code can be found in appendix G.

Chapter 5

Numerical Results

The numerical solutions using the parameter values listed in table 2.1 indicate that the pressure rises rapidly to a global maximum at the steam generation boundary when compared to the time it takes for the inclusion to boil off the water vapour. The vapour producing the pressures at the steam generation boundary diffuses into the magma region, reducing the high initial pressures at the flash front. The typical solutions, figure 5.1, also indicate that the amount of vapour produced decreases over time as the liquid in the inclusion boils away. This can be understood physically: as the steam generation boundary moves towards the centre of the inclusion, the surface area over which the heating occurs decreases. The parameter values listed in table 2.1 indicate a maximum dimensionless pressure of approximately 50 which is 5Mpa when reverted to dimensional units. This suggests that for the typical parameters being used, an ejectum would explode as the pressure exceeds the 2Mpa tensile strength limit. This is consistent with the data from Ian Schipper, shown in figure 5.6, which indicates that the surviving ejecta have a higher permeability than the value 10^{-14} m^2 that has been taken as typical.

The typical numerical solutions also reveal that the dominant temperature gradient is on the magma side of the steam generation boundary. The numerical model has been set up so that the mesh steps on either side of the steam generation boundary are of equivalent size. The dominant temperature gradient is therefore determined by the change in temperature on either side of that front. The temperature at the flash front is closer to that of the initial temperature of the inclusion than the temperature of the magma, and so the magma region has a
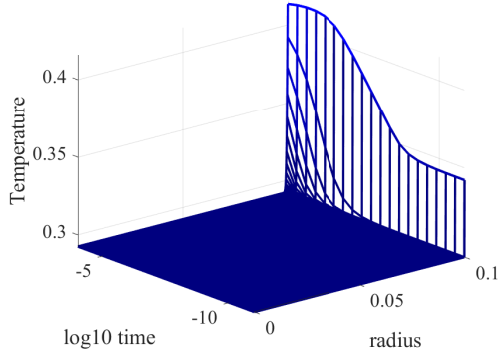
a) Temperature in the inclusion
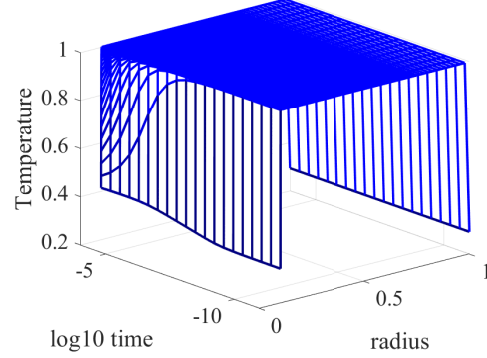
b) Temperature in the magma region
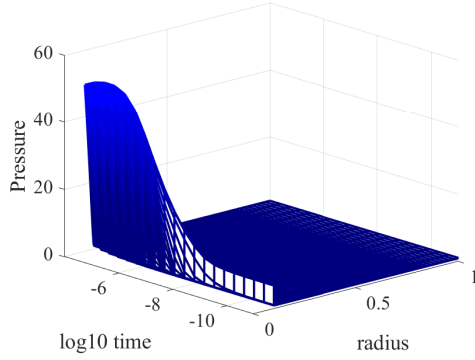
c) Pressure in the magma region
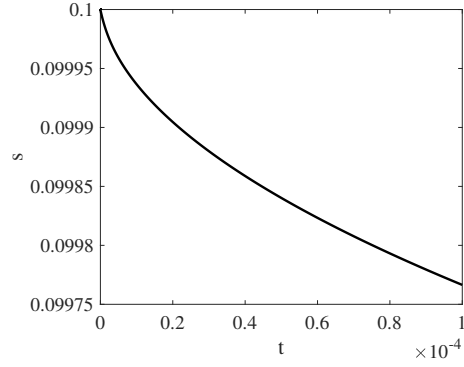
d) Position of the flashing front
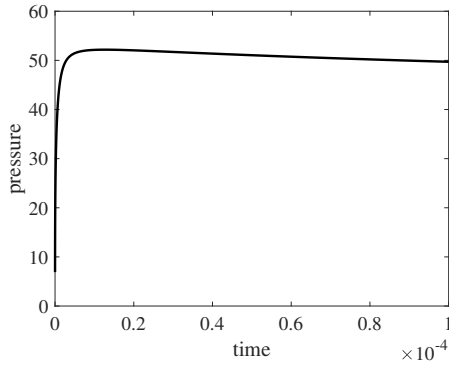
e) Pressure at the flashing front
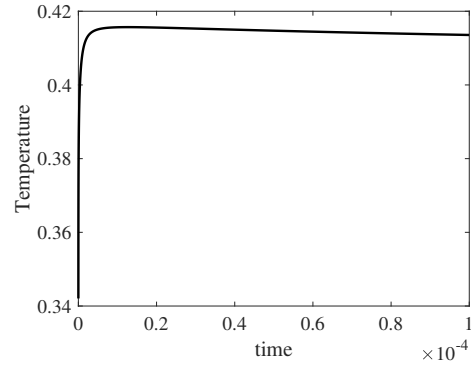
f) Temperature at the flashing front

Figure 5.1: Numerical results using the typical parameters in table 2.1. With the smallest mesh size fixed at 10 microns and 400 mesh points in the magma and 200 in the inclusion. Figures (a), (b), (c) are 3 dimensional plots of non-dimensional temperature or dimensional pressure versus log base 10 of non-dimensional time versus non-dimensional radius r. Figures (d), (e) and (f) are all plotted against non-dimensional time.

larger temperature difference and therefore a larger temperature gradient. This is consistent with the approximate temperature gradients at the flash front calculated in chapter 3.3.

Figure 5.2: This graph shows the velocity of the steam generation boundary for numerical solutions using typical parameters (table 2.1). With the smallest mesh size fixed at 10 microns and 800 mesh points in the magma and 200 in the inclusion. This graph details the initial change in non-dimensional velocity versus non-dimensional time and shows an initial spike that dec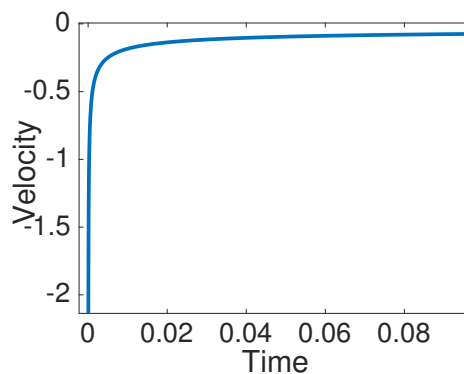elerates and plateaus with time. Velocity in the negative direction shows the flash front moving towards the centre of the inclusion.

In figure 5.1 the temperature in both the magma and the inclusion remain predominately at their initial values. In both regions there is a rapidly varying boundary layer. In the magma region there is also evidence of a thermal boundary layer at the outer surface of the ejectum. This boundary layer has been ignored in the analysis in chapter 3. The numerical results, figure 5.1, also show that the vapour at the flash front diffuses into the magma at a relatively fast rate compared to the temperature.

If the temperature at the flash front drops it is possible for liquid in the inclusion to exceed its boiling temperature, as the boiling temperature is by definition the temperature at the steam generation boundary. This results in a widening of the two-phase region at the steam generation boundary, which is assumed in the numerics to have no size. The widening of the boundary is represented by a change in direction of the temperature gradient in the inclusion at the flash front. This would, through the boundary equation 2.33, reduce the speed of the steam generation boundary. The numerical simulations for typical parameters, in table

2.1, show that the temperature in the inclusion never exceeds that of the boundary. The velocity of the steam generation boundary for typical numerical solutions shows an initial rapid change in the velocity of the steam generation boundary towards the centre of the inclusion. This is driven by a large difference in temperature at the steam generation boundary at initial times. The velocity of the steam generation boundary plateaus after this initial change. This plateau observed in the numerical results for typical parameters is likely due to the dominant temperature gradient at the flash front in the magma decreasing.

5.1   Numerical Convergence

The maximum pressure at the flashing front is expected to be sensitive to the mesh size, due to the unbounded initial temperature and pressure gradients created as the mesh size decreases. Figure 5.3 shows that maximum pressure converges as the smallest mesh size decreases. However, the time taken for maximum pressure to be reached does not converge as the smallest mesh size is decreased, see figure 5.3. This suggests that the time it takes for maximum pressure to be recorded depends on the initial temperature gradient, which is set using in the smallest computational mesh size in the numerical simulations in figure 5.3.

The results in figure 5.3 suggest that for the typical parameter values with 800 and 200 mesh points in the magma and the inclusion respectively, a smallest mesh size in dimensionless r of 10^{-5} (one micron when converted back to dimensional units) will give a dimensional maximum pressure which is accurate within one atmosphere. The ramp size of 10 microns that has been used in many of the calculations for the typical parameters will produce a maximum pressure that, when converted back to dimensional units, is accurate to within four atmospheres.

Figure 5.3 shows that the time taken to produce the maximum pressure at the steam generation boundary depends on the smallest computational mesh size (which in this numerical simulation is the same as the ramp size). Both the temperature and pressure gradients also depend on this computational mesh size.
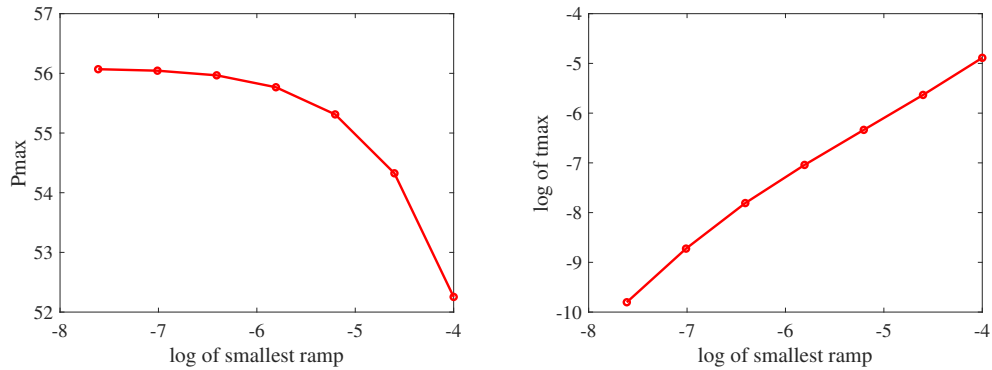
The relationship between the time taken to produce maximum pressure and the temperature and pressure gradients can be explored by fixing an initial temperature gradient. This is achieved by varying the distance that the ramp is operating over, but having this independent of the small computation mesh size. The results of this show that the time it takes to reach maximum pressure is approximately constant for mesh sizes 10^{-5} and smaller and is therefore independent of it. However, the maximum pressure does vary with the ramp size and this shows that the initial temperature gradient controls the time it takes for maximum pressure to be reached. The pressures developed in figure 5.4 are smaller that those in 5.3. This is due to the initial temperature gradients observed in 5.3 being larger.

Figure 5.4 also shows that the time taken for this maximum pressure to be reached is approximately constant with smallest mesh size below 10^{-5}. This suggests that the time it takes to reach maximum pressure is independent on mesh size. It, like the maximum pressure, depends on the ramp distance from the temperature gradient. The maximum pressure in figure 5.4 also shows convergence, seen in figure 5.3, as the ramping distance of the temperature initial gradient is decreased. The time it takes for the maximum pressure to be reached does not show signs of convergence in figure 5.4, which is consistent with figure 5.3.

5.2   Sensitivity Analysis

The model and the typical solutions depend on the parameters detailed in table 2.1. However, these physical properties may vary. Some of these properties are the permeability, porosity and the ratio of the inclusion to the ejectum radii.

Figure 5.5 shows a sensitivity analysis that demonstrates how the maximum pressure at the flash front is affected by permeability, porosity and the ratio of the inclusion to the ejectum radii. As expected, as the permeability decreases the predicted maximum pressure increases sharply; increased porosity means an increase in the number of pores for the vapour to escape, lowering the maximum pressure; a smaller ratio of inclusion to magma results in less water being available in the inclusion, less vapour, and therefore producing a lower maximum

a) Maximum pressure at the flash front
verses smallest step size

b) Time it takes for maximum pressure
to be reached versus smallest step size

Figure 5.3: Graphs (a) shows the convergence of the maximum non-dimensional pressure as the smallest ramp (smallest mesh size) decreases. The smallest mesh size is initially set at 10^{-4} and it is then divided by the values 4, 16, 64, 256, 1024 and 4096. Graph (b) plots the time is takes for this maximum pressure to be reached versus log base 10 of the smallest ramp size. (a) and (b) both use the typical parameters in table 2.1 and have 800 mesh points in the magma and 400 in the inclusion.
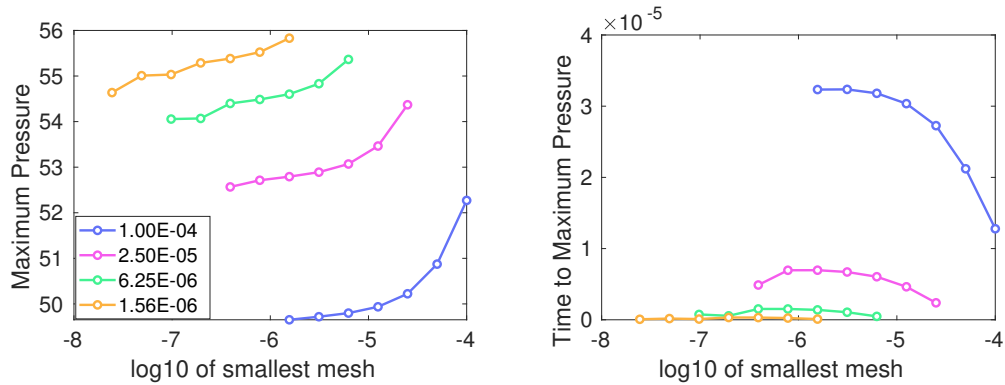
a) Maximum pressure at the flash front
versus smallest step size and ramp size

b) Time it takes for maximum pressure
to be reached versus smallest step size
and ramp size

Figure 5.4: Graph (a) details the maximum pressure at the flash front and graph (b) the time at which this maximum pressure is achieved plotted against the smallest computational step size at various initial ramping distances from the flash to magma or inclusion regions (shown in the legend as non-dimensional r values). Please note that the larger the ramping distance the shallower the initial gradient (therefore lowering the pressure). (a) and (b) both use the typical parameters in table 2.1 and have 1600 mesh points in the magma.

pressure than for larger inclusion to ejecta ratios. However, inclusion to ejecta ratios of above approximately 0.4 cause an error in the computation of the model's boundary temperature. This is due to a lack of magma available to heat the inclusion and results in excess water in the inclusion, which is not evaporated. The computation of this model assumes all the water in the inclusion is evaporated.
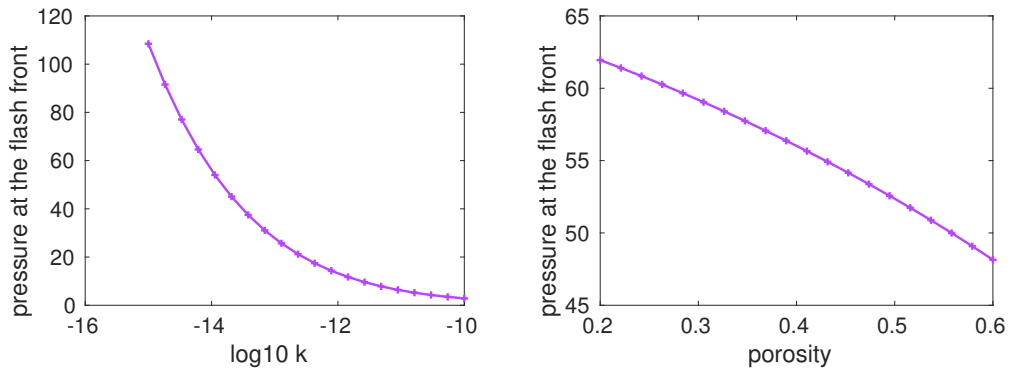
a) Maximum non-dimensional pressure at the flash front versus permeability ranging from 10^{-10}m^2 and 10^{-15}m^2

b) Maximum non-dimensional pressure at the flash front versus porosity ranging from 0.2 and 0.6
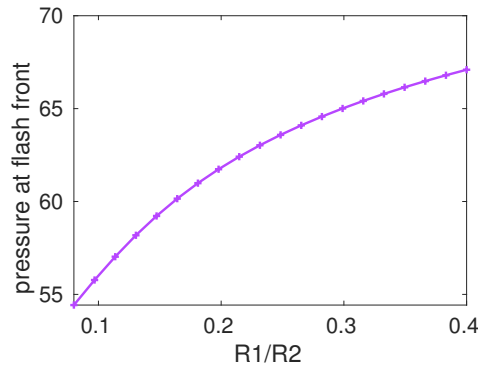
c) Maximum non-dimensional pressure at the flash front versus ratio of inclusion size with ejecta radii, ranging from 0.008 and 0.4

Figure 5.5: The numerical simulations in figures (a), (b) and (c) all use the typical parameters, from table 2.1, for all parameters apart from permeability in (a), porosity in (b) and radius of the inclusion and the ejecta in (c). The smallest mesh size is fixed at 10 microns and 400 mesh points in the magma and 200 in the inclusion are used.

In the sensitivity analysis it has been assumed that the permeability, porosity and
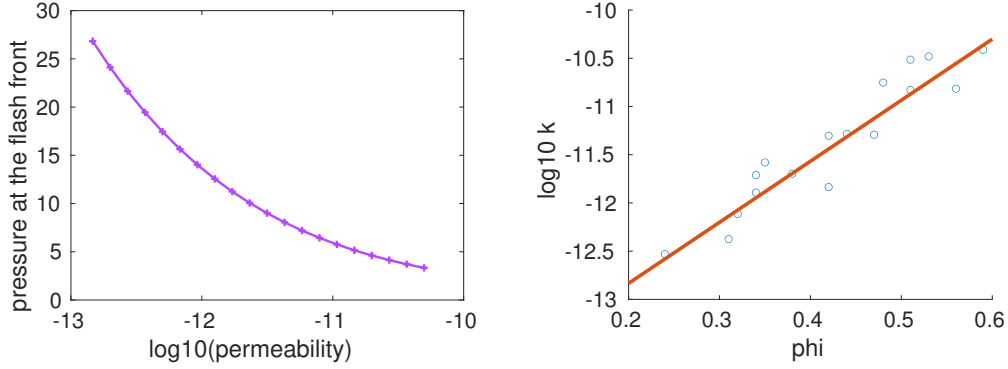
a) Maximum non-dimensional pressure at the flash front versus log base 10 of the permeability (units m^2)

b) Log of permeability (units m^2) versus porosity of measured samples of Surtseyan ejecta

Figure 5.6: In figure (a) the maximum pressure is simulated using $\log_{10} k = 6.33\phi - 14.1$ and porosity ranging from 0.2 to 0.6. The smallest mesh size used in figure (a) was 10 microns 400 mesh points in the magma and 200 in the inclusion are used. Figure (b) plots the log of permeability versus porosity of measured samples of Surtseyan ejecta (data provided by Ian Schipper [40]). This includes the best linear fit of $\log_{10} k = 6.33\phi - 14.1$.

the ratios between the inclusion and the ejecta radii can change independently of each other. However porosity and permeability values are usually highly correlated. Figure 5.6 showing the permeability and porosity measurements of a of Surtseyan ejecta indicate a relationship between porosity and permeability that can be approximated by:

$$\log_{10} k = 6.33\phi - 14.1. \tag{5.1}$$

This approximation is used in figure 5.6 to relate the porosity and permeability in the numerical simulations. The maximum pressures produced are comparable with those of the varying permeability but fixed porosity, simulations in figure 5.5. The numerical simulations in figure 5.6, along with the non-dimensional tensile strength of magma, $p_c = 20$, suggest that ejecta with permeability less than approximately $10^{-12.5}$ will rupture.

5.3 Alternate initial profile

As previously discussed, the step function at the steam generation boundary produces unbounded pressure and temperature gradients as the mesh size is reduced. This was handled by using a ramp function. The maximum pressure at the flash front is shown to converge.
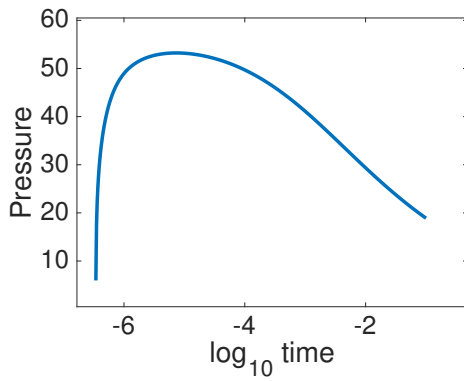
Figure 5.7: Non-dimension pressure at the flash front vs log of the non-dimensional time. This numerical simulation uses the typical parameters, table 2.1 and 400 mesh points in the magma with 200 in the inclusion.
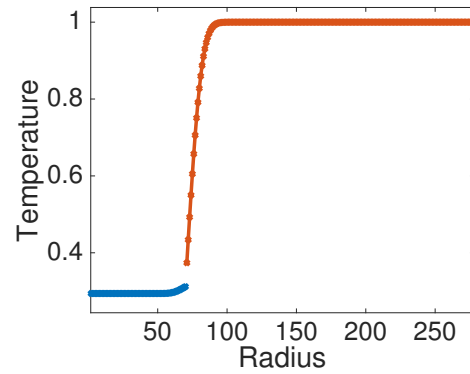
Figure 5.8: The initial non-dimensional temperature profile calculated using the work for chapter 3. The radius is given by the coordinate transformation in chapter 3.

As an alternative to the ramp function, the temperature profiles for chapter 3 can be used to give the initial temperatures in the numerical simulations. This method uses the temperature profiles evaluated at some time, t_e, determined by the time it takes for the 10 micron section of magma to change from its initial temperature. This temperature profile at t_e, figure 5.8, allows for the mesh to be refined and, like the ramp solution, leads to convergence in maximum pressure. The use of the adjusted initial conditions produces results consistent with the ramp function initial conditions. Figure 5.7 shows the results using the alternative initial conditions.

Chapter 6

Approximation for the upper-bound on the maximum pressure

An approximation for the early time behaviour of pressure at the flashing front provides an upper bound for the maximum pressure developed. In this approximation the non-dimensional equation derived from the conservation of vapour mass is considered, equation 2.29. This equation describes the change in vapour density in the magma region. This is driven predominantly by the temperature differences between the magma and the flash front. The temperature gradient between the steam generation boundary and the inclusion also makes a contribution to the change in vapour density. This contribution is ignored in this analysis because, as shown in chapter 3.3, the temperature gradient in the magma is dominant. Likewise, the movement of the steam generation boundary is also neglected. Ignoring the movement of the steam generation boundary is supported by the numerics, for typical parameters, which shows the flash front moving less than 5 microns before maximum pressure is reached. This is less than typical pore size in the magma.

The boundary condition, equation 2.33, relates the temperature and pressure at the flash front. The early time pressure behaviour can be approximated as:

$$p\frac{\partial p}{\partial r} \approx -\frac{T}{f_{10}f_3}\left.\frac{\partial T}{\partial r}\right|_{r=\varepsilon} \tag{6.1}$$

where $\left.\frac{\partial T}{\partial r}\right|_{r=\varepsilon}$ is the temperature gradient between the magma region and the

57

steam generation boundary. This equation neglects the heat flow into the inclusion.

$\frac{\partial T}{\partial r}\Big|_{r=\varepsilon}$ can be approximated using the asymptotic temperature equations from chapter 3, and by adapting the magma temperature gradient equation, equation 3.14. Equation 3.14 is undefined at initial time, but it provides a ramped temperature if the time origin is shifted by replacing time with $t + t_e$, where $t_e \geq 0$ is an initial time (time elapsed after the theoretical step change in temperature between the magma and the inclusion). This is one way to acknowledge that the processes of emplacement of the inclusion is unlikely to give a step change in the temperature at the surface of the inclusion. This initial time can be considered an emplacement time and this may be more faithful to the physical situation. Including the time of emplacement time, t_e, in equation 3.14 gives:

$$\frac{\partial T}{\partial r}\Big|_{r=\varepsilon} = \frac{(1 - T_f)}{\delta_m \sqrt{\pi(t + t_e)}}. \tag{6.2}$$

Thus, the equation describes the temperature flux from the initial temperature profile. This initial temperature profile is ramped, but the initial step function can be recovered as the emplacement time reduces to zero. The use of an emplacement time helps to avoid issues arising from the step function at the steam generation boundary and the singular point it creates. The emplacement time relates, through the similarity solution, to the distance, r_{ramp}, over which the temperature at the flash front ramps to that of the magma. This distance $r_{ramp} \approx 4\delta_m\sqrt{t_e}$ is derived in appendix D.3.1. Equations 6.2 and 6.1 can be combined to create the following approximation for early time pressure behaviour at the flash front:

$$p\frac{\partial p}{\partial r} \approx -\frac{T(1 - T)}{f_{10}f_3\delta_m\sqrt{\pi(t + t_e)}}. \tag{6.3}$$

The pressure in this system is driven by the conservation of vapour mass equation 2.29. This equation can be rewritten using the ideal gas law as follows:

$$\frac{\partial}{\partial t}\left(\frac{p}{T}\right) = \frac{f_{11}}{r^2}\frac{\partial}{\partial r}\left(r^2\frac{p}{T}\frac{\partial p}{\partial r}\right), \quad r > s(t). \tag{6.4}$$

Then by considering only r values close to the flash front, equation 6.4 can be

reduced further to:

$$\frac{\partial}{\partial t}\left(\frac{p}{T}\right) = f_{11}\frac{\partial}{\partial r}\left(\frac{p}{T}\frac{\partial p}{\partial r}\right), \quad r > s(t), \quad r - \varepsilon << 1. \tag{6.5}$$

By taking advantage of the relatively slow rate of change of temperature, equation 6.5 can be simplified by treating the temperature as constant. This simplification allows the density equation to be simplified to the follow pressure equation:

$$\frac{\partial p}{\partial t} = f_{11}\frac{\partial}{\partial r}\left(p\frac{\partial p}{\partial r}\right), \quad r > s(t), \quad r - \varepsilon << 1. \tag{6.6}$$

The pressure change at early times in this system is driven by the influx of vapour at the steam generation boundary. This vapour propagates into the magma from the steam generation boundary. Using the diffusivity in the vapour pressure equation as a rough estimate $\Delta r \approx \sqrt{f_{11}t}$ for distance the vapour propagates from the flash front can be taken. This estimate, along with the spatially constant initial pressures, suggest the following approximation at the steam generation boundary can be made to equation 6.6:

$$\frac{\partial p}{\partial t} \approx -\frac{f_{11}}{\Delta r}\left(p\frac{\partial p}{\partial r}\right), \quad r > s(t), \quad r - \varepsilon << 1 \tag{6.7}$$

$$\approx -\sqrt{\frac{f_{11}}{t}}\left(p\frac{\partial p}{\partial r}\right), \quad r > s(t), \quad r - \varepsilon << 1. \tag{6.8}$$

By substituting equation 6.3 into equation 6.7 the following equation:

$$\frac{\partial p}{\partial t} \approx \sqrt{\frac{f_{11}}{t}}\left(\frac{T(1-T)}{f_{10}f_3\delta_m\sqrt{\pi(t+t_e)}}\right), \quad r = s(t), \tag{6.9}$$

describes the approximate early time pressure behaviour at the steam generation boundary. Following the derivation in appendix D.3.2, the early time pressure behaviour can be approximated as:

$$p_e \approx A\left(\ln\left(2t + t_e + 2\sqrt{t^2 + tt_e}\right) - \ln t_e\right) + 1, \tag{6.10}$$

where $A = \frac{T(1-T)\sqrt{f_{11}}}{f_3 f_{10}\delta_m\sqrt{\pi}}$ with the temperature at the flash front T taken to be approximately 0.4.

The times required to reach maximum pressure at the steam generation boundary, t_m, is estimated by calculating when p_e intersects with the pressure null surface at the flash front. The pressure null surface occurs when $\frac{\partial p}{\partial t} = 0$. This can be approximated using the density null surface if the temperatures remain of order one. The density null surface provides a quasi-steady state equation:

$$\frac{\partial}{\partial r} \left(\frac{p}{Tr^2} \frac{\partial p}{\partial r} \right) = 0, \quad r > s(t), \tag{6.11}$$

with a solution for the upper bound on the quasi-steady state pressure, p_u,

$$p_u^2 = -\frac{2C_1}{r} + 2C_1 + 1, \tag{6.12}$$

where

$$C_1 = -\frac{\varepsilon^2(1-T)}{f_3 f_{10} \delta_m \sqrt{\pi(t+t_e)}}$$

derived in appendix D.3.3. At $r = \varepsilon$ this upper bound for the maximum pressure is:

$$p_u = \sqrt{\frac{B_1}{\sqrt{t+t_e}} + 1} \tag{6.13}$$

$$B_1 = \frac{2\varepsilon(1-\varepsilon)(1-T)}{f_3 f_{10} \delta_m \sqrt{\pi}}, \tag{6.14}$$

which can be closely approximated at early times by:

$$p_u = \frac{B_2}{(t+t_e)^{\frac{1}{4}}} \tag{6.15}$$

$$B_2 = \sqrt{\frac{2\varepsilon(1-\varepsilon)(1-T)}{f_3 f_{10} \delta_m \sqrt{\pi}}}. \tag{6.16}$$

A lower bound for t_m can be provided by dropping the initial pressure term from equation 6.10 and equating the resulting equation with equation 6.15. The lower bound on t_m is given by:

$$\frac{B_2}{(t_m+t_e)^{\frac{1}{4}}} \approx A \left(\ln \left(2t_m + t_e + 2\sqrt{t_m^2 + tt_e} \right) - \ln t_e \right). \tag{6.17}$$

The right-hand side of equation 6.17 is approximated in appendix D.3.4 to be:

$$2A\sqrt{\frac{t_m}{t_e}} \approx A\left(\ln\left(2t_m + t_e + 2\sqrt{t_m^2 + tt_e}\right) - \ln t_e\right) \qquad (6.18)$$

using the Taylor series expansions of the square root and log as well as considering that t is approaching zero at time t_m.

Using the t_m approaching zero approximation the left-hand side of equation 6.17 can be reduced to:

$$\frac{B_2}{(t_e)^{\frac{1}{4}}} \qquad (6.19)$$

which can be equated to the approximation in equation 6.18 to form:

$$\frac{B_2}{(t_e)^{\frac{1}{4}}} = 2A\sqrt{\frac{t_m}{t_e}}. \qquad (6.20)$$

Equation 6.20 can then be solved to find the lower bound on t_m:

$$t_m = \left(\frac{B_2}{2A}\right)^2\sqrt{t_e}. \qquad (6.21)$$

This lower bound for the time taken to reach maximum pressure depends on the emplacement time, which is given by the ramping distance. This dependence is also seen in the numerical simulations in chapter 5.

The maximum pressure (p_{max}) at the flash front has an upper bound estimate of

$$p_{max} = \frac{B_2}{(t_e)^{\frac{1}{4}}}. \qquad (6.22)$$

Using the equivalent length scale, $r_{ramp} \approx 4\delta_m\sqrt{t_e}$, to replace t_e, the dimensionless maximum pressure at the flash front has an upper bound at:

$$p_{max}^2 = \frac{4B_2{}^2\delta_m}{r_{ramp}} \qquad (6.23)$$

$$= \frac{8\varepsilon(1-\varepsilon)(1-T_f)}{f_3 f_{10}\sqrt{\pi}r_{ramp}} \qquad (6.24)$$

$$= \frac{8K_e T_m \mu_v \varepsilon(1-\varepsilon)(1-T_f)}{\rho_{v0} h_{vl} k p_0\sqrt{\pi}r_{ramp}} \qquad (6.25)$$

where $T_f \approx 0.4$. Equation 6.25 can be used as a criterion for rupture by considering that the pressure can not exceed the typical tensile strength of magma, 2MPa or $p_{max} = 20$ in dimensionless units. Comparisons between the upper bound of the maximum pressure and the simulations are discussed in chapter 7. Together with comparisons with the criterion for rupture from the previous model.

Chapter 7

Comparisons

7.1 Asymptotic temperature profiles vs Numerical simulations

The asymptotic temperature profile from chapter 3 can be used to help verify the numerical results. Figure 7.1 shows the numerical simulations and theoretical temperature profiles plotted against the similarity variable, η, derived in chapter 3. The numerical simulations in the inclusion and the asymptotic temperature profile show close agreement for the parameters used. The numerical simulations and theoretical temperature profile in the magma between $0.5 < \eta < 2$ show the numerical simulations produce temperatures that are consistently less than the theoretical temperature profile. However for the majority of the graph there is a close agreement between the theoretical and numerical results.

The magma temperature result from figure 7.1 shows that the numerical temperatures produced are lower than the theoretical temperature profile. The asymptotic temperature profile was calculated by fixing the steam generation boundary, but the numerical simulations include the movement of the steam generation boundary in the calculation. In figure 7.2 the advection terms have been removed from the differential equations and the resulting numerical simulations show a much closer agreement between the numerics and the asymptotic profile in the magma region. These advection terms in the equation originate from the Landau transformations, which freeze the boundary in the numerics. Removing them means that the movement of the boundary is

neglected.

7.2   Upper-bound on maximum pressure vs numerical results

The upper-bound for the maximum pressure developed at the flash front is given by the non-dimensional equation:

$$p_{max}^2 = \frac{8K_e T_m \mu_v \varepsilon (1-\varepsilon)(1-T_f)}{\rho_{v0} h_{vl} k p_0 \sqrt{\pi} r_{ramp}}. \tag{7.1}$$

Figure 7.3 shows that the upper-bound on the maximum pressure is not a tight upper-bound. However the shape of the upper-bound of the maximum pressure at the flash front is similar to that of the simulated numerical results with permeability set by the porosity and the porosity ranging from 0.2 to 0.6. This similarity is clearer if the maximum pressure is presented on a log scale, as in figure 7.3.

This similarity allows for a closer theoretical estimate to the maximum pressures to be considered. This is achieved by taking the average of the ratio between the upper-bound and the simulated maximum pressure, and using this value to obtain a fit of the upper-bound on the maximum pressure to the simulations, thus producing a closer theoretical estimate of the maximum pressure (P_{est}):

$$P_{est} = 0.43 \sqrt{\frac{8K_e T_m \mu_v \varepsilon (1-\varepsilon)(1-T_f)}{\rho_{v0} h_{vl} k p_0 \sqrt{\pi} r_{ramp}}}. \tag{7.2}$$

Figure 7.2 compares the theoretical estimate of the maximum pressure, produced from fitting to the simulated results, to those simulated results and it shows it to be a reasonable fit with in the ranges of Ian Schipper's data. This allows for the theoretical estimate of the maximum pressure to be used to give a prediction from the maximum pressures developed at the flash front in an ejecta, instead of running the simulation.
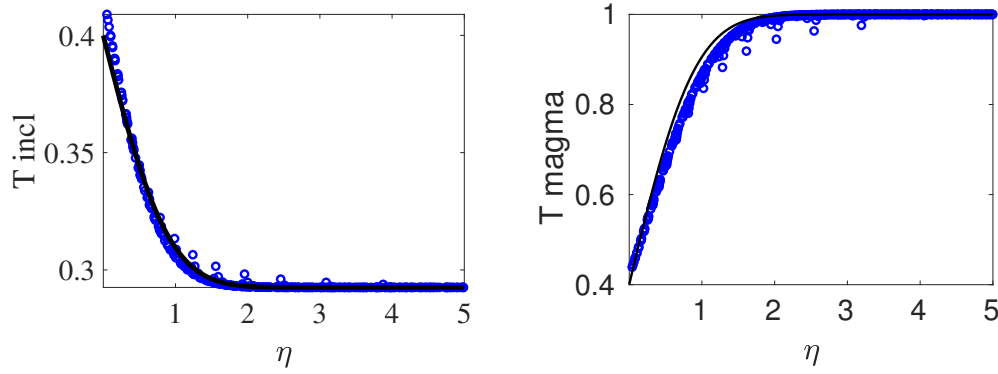
Figure 7.1: The graphs above contain the simulated numerical non-dimensional temperatures (blue circles) in the inclusion and the magma plotted against the similarity variable from chapter 3. These numerical simulations use the typical parameters for table 2.1 and a smallest mesh size of 10 microns. They also show the theoretical similarity solutions (black line) using 0.4 as the initial temperature of the flash front.
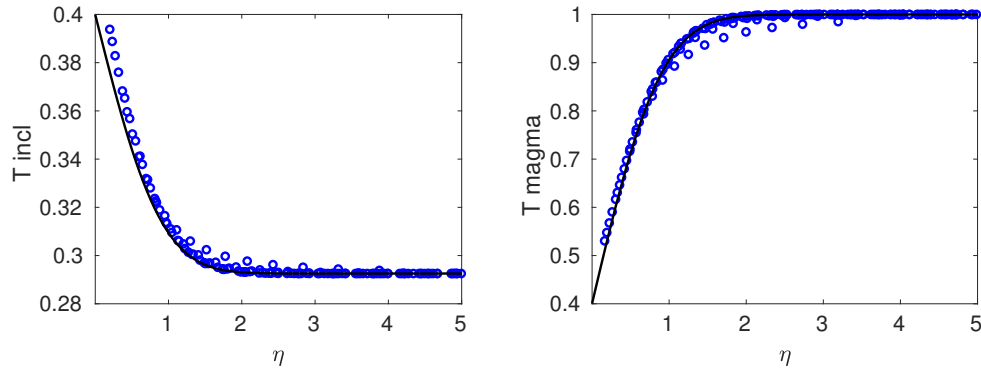
Figure 7.2: The graphs above contain the simulated numerical non-dimensional temperatures when advection is not considered (blue circles) in the inclusion and the magma plotted against the similarity variable from chapter 3. These numerical simulations use the typical parameters for table 2.1 and a smallest mesh size of 10 microns. They also show the theoretical similarity solutions (black line) using 0.4 as the initial temperature of the flash front.
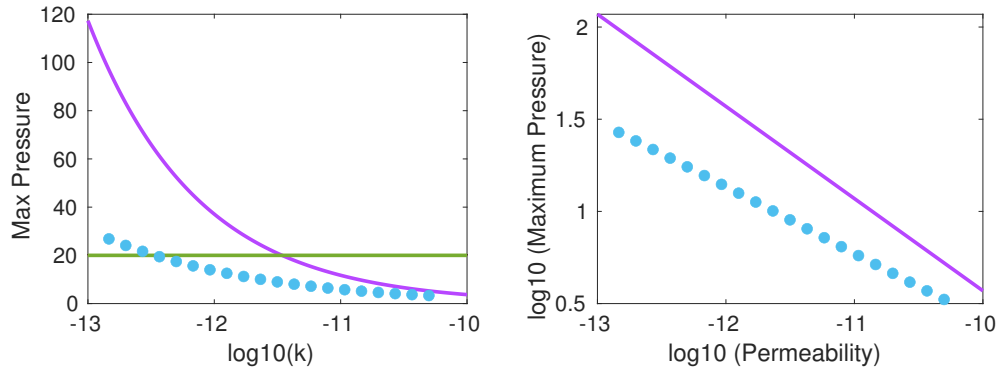
Figure 7.3: These graphs show the the simulated maximum pressure (blue circles) and the calculated upper-bound pressures at the flash front (purple line) plotted against log10 of permeability (the graph on the right has log10 pressures), for various permeabilities and porosities matching Ian Schipper's data. The green line indicates the tensile strength of magma at dimensional 2 MPa.
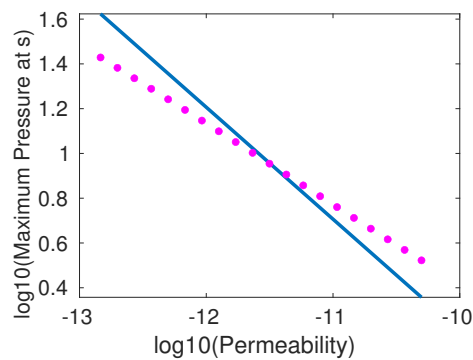
Figure 7.4: This graph shows the simulated maximum pressure (purple circles) and theoretical estimate of the maximum pressure (blue line), from equation 7.2, plotted against log10 of permeability, for various permeabilities matching Ian Schipper's data.

7.3 The previous model vs the upper-bound on maximum pressure and the numerical simulations

The upper-bound on the maximum pressure, equation 6.25, is compared to the previous criterion for rupture published by McGuinness et al. [[31]]:

$$p_{max}^2 = \frac{7RT_m K(T_m - T_0)(1-\varepsilon)\mu_v}{Mh_{vl}k},$$ (7.3)

by converting both criteria back to dimensional units and expanding some of the typical dimensionless parameters in equation 6.25 giving:

$$p_{max}^2 = \frac{8K_e T_m \mu_v (1-\varepsilon)(1-T_f)}{h_{vl}k} \frac{R_g T_m}{M} \frac{\varepsilon}{\sqrt{\pi} r_{ramp}}.$$ (7.4)

Equation 7.3 can be rewritten using the parameters from table 2.1 to give:

$$p_{max}^2 = \frac{7K_e T_m \mu_v (1-\varepsilon)(1-\frac{T_i}{T_m})}{h_{vl}k} \frac{R_g T_m}{M}$$ (7.5)

$$= \frac{7K_e T_m \mu_v (1-\varepsilon)(1-T_0)}{h_{vl}k} \frac{R_g T_m}{M}.$$ (7.6)

It is clear that equation 7.6 and equation 7.4 are close to identical. The most pronounced difference is the factor $\frac{\varepsilon}{\sqrt{\pi} r_{ramp}}$ in the upper-bound on the maximum pressure at the steam generation boundary in chapter 6. This new factor originated from the temperature gradient in the magma calculated in chapter 3, using an analysis of the thermal boundary layer in the magma. In the previous model the temperature gradient $\left(\frac{T_m - T_0}{0.28\varepsilon}\right)$ was estimated using a length scale approximated by the amount of magma required to vaporise the water in the inclusion as well as a temperature equation that is decoupled from the pressure. The upper-bound for the maximum pressure at the flash front will produce a higher temperature gradient when compared to the previous model due to the much smaller and more accurate length scale used in the calculation.

Other minor differences between equations 7.6 and 7.4 include the coefficient 8 in place of 7 and the use of the approximate flash front temperature, T_f, instead of the non-dimensional inclusion temperature, T_0, used in the previous model.

The dimensional pressures seen in the previous model, [[20],[31]] , differ from the numerical simulations seen in chapter 5, with the previous pressures reaching approximately 2 MPa and the numerical simulations reaching about 5 MPa at the same typical parameter values. This is partly due to the temperature gradient at the boundary calculation using a much smaller length scale (ramping distance), thus driving up the temperatures and pressures in the new model. This increase in pressure affects the lower limit of the permeability for intact ejecta (at tensile strength 2 MPa using the typical values from Table 2.1). In the previous model this was of order 10^{-14}m; and in the numerical simulations this criterion for rupture was much higher at $10^{-12.5}$m.

A noticeable difference between the numerical solutions in this thesis and the previous model is the temperature diffusion in the inclusion. The previous model had an assumption that the inclusion would heat in a uniform manner. The numerical solutions from the new model show clearly that this is not the case and there is a small layer of varying temperature at early times, while the remainder of the inclusion stays at a constant initial temperature.

It was also assumed in the previous model that the velocity of the steam generation boundary is constant. In the new model the velocity of steam generation boundary initially shows a rapid change in magnitude due to the infinite gradients at the boundary, then the magnitude decreases and plateaus. The assumption of a constant velocity outside the early time behaviour is consistent with the numerical simulations. The maximum pressure at the flash front occurs at early times and has been shown in the numerical convergence work to depend on the infinite temperature gradients at the boundary. Therefore the early time behaviour of the velocity and the infinite temperature gradients at the boundary are important when producing a value for the maximum pressure in the simulations.

7.3.1 Discussion

The numerical solutions, using the typical parameter values in table 2.1, suggest a maximum pressure of approximately 5 MPa using the minimum step size of 10 microns and 400 mesh points in the magma and 200 in the inclusion. This pressure exceeds the tensile strength of the magma and under these conditions ejecta should explode when permeabilities are about 10^{-14}m^2. This is consistent with the data provided by Ian Schipper.

The numerical convergence study in chapter 5 shows the maximum pressure depends on the initial temperature gradient at the flash front, but will converge to 5.6 Mpa for the typical parameter values in table 2.1. However, the time it takes for this maximum pressure to be reached also depends on the initial temperature gradient at the flash front and this does not show signs of convergence. This suggests that the maximum pressure is produced instantaneously in the limit of the smallest ramp distance tending to zero.

Unpublished data (provided by Ian Schipper [40]) details the porosities and permeabilities of various ejecta. This data has been collected through the examination of the vesicle textures in lapilli using an X-ray microtomograph. The permeability is calculated by simulating a single-phase gas using Lattice Boltzmann simulations. Lattice Boltzmann simulations are constructed using a fluid density across a lattice; this fluid density is simulated using streaming and collision processes. The unpublished data contains no information concerning the sizes of the ejecta and the inclusion. However, the sensitivity analysis, figure 5.5, shows that a change in permeability will have a far greater affect on the maximum pressure than a varying ratio of inclusion size to ejecta radii. This data of intact ejecta, shown in figure 5.6, shows surviving ejecta with permeability of $10^{-12.5}$ or greater and this is consistent with the numerical simulations. This data also suggests a range of typical permeabilities between $10^{-12.5}$m^2 and $10^{-10.5}$m^2, which affects the values of the physical constants in table 2.2.

The typical dimensionless parameter values calculated at a permeability of $10^{-12.5}$m^2 still show that the f_{15} parameters values dominate f_{12}, f_{13} and f_{14}, which justifies the simplification of the energy conservation equation by neglecting these terms. However, at a permeability of $10^{-10.5}$m^2 this is not the case and the dominant parameters are f_{12} and f_{14}. Therefore, the parameter size

Typical values with permeabilities ranging $10^{-12.5} \text{m}^2$ and $10^{-10.5} \text{m}^2$			
Parameter	**Value**	**Typical Value at $k = 10^{-12.5}$**	**Typical Value at $k = 10^{-10.5}$**
f_{10}	$\frac{kp_0}{\mu_v R_2 \phi v_{v0}}$	2×10^{-3}	0.22
f_{11}	$\frac{t_0 k p_0}{\phi \mu_v R_2^2}$	4.4	443
f_{12}	$\frac{t_0 \rho_{v0} c_{pv} k p_0}{\rho_e c_e \mu_v R_2^2}$	1.3×10^{-3}	0.13
f_{13}	$\frac{\phi p_0}{\rho_e c_e T_m}$	2.3×10^{-5}	2.3×10^{-5}
f_{14}	$\frac{k t_0 p_0^2}{\rho_e c_e T_m R_2^2 \mu_v}$	2.9×10^{-4}	0.028
f_{15}	$\frac{K_e t_0}{R_2^2 \rho_e c_e}$	0.0025	0.0025

Table 7.1: This table contains typical dimensionless parameter values for the reduced model using the typical values of the physical constants in table 2.1 and the range of permeabilites set by the data [40]

.

cannot be used as a justification at this permeability for these terms in the energy conservation equation to be ignored. However, at a larger permeability the magma would allow the vapour in the magma to escape at a much faster rate. This is apparent in parameter f_{11}, which can be used to estimate the nonlinear diffusivity of pressure. It follows that the change of pressure with radius (*r*) would be much lower because the pressure is not building up at the flash front as the vapour can flow more readily through the magma. Therefore the temperature diffusion term in the energy conservation equation would be expected to be dominant.

The results show that upstream differencing has little affect on the solutions as diffusion terms dominate the advection terms. However, at early times in the inclusion, if the differencing is reversed then this causes a temperature drop below the initial inclusion temperature. This is caused by the diffusion error introduced by the reversed upstream differencing. As the diffusion terms dominate this suggests a more efficient central difference scheme could be used instead of the upstream differencing scheme in further modelling. This method was not originally used as it was not previously clear if the advection terms would dominate (due to the vapour flow or the moving boundary at the flash front). If the advection terms dominate it would be necessary to consider the directions of the flow in finite differencing methods.

In previous modelling and in this thesis the fragmentation pressure has been considered to be 2 MPa, the tensile strength of the magma. It is also assumed that the fragmentation pressure did not depend on the porosity of the magma. However, studies by Spieler et. al [45] have empirically shown that the fragmentation threshold of pyroclastic rocks increases as the porosity decreases. If the critical pressure is taken to be 6 MPa, which is consistent with the fragmentation pressure for porosity between 0.2 and 0.3 seen in Spieler et. al [45], the calculated permeability lower limit from the numerical simulations would be approximately 10^{-14}. The upper-bound for the maximum pressure at the flash front is not a tight upper-bound. However the theoretical estimate of the maximum pressures found by fitting it to the simulated data gives a reasonably close prediction of the values for the maximum pressure that may be produced at the flash front. Using this estimate the relationship between the tensile strength and the lower bound on the permeability can be estimated, see figure 7.5.
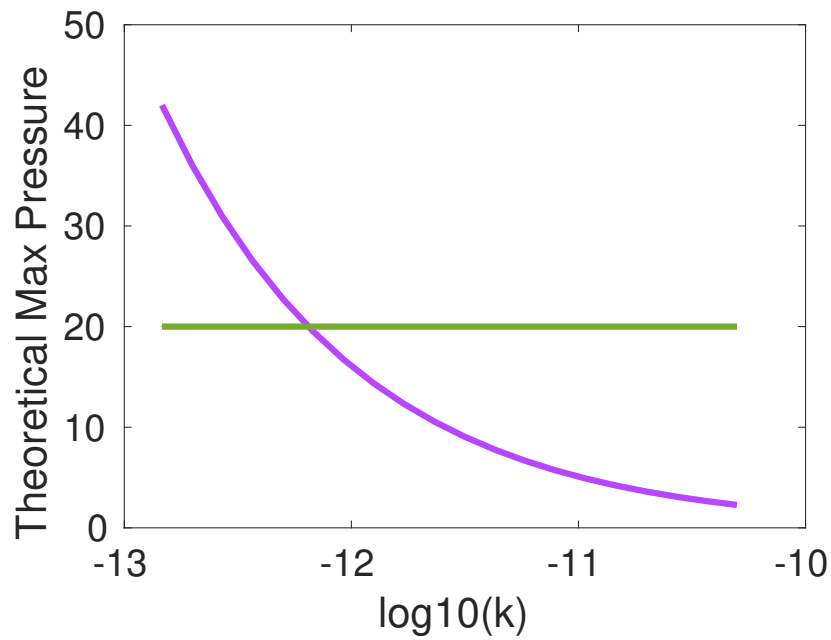
Figure 7.5: This graph plots the theoretical estimate of the maximum pressure (purple line), from equation 7.2, plotted against log10 of permeability, for various permeabilities and porosities matching Ian Schipper's data [40]. The green line represents the tensile strength of magma and all permeabilities that produce pressures above this line are expected to lead to rupture.

Chapter 8

Conclusion

The purpose of this thesis has been to construct a mathematical model to expand and improve upon an existing model of Surtseyan ejecta behaviour [[20],[31]]. The existing model firstly assumed that the pressure and the temperature were not coupled and that the inclusion heated in a uniform manner. The aim of this research was to use a systematic reduction of the resulting coupled nonlinear partial differential equations that arise from mass, momentum and energy conservation to more closely represent the physical nature of Surtseyan ejecta. Further aims were to retain a criterion for rupture of the ejectum and to help validate the model with the aid of analytical solutions.

The numerical solutions can be split into two separate categories, depending on the mesh used in the spatial discretisation. The first mesh is a log-based mesh centred around the steam generation boundary. This mesh is non-uniform and leads to the use of the Taylor expansion methods to calculate derivatives, which are only first-order accurate. The second mesh is a uniform mesh achieved by using an arctan co-ordinate transformation. This mesh does not require the Taylor expansion methods for the second-order derivatives in the density equation and is, as a result, second-order accurate. This arctan co-ordinate transformation allowed for the smallest mesh size and the number of mesh points to be easily varied compared to the log mesh. Due to the uniform nature of the arctan mesh it was more straightforward to construct the derivatives using finite differencing methods.

The numerical simulations for the maximum pressure at the flash front show

convergence, but the time it takes to reach this maximum pressure does not. This is due to the initial infinite temperature gradient at the flash front. In the numerics a ramp function was used to set the initial gradient and both the maximum pressure at the flash front and the time it takes for it to be reached depend on this ramping distance. This can also be seen in the asymptotic temperature profiles at initial times. As the asymptotic temperature gradients at the flash front are proportional to $\frac{1}{\sqrt{t}}$ this is not defined at initial times. Therefore an emplacement time needs to be considered and like the numerical solutions this time can be related to a length through the similarity solution. It would be interesting to consider in further modelling the process of how the inclusion is entrained in the magma because this will affect the maximum pressures reached.

The results also show that if the limit is taken as t_e tends to zero, this corresponds to the limit as the ramping initial temperature profile approaches the step change in temperature, the theoretical maximum temperature obtained is unbounded. This indicates that the model is mathematically ill-posed for step function initial temperatures. This is another reason why further study into how the inclusions are entrained in the magma would be helpful.

The numerical simulations show a boundary layer of rapid heating or cooling on either side of the steam generating boundary. At the chosen typical parameter values in table 2.1 the maximum dimensional pressure was calculated to be 5 MPa. A pressure of 5 MPa exceeds the tensile strength of the magma (2 MPa). At this pressure it is expected that the ejecta would rupture. This is consistent with the data provided by Ian Schipper, figure 5.6, which shows no surviving ejecta with permeabilities less than $10^{-12.5}$ m^2. The numerical simulations also suggest a lower bound on the permeability of $10^{-12.5}$ m^2, which is consistent.

An upper-bound for the maximum pressure at the flash front was produced by considering the early time behaviour of pressure at the flashing front. This was achieved by reducing the density equation 2.38 using a modified initial temperature gradient in the magma, equation 6.2, and the flux condition at the boundary, equation 2.33. In this approximation the heat flux from the inclusion is neglected and it is assumed that 'early time' is defined by the time before the steam generation boundary can significantly affect the pressures. The early time

pressure behaviour at the boundary:

$$p_e \approx A \left(\ln \left(2t + t_e + 2\sqrt{t^2 + tt_e} \right) - \ln t_e \right) + 1, \tag{8.1}$$

is equated with the pressure null surface to provide an estimate for the lower bound on the time it takes to reach maximum pressure:

$$t_m = \left(\frac{B_2}{2A} \right)^2 \sqrt{t_e}. \tag{8.2}$$

The quasi-steady state equation derived from the pressure null surface is used to find an upper bound of the maximum pressure at the flash front:

$$p_{max}^2 = \frac{8K_e T_m \mu_v (1 - \varepsilon)(1 - T_f)}{h_{vl} k} \frac{R_g T_m}{M} \frac{\varepsilon}{\sqrt{\pi} r_{ramp}},$$

although this is not a tight upper limit, but was fitted to the numerical solutions. The resulting equation for maximum pressure is more consistent with the simulations and the data. This theoretical estimate of the maximum pressure could be used for ejecta with porosity between 0.2 and 0.6 to predict whether or not we expect the maximum pressure to exceed the critical pressure determined buy the tensile strength.

Improvements to this numerical model can be made by considering some of the underlying assumptions. In all current models describing the behaviour of Surtseyan ejecta it is assumed that a single spherical inclusion is entrained in a spherical magma bomb. This is not physically accurate as ejecta often contain more than one inclusion distributed around the ejecta. There is also evidence that some of the larger Surtseyan ejecta contain previously erupted ejecta inside as inclusions. In further modelling of ejecta behaviour consideration needs to be given to the effect that multiple random distributed inclusions, of varying sizes, would have on the maximum pressure. This is a challenging problem as this model relies on the spherical symmetry to reduce it to one dimensional problem.

It is also assumed that the inclusion is not compressible. There is evidence in Schipper's 2016 paper [39] that the inclusion does undergo compression and crystallisation due to the pressure build-up and this process of relieving pressure was not included in the mathematical model. Evidence of compression is also

seen in the void space surrounding the inclusions in ejecta. The compression and crystallisation process can greatly affect the maximum pressure, especially if it is over a small-time frame. The numerical simulations show high pressures acting over a small area, approximately 10 microns, for a short period of time before the pressure drops below breaking pressure. Therefore a small deformation in the inclusion (or the magma) could relieve the strain long enough for the ejectum to survive pressures higher than breaking pressure (2Mpa) . The numerical simulations could therefore be significantly affected by compression and crystallisation processes. An improvement needed in this model is to include these effects to more accurately match what is happening physically in Surtseyan ejecta.

Another area in the model that could use further work is the initial entrainment of the inclusion into the magma. How the inclusions are entrained in the magma inside the volcano is not well understood. The leading theory mentioned in the literature review, section 1.2, assumes this entrainment is caused by magma turbulence and mixing. A model for the magma and water slurry mix in the volcanic vent could provide answers as to how this mixing occurs and also improve the initial boundary considerations in the current model and provide a initial temperature gradient that is not infinite at the steam generation boundary.

In the future it would be helpful to more rigorously test the numerical simulations and the theoretical estimate of the maximum pressure against a larger data set of porosities, permeabilites and ratios of inclusion and ejecta radius from intact Surtseyan ejecta.

To conclude, this thesis has developed a more rigorous mathematical model for the behaviour of Surtseyan ejecta. This model has been solved numerically, producing maximum pressures that are consistent with data from intact Surtseyan ejecta. Also, fitting the upper bound of the maximum pressure to the simulations produces a reasonably close prediction for the maximum pressure expected to develop at the flash front in the Surtseyan ejecta. This theoretical estimate of the maximum pressure can be used to replace the previous criterion for rupture and produces results for the lower bound on the permeability that is consistent with the data provided by Ian Schipper [40].

Appendix A

Energy Conservation for a moving fluid

The energy conservation for a moving fluid equation, equation 2.1, in terms of pressure and temperature can be derived from the pointwise conservation of enthalpy equation for a moving fluid with no sources or sinks [22]. The enthalpy equation:

$$\frac{\partial}{\partial t}(\rho h) + \nabla \cdot (\rho h \mathbf{v}) = -\nabla \cdot \mathbf{q} + \frac{\partial p}{\partial t} + \mathbf{v} \cdot \nabla p + \tau : \nabla \mathbf{v} \tag{A.1}$$

where ρ is the fluid density of some liquid or gas, h is the specific enthalpy, $\mathbf{v}$ is the local fluid velocity vector and $\mathbf{q}$ is the heat flux. The viscous dissipation term, $\tau : \nabla \mathbf{v}$, involves taking the double dot product of the deviatoric stress tensor, τ, and the gradient of the local fluid velocity vector to form a scalar. This viscous dissipation term is generally small, so can dropped from the energy equations. Also, as the ejectum is in free fall during the time of interest, and all gravity terms will be small, they can reasonably be neglected.

In order to derive equation 2.1 first consider a mass conservation equation in terms of enthalpy [4] [17]:

$$\frac{\partial \rho}{\partial t} + \nabla \cdot (\rho \mathbf{v}) = 0, \tag{A.2}$$

which allows the left hand-side of equation A.1 to be rewritten as:

$$\rho \left(\frac{\partial h}{\partial t} + \mathbf{v} \cdot \nabla h \right), \tag{A.3}$$

The enthalpy in a thermodynamic system equation is:

$$h = U + \frac{p}{\rho},$$

(A.4)

where U is the specific internal energy and the differential relationship between enthalpy, specific entropy, S, and pressure in homogeneous systems is:

$$dh = TdS + \frac{dp}{\rho}.$$

(A.5)

Change of entropy can be described as:

$$dS = \left(\frac{\partial S}{\partial T}\right)_p dT + \left(\frac{\partial S}{\partial p}\right)_T dp.$$

(A.6)

Noting that the specific heat at constant pressure, c_p, is equivalent to:

$$c_p = T\left(\frac{\partial S}{\partial T}\right)_p$$

(A.7)

and using Maxwell's relations:

$$\left(\frac{\partial S}{\partial p}\right)_T = \left(\frac{\partial (\frac{1}{\rho})}{\partial p}\right)_T$$

(A.8)

which relates to the coefficient of isothermal compressibility:

$$\beta = -\rho \left(\frac{\partial (\frac{1}{\rho})}{\partial p}\right)_T$$

(A.9)

equation A.6 can now be rewritten as:

$$TdS = c_p dT - \frac{\beta T}{\rho} dp.$$

(A.10)

Hence:

$$dh = c_p dT + \left(\frac{1 - \beta T}{\rho}\right) dp,$$

(A.11)

and by using Fourier's law for heat conduction $q = -K\nabla T$, where K is the thermal conductivity of the fluid, the pointwise conservation equation for energy

can be written as:

$$\rho \left(\frac{\partial h}{\partial t} + \mathbf{v} \cdot \nabla h \right) = -\nabla \cdot \mathbf{q} \tag{A.12}$$

$$\rho c_p \left(\frac{\partial T}{\partial t} + \mathbf{v} \cdot \nabla T \right) - \beta T \left(\frac{\partial p}{\partial t} + \mathbf{v} \cdot \nabla p \right) = \nabla \cdot (K \nabla T). \tag{A.13}$$

These equations are also seen in [4] and [17] for stationary fluids with the total derivatives $\frac{\partial}{\partial t} + \mathbf{v} \cdot \nabla$ replaced by partial derivatives.

Appendix B

The Steam Generation Boundary equations

In order to consider the behaviour of the steam generation boundary it is necessary to integrate across the moving boundary in the energy conservation equations in averaged enthalpy form. These equations are an averaging across a representative elementary volume of porous medium of equation A.1. In the inclusion this is:

$$\frac{\partial}{\partial t}\left[\phi\rho_l h_l + (1-\phi)\rho_m h_m\right] + \nabla \cdot (\phi\rho_l h_l \mathbf{v}_l) = K_i \nabla^2 T + \phi\left[\frac{\partial p}{\partial t} + \mathbf{v}_l \cdot \nabla p\right] \quad \text{(B.1)}$$

and in the magma:

$$\frac{\partial}{\partial t}\left[\phi\rho_v h_v + (1-\phi)\rho_m h_m\right] + \nabla \cdot (\phi\rho_v h_v \mathbf{v_v}) = K_e \nabla^2 T + \phi\left[\frac{\partial p}{\partial t} + \mathbf{v_v} \cdot \nabla p\right]. \quad \text{(B.2)}$$

By assuming spherical symmetry, equations B.1 and B.2 can be reduced to a single spatial variable: radial distance to front, r. Thus reducing the equation to two variables r and t. Only the radial components of motion are considered, producing:

$$\frac{\partial}{\partial t}\left[\phi\rho_l h_l + (1-\phi)\rho_m h_m\right] + \frac{\partial}{\partial r}(\phi\rho_l h_l v_l) = K_i \nabla^2 T + \left[\phi\frac{\partial p}{\partial t} + \phi v_l \frac{\partial p}{\partial r}\right] \quad \text{(B.3)}$$

$$\frac{\partial}{\partial t}\left[\phi\rho_v h_v + (1-\phi)\rho_m h_m\right] + \frac{\partial}{\partial r}(\phi\rho_v h_v v_v) = K_e \nabla^2 T + \left[\phi\frac{\partial p}{\partial t} + \phi v_v \frac{\partial p}{\partial r}\right] \quad \text{(B.4)}$$

81

where $u = \phi v_v$ and $u_l = \phi v_l$.

A coordinate transform, $R = r - s(t)$, to make $R = 0$ the position of the steam generation boundary requires a change in the spatial and temporal derivatives:

$$\frac{\partial f(R(r,t),t)}{\partial t}\bigg|_r = \frac{\partial f}{\partial R}\frac{\partial R}{\partial t} + \frac{\partial f}{\partial t}\bigg|_R = -\dot{s}\frac{\partial f}{\partial R} + \frac{\partial f}{\partial t}\bigg|_R \qquad (B.5)$$

$$\frac{\partial}{\partial r}\bigg|_t = \frac{\partial}{\partial R}\bigg|_t \qquad (B.6)$$

in equations B.3 and B.4, producing:

$$\frac{\partial}{\partial t}\left[\phi\rho_l h_l + (1-\phi)\rho_m h_m\right] - \dot{s}\frac{\partial}{\partial R}\left[\phi\rho_l h_l + (1-\phi)\rho_m h_m\right] + \frac{\partial}{\partial R}\left(\phi\rho_l h_l v_l\right)$$
$$= K_i\nabla^2 T + \left[\phi\frac{\partial p}{\partial t}\bigg|_R + \phi(v_l - \dot{s})\frac{\partial p}{\partial R}\right] \qquad (B.7)$$

$$\frac{\partial}{\partial t}\left[\phi\rho_v h_v + (1-\phi)\rho_m h_m\right] - \dot{s}\frac{\partial}{\partial R}\left[\phi\rho_v h_v + (1-\phi)\rho_m h_m\right] + \frac{\partial}{\partial R}\left(\phi\rho_v h_v v_v\right)$$
$$= K_e\nabla^2 T + \left[\phi\frac{\partial p}{\partial t}\bigg|_R + \phi(v_v - \dot{s})\frac{\partial p}{\partial R}\right]. \qquad (B.8)$$

This is then integrated with respect to the volume of a spherical shell with $R = 0^-$ to $R = 0^+$ in order to capture the energy jump condition across the boundary. In the limit, this removes all terms apart from those containing radial derivatives. The jump condition is:

$$-\dot{s}\phi(\rho_v h_v - \rho_l h_l) + \phi(\rho_v h_v v_v - \rho_l h_l v_l) = [K\nabla T]_-^+ + \phi(v_v - v_l)p \qquad (B.9)$$

where $[K\nabla T]_-^+ = [K_e\nabla T(0^+) - K_i\nabla T(0^-)]$ ensures that energy is conserved across the boundary.

The same process can be used to create a jump condition for the conservation of mass equations. Using the same coordinate transform, the conservation of liquid mass in the inclusion is:

$$\frac{\partial\rho_l}{\partial t}\bigg|_R - \dot{s}\frac{\partial\rho_l}{\partial R} + \frac{\partial}{\partial R}(\rho_l v_l) = 0, \qquad (B.10)$$

and for the vapour in the magma is:

$$\frac{\partial \rho_v}{\partial t}\bigg|_R - \dot{s}\frac{\partial \rho_v}{\partial R} + \frac{\partial}{\partial R}(\rho_v v) = 0. \tag{B.11}$$

Integrating across the steam generation boundary in a similar way to the conservation of energy jump condition gives the mass condition:

$$\dot{s}(\rho_l - \rho_v) - \rho_l v_l + \rho_v v_v = 0. \tag{B.12}$$

Using both the energy and mass jump conditions and considering that the latent heat of vaporisation is $h_v - h_l = h_{vl}$ gives the boundary condition:

$$\phi \rho_v h_{vl}(v - \dot{s}) = \phi \rho_l h_{vl}(v_l - \dot{s}) = [K\nabla T]_-^+ + \phi(v_v - v_l)p. \tag{B.13}$$

Appendix C

Details on Model Rescaling

C.1 Steam Generation Boundary

In Surtseyan ejecta all the vapour is generated at the steam generation boundary. As vapour is produced from the boiling liquid at the surface of the inclusion, balancing the amount of liquid swept by the steam generation boundary, $\dot{s}\rho_l$, and the amount of steam crossing the front, $v_s\rho_s$, will give the following equation describing the velocity of the steam generation boundary:

$$\frac{R_2}{t_0}\dot{\tilde{s}}\rho_{l0}\tilde{\rho}_l = v_{v0}\rho_{s0}\tilde{v}_v\rho_v.$$

Then by taking the rescaling for the velocity of the vapour as $v_{v0} = \frac{R_2\rho_{l0}}{t_0\rho_{v0}}$ the equation can be further simplified to produce:

$$\dot{\tilde{s}}\tilde{\rho}_l = \tilde{v}_v\rho_v.$$

Using the rescalings in section 2.2, the conservation of mass equation across the steam generation boundary can be reduced to:

$$\frac{R_2}{t_0}\dot{\tilde{s}}(\rho_{l0}\tilde{\rho}_l - \rho_{v0}\tilde{\rho}_v) - \rho_{l0}v_{l0}\tilde{\rho}_l\tilde{v}_l + \rho_{v0}\tilde{\rho}_v v_{v0}\tilde{v}_v = 0.$$

Then by combining parameters $f_1 = \frac{\rho_{v0}}{\rho_{l0}}$ and $f_2 = \frac{v_{l0}t_0}{R_2}$ to form:

$$\dot{\tilde{s}}(\tilde{\rho}_l - f_1\tilde{\rho}_v) = f_2\tilde{\rho}_l\tilde{v}_l - \tilde{\rho}_v\tilde{v}_v,$$

the various sizes of the terms can be considered and the smaller terms neglected.

The energy conservation equation across the boundary is rescaled in the same manner as the mass conservation equation across the boundary to form:

$$\phi\rho_{v0}\tilde{\rho}_vh_{vl}\left(v_{v0}\tilde{v}_v - \frac{R_2}{t_0}\dot{\tilde{s}}\right) = \left[\frac{KT_m}{R_2}\tilde{\nabla}\tilde{T}\right]_-^+ + \phi(v_{v0}\tilde{v}_v - v_{l0}\tilde{v}_l)p_a\tilde{p}.$$

The parameters can be grouped together and the coefficient of the temperature gradient in the magma and the inclusion considered. The only difference between these two coefficients is the effective thermal conductivities. These effective thermal conductivities are taken from Robertson's report [35], which contains fits of data taken from both wet and dry igneous rock at various porosity. The representative values chosen in this model are $\phi = 0.4$, $K_e = 2$ W/m/K for air/vapour filled rock and $K_i = 3$ W/m/K for wet rock. As the values chosen for K_e and K_i are approximately equal, in the model K_i will be approximated by K_e. This allows for the coefficients of the temperature gradients to be further simplified to:

$$\tilde{\rho}_v(\tilde{v}_v - f_1\dot{\tilde{s}}) = \frac{K_eT_m}{v_{v0}R_2\phi\rho_{v0}h_{vl}}\left[\tilde{\nabla}\tilde{T}\right]_-^+ + \frac{p_a}{\rho_{v0}h_{vl}}\left(\tilde{v}_v - \frac{v_{l0}}{v_{v0}}\tilde{v}_l\right)\tilde{p}.$$

By setting $f_4 = \frac{p_a}{\rho_{v0}h_{vl}}$, $f_5 = \frac{v_{l0}}{v_{v0}}$ and the Stefan number to $f_3 = \frac{v_{v0}R_2\phi\rho_{v0}h_{vl}}{K_eT_m}$ the equation becomes:

$$\tilde{\rho}_v(\tilde{v}_v - f_1\dot{\tilde{s}}) = \frac{1}{f_3}\left[\tilde{\nabla}\tilde{T}\right]_-^+ + f_4(\tilde{v}_v - f_5\tilde{v}_l)\tilde{p}.$$

C.2 The Inclusion Rescaling

The dimensional equation 2.12, the equation of state, is scaled as follows:

$$\tilde{\rho}_l = 1 + f_6(\tilde{p} - 1) - f_7(\tilde{T} - T_n) \tag{C.1}$$

where $T_n = \frac{T_R}{T_m}$, $f_6 = \frac{\beta_e p_a}{\rho_{l0}}$ and $f_7 = \frac{\alpha T_m}{\rho_{l0}}$. As f_6 is shown to be small in table 2.2 it can be assumed that the effects of thermal expansion will dominate the density variations in the inclusion.

The parameters f_2, present in the mass conservation equation, and f_5, in the energy conservation equation, both contain the velocity scaling in the inclusion (v_{l0}). An estimate for this value can be made by taking the change in the inclusion size over the time it takes for the inclusion to heat the water to its critical temperature (T_{crit}).

To estimate the change in the inclusion size it is firstly assumed that there are no losses in liquid mass in the inclusion. This inclusion mass can then be described as the volume multiplied by the density and then, assuming all the expansion is due to thermal expansion, this gives:

$$(R_1 + \Delta R_1)^3[\rho_l - \alpha(T_{crit} - T_R)] = R_1^3 \rho_{l0},$$

when the inclusion starts at a radius R_1, with a density ρ_{l0} and temperature T_0 and expands to a new radius $R_1 + \Delta R_1$. This change in radius in the inclusion is assumed to be small, allowing the cubic $(R_1 + \Delta R_1)^3$ to be approximated as $(R_1^3 + 3\Delta R_1 R_1^2)$. This allows for the change in radius in the inclusion to be estimated as:

$$\Delta R_1 \approx R_1 \left(\frac{\alpha(T_{crit} - T_R)}{3(\rho_l - \alpha(T_{crit} - T_R))} \right).$$

The time it takes for the inclusion to be heated using only conduction to the critical temperature of water can be estimated from the conduction equation as:

$$t_s \approx \frac{R_1^2((1 - \phi)\rho_m c_{pm} + \phi \rho_v c_{pv})}{K_i}.$$

By assuming that the change in radius occurred in the time it took for the inclusion to heat to the critical temperature of water we obtain the following

estimate for the velocity scaling in the inclusion:

$$v_{l0} \approx \frac{\alpha K_i (T_{crit} - T_R)}{3R_1 ((1 - \phi)\rho_m c_{pm} + \phi \rho_v c_{pv})(\rho_l - \alpha(T_{crit} - T_R))}. \tag{C.2}$$

The velocity scaling in the inclusion is estimated to be of the order 10^{-5} using equation C.2 and the typical parameters in table 2.1. The relatively small velocity scaling in the inclusion results in the small sizes of f_2 and f_5 in table 2.2 allowing them to be neglected for the mass and energy conservation equations across the steam generation boundary.

The mass conservation in the inclusion is rescaled to:

$$\phi \frac{\partial \tilde{\rho}_l}{\partial \tilde{t}} + f_2 \tilde{\nabla} \cdot (\tilde{\rho}_l \tilde{\mathbf{u}}_l) = 0.$$

This contains the parameter f_2, which can be neglected, which allows the density of the liquid in the inclusion to be considered constant. Physically this means that the liquid in the inclusion does not move until the boundary reaches it and it flashes to steam.

The energy conservation equation in the inclusion, noting that $\mathbf{u}_l$ is negligible, reduces to:

$$\frac{\partial \tilde{T}}{\partial \tilde{t}} - f_8 \tilde{T} \frac{\partial \tilde{p}}{\partial \tilde{t}} = \frac{f_9}{\tilde{r}^2} \frac{\partial}{\partial \tilde{r}} \left(\tilde{r}^2 \frac{\partial \tilde{T}}{\partial \tilde{r}} \right),$$

with the parameters $f_8 = \frac{\phi \beta p_a}{\rho_i c_i}$ and $f_9 = \frac{K_i t_0}{R_2^2 \rho_i c_i}$. f_8 is determined in table 2.2 to be small, allowing the advective term to be neglected.

C.3   Rescaling the Magma equations

The ideal gas law allows setting $\rho_{v0} = \frac{M p_0}{R_g T_m}$, which can be rescaled to:

$$\tilde{\rho}_v = \frac{\tilde{p}}{\tilde{T}}.$$

As the model only assumes radial velocity ($\mathbf{u} = \phi v$), due to the spherical symmetry assumption, Darcy's law can by reduced to

$$\tilde{v}_v = -f_{10} \tilde{\nabla} \tilde{p}$$

where $f_{10} = \frac{kp_0}{\mu_v R_2 \phi v_{v0}}$.

As it is possible to have turbulent flow, the Forcheimer equation, which combines Darcy flow with the Ergun equation [5], is considered:

$$\nabla p = -\frac{\mu_v}{k}\mathbf{u} - \frac{\rho_v C_f}{\sqrt{k}}\mathbf{u}|\mathbf{u}|,$$

where C_f is an order one coefficient. The non-dimensional equation is produced as follows:

$$\frac{p_0}{R_2}\tilde{\nabla}\tilde{p} = -\frac{\mu_v \phi v_{v0}}{k}\tilde{v}_v - \frac{\rho_{v0}\tilde{\rho}_v C_f \phi^2}{\sqrt{k}}\tilde{v}_v|\tilde{v}_v|$$

$$\implies \frac{kp_0}{R_2 \mu_v v_{v0}\phi}\tilde{\nabla}\tilde{p} = -\tilde{v}_v - \frac{\rho_{v0}\tilde{\rho}_v C_f \phi \sqrt{k}}{\mu_v v_{v0}}\tilde{v}_v|\tilde{v}_v|$$

$$\implies f_{10}\tilde{\nabla}\tilde{p} = -\tilde{v}_v - \delta_f \tilde{\rho}_v \tilde{v}_v|\tilde{v}_v|$$

$$\implies \delta_f = \frac{\rho_{v0}C_f \phi \sqrt{k}}{\mu_v v_{v0}}.$$

The constant $\delta_f \approx 0.08$ using the the typical parameters in table 2.1. As $\delta_f << 1$ the Ergun term is not required. This can also be confirmed using the pore Reynolds number:

$$Re_p = \frac{\rho_l \sqrt{k}\phi|u|}{\mu_v} \approx 0.01,$$

which confirms laminar flow and the use of Darcy's Law in this model.

Apply Darcy's law and rescaling the conservation of mass equation produces:

$$\frac{\partial \tilde{\rho}_v}{\partial \tilde{t}} = f_{11}\tilde{\nabla} \cdot (\tilde{\rho}_v(\tilde{\nabla}\tilde{p})),$$

where $f_{11} = \frac{t_0 kp_0}{\phi \mu_v R_2^2}$. This can be simplified further, as the assumed spherical symmetry allows only for variations in the radius, reducing the equation further to:

$$\frac{\partial \tilde{\rho}_v}{\partial \tilde{t}} = \frac{f_{11}}{\tilde{r}^2}\frac{\partial}{\partial \tilde{r}}\left(\tilde{\rho}_v \tilde{r}^2 \frac{\partial \tilde{p}}{\partial \tilde{r}}\right).$$

The rescaling of the energy conservation equation, remembering that $\rho_e c_e$ in the ranges of temperature and pressures in this model is dominated by the thermal

capacity of the rock material (allowing it be treated as a constant), produces:

$$\frac{\partial \tilde{T}}{\partial \tilde{t}} - f_{12}\tilde{\rho}_v \frac{\partial \tilde{p}}{\partial \tilde{r}} \frac{\partial \tilde{T}}{\partial \tilde{r}} - f_{13}\frac{\partial \tilde{p}}{\partial \tilde{t}} + f_{14}\left(\frac{\partial \tilde{p}}{\partial \tilde{r}}\right)^2 = \frac{f_{15}}{\tilde{r}^2}\frac{\partial}{\partial r}\left(\tilde{r}^2\frac{\partial \tilde{T}}{\partial \tilde{r}}\right),$$

where $f_{12} = \frac{t_0 \rho_{v0} c_{pv} k p_0}{\rho_e c_e \mu_v R_2^2}$, $f_{13} = \frac{\phi p_0}{\rho_e c_e T_m}$, $f_{14} = \frac{k t_0 p_0^2}{\rho_e c_e T_m R_2^2 \mu_v}$ and $f_{15} = \frac{K_e t_0}{R_2^2 \rho_e c_e}$. Then this is reduced further when f_{12}, f_{13} and f_{14} are neglected due to their small size leaving the energy conservation equation in the magma as:

$$\frac{\partial \tilde{T}}{\partial \tilde{t}} = \frac{f_{15}}{\tilde{r}^2}\frac{\partial}{\partial r}\left(\tilde{r}^2\frac{\partial \tilde{T}}{\partial \tilde{r}}\right). \tag{C.3}$$

Appendix D

Calculation details for the Asymptotic Temperature Solutions and the Upper-bound on the Maximum Pressure

D.1 Region of rapidly varying temperature in the magma

Equation 3.4 describes the rapidly varying temperature behaviour in the boundary layer surrounding the steam generation boundary assuming that times are early enough that the steam generation boundaries movement can be reasonable ignored. Equation 3.4, with the boundary conditions $T(0,t) = T_f$ and T tends to 1 as $\sigma \to \infty$, can be solved using the similarity solution $\eta = \frac{t}{\sigma^2}$.

The chosen similarity solution substituted into equation 3.4 gives:

$$\frac{\partial T}{\partial \eta} \frac{\partial \eta}{\partial t} = \frac{\partial}{\partial \sigma} \left(\frac{\partial T}{\partial \eta} \frac{\partial \eta}{\partial \sigma} \right)$$

$$\implies \frac{\partial T}{\partial \eta} \frac{1}{\sigma^2} = \frac{\partial}{\partial \sigma} \left(\left[\frac{-2\eta}{\sigma} \right] \frac{\partial T}{\partial \eta} \right)$$

$$= \left(\frac{-2}{\sigma} \frac{\partial \eta}{\partial \sigma} \frac{\partial T}{\partial \eta} \right) + \left(\frac{2\eta}{\sigma^2} \frac{\partial T}{\partial \eta} \right) + \left(\frac{-2\eta}{\sigma} \frac{\partial^2 T}{\partial \eta^2} \frac{\partial \eta}{\partial \sigma} \right)$$

$$= \left(\frac{4\eta}{\sigma^2}\frac{\partial T}{\partial \eta}\right) + \left(\frac{2\eta}{\sigma^2}\frac{\partial T}{\partial \eta}\right) + \left(\frac{4\eta^2}{\sigma^2}\frac{\partial^2 T}{\partial \eta^2}\right)$$

$$\implies \frac{\partial T}{\partial \eta} = 6\eta\frac{\partial T}{\partial \eta} + 4\eta^2\frac{\partial^2 T}{\partial \eta^2}. \tag{D.1}$$

Then, by using the substitution $w = \frac{\partial T}{\partial \eta}$, a solution for the temperature gradient in terms of η can be found:

$$\frac{1 - 6\eta}{4\eta^2} = \frac{w'}{w}$$

$$\implies \ln[w] = \frac{-1}{4\eta} - \frac{3}{2}\ln[\eta] + c$$

$$\implies w = Ae^{-\frac{1}{4\eta}}\eta^{\frac{-3}{2}}$$

An equation for T can be found using the substitution $x = \frac{1}{2\eta}$ this gives:

$$\frac{-1}{4\eta^{\frac{3}{2}}}\frac{\partial T}{\partial x} = Ae^{-x^2}\eta^{\frac{-3}{2}}$$

$$\implies \frac{\partial T}{\partial x} = -4Ae^{-x^2} \tag{D.2}$$

and then integrating from infinity to $\frac{1}{2\sqrt{\eta}}$ produces:

$$T = 2A\sqrt{\pi}(1 - \text{erf}(\frac{\sigma}{2\sqrt{t}})) + T^*. \tag{D.3}$$

Furthermore, by applying the boundary conditions $T(0,t) = T_f$ and with T tending to 1 as $\psi \to \infty$, this gives:

$$T = (T_f - 1)\left(1 - \text{erf}(\frac{\sigma}{2\sqrt{t}})\right) + 1. \tag{D.4}$$

D.2 Region of rapidly varying temperature in the Inclusion

Equation 3.10 describes the rapidly varying temperature behaviour in the boundary layer surrounding the steam generation boundary, in the inclusion, assuming that times are early enough that the steam generation boundaries movement can be reasonably ignored. Equation 3.10 with the boundary conditions $T(0,t) = T_f$ and T tending to T_0 as $\psi \to \infty$ can be solved using the similarity solution $\eta = \frac{t}{\psi^2}$.

The chosen similarity solution substituted into equation 3.10 follows a similar derivation to that for the magma region:

$$\frac{\partial T}{\partial \eta} \frac{\partial \eta}{\partial t} = \frac{\partial}{\partial \psi} \left(\frac{\partial T}{\partial \eta} \frac{\partial \eta}{\partial \psi} \right)$$

$$\implies \frac{\partial T}{\partial \eta} = 6\eta \frac{\partial T}{\partial \eta} + 4\eta^2 \frac{\partial^2 T}{\partial \eta^2}. \tag{D.5}$$

Like in the magma region, the substitution $w = \frac{\partial T}{\partial \eta}$ followed by $x = \frac{1}{2\eta}$ is used to form the following equation:

$$\frac{\partial T}{\partial x} = -4Ae^{-x^2}, \tag{D.6}$$

which is integrated from infinity to $\frac{1}{2\sqrt{\eta}}$ producing:

$$T = 2A\sqrt{\pi}(1 - \text{erf}(\frac{\psi}{2\sqrt{t}})) + T^*. \tag{D.7}$$

This is similar to the equation produced in the magma region and by applying the boundary conditions $T(0,t) = T_f$ and T tending to T_0 as $\psi \to \infty$ this gives:

$$T = (T_f - T_0)(1 - \text{erf}(\frac{\psi}{2\sqrt{t}})) + T_0. \tag{D.8}$$

D.3   Maximum Pressure Analysis Details

D.3.1   Deriving the ramping distance at t_e

The initial temperature profile for magma, equation 3.14, was derived using a similarity solution which included the variable $\eta = \frac{t}{\sigma}$. For early time pressure calculations and emplacement time is added to create a ramp function. This ramp function allows the singularity at the flash front to be avoided. The step function in the initial temperature profile is retained by setting the emplacement time to zero. For the emplacement time t_e to be considered in this calculation the previous variable for time t is equivalent to $t_{new} + t_e$. From this point on t_{new} will be referred to as t. The initial temperature profile for magma is therefore rewritten as:

$$T = (T_f - 1)\left(1 - \operatorname{erf}(\frac{\sigma}{2\sqrt{t+t_e}})\right) + 1. \tag{D.9}$$

The ramping distance r_{ramp} can be estimated using the error function by noting that when the argument of the error function equals two the result is approximately one, $\operatorname{erf}(2) = 0.995$ (3sf). The argument of the error function at initial time $\frac{\sigma_{(t=0)}}{2\sqrt{t_e}}$ written in terms of r is $\frac{r_{(t=0)} - \varepsilon}{\delta_m \sqrt{t_e}}$. The ramping distance $r_{ramp} = r_{(t=0)} - \varepsilon$. Therefore the ramping distance can be estimated as:

$$\frac{r_{ramp}}{2\delta_m\sqrt{t_e}} \approx 2$$

$$\implies r_{ramp} \approx 4\delta_m\sqrt{t_e}.$$

D.3.2   Deriving the approximate early time pressure behaviour equation at the flash front

The approximate early time pressure behaviour equation at the flash front is:

$$\frac{\partial p}{\partial t} \approx \frac{A}{\sqrt{(t^2 + t_e t)}}, \quad r = s(t),$$

$$\implies A = \frac{T(1 - T)\sqrt{f_{11}}}{f_3 \delta_m \sqrt{\pi}}$$

where the temperature at the flash front T is approximated to be 0.4, which is justified in chapter 3. By completing the square and using the substitutions

$u = t + \frac{t_e}{2}$ and $w = \frac{2u}{t_e}$ the following equations are formed:

$$\frac{\partial p}{\partial t} \approx \frac{A}{\sqrt{(t + \frac{t_e}{2})^2 - \frac{t_e^2}{4}}}$$

$$\implies \int \partial p \approx \int \frac{A}{\sqrt{u^2 - \frac{t_e^2}{4}}} \partial u$$

$$\approx \int \frac{A}{\sqrt{w^2 - 1}} \partial w,$$

then by applying the trigonometric substitution $w = \sec(x)$ and using the $\sec^2(x) - 1 = \tan^2(x)$ identity to form equation:

$$\int \partial p \approx \int \frac{A \sec(x) \tan(x)}{\sqrt{(\sec(x))^2 - 1}} \partial x$$

$$\approx \int A \sec(x) \partial x,$$

which can be integrated to form the following equation for approximate early time pressure behaviour, p_e:

$$p_e \approx A \ln|\sec(x) + \tan(x)| + c$$

$$\approx A \ln \left| \frac{1}{t_e} \left(2t + t_e + 2\sqrt{t^2 + tt_e} \right) \right| + c$$

$$\approx A \left(\ln \left(2t + t_e + 2\sqrt{t^2 + tt_e} \right) - \ln t_e \right) + c.$$

Note that the absolute values have been dropped due to t and t_e being positive time values. The constant c can now be determined by considering the initial pressure at the time of emplacement, $t = 0$, to be atmospheric pressure. The approximate early time pressure behaviour equation is:

$$p_e \approx A \left(\ln \left(2t + t_e + 2\sqrt{t^2 + tt_e} \right) - \ln t_e \right) + 1. \tag{D.10}$$

D.3.3 Quasi-steady state pressure

The quasi-steady state pressure equation:

$$\frac{\partial}{\partial r}\left(\frac{p}{Tr^2}\frac{\partial p}{\partial r}\right) = 0, \quad r > s(t)$$

produces the following solution:

$$p\frac{\partial p}{\partial r} = \frac{C_1 T}{r^2} \tag{D.11}$$

$$\implies p_q^2 = \int \frac{2C_1 T}{r^2}\partial r, \tag{D.12}$$

where p_q is the quasi-steady state pressure. Since the temperatures in this system are less than or equal to one (the non-dimensional initial temperature in the magma), an upper bound for the quasi-steady state pressure can be given by setting the temperature T to equal 1. This produces the following equation for the upper bound of the quasi-steady state pressure, p_u:

$$p_u^2 = -\frac{2C_1}{r} + C_2. \tag{D.13}$$

C_1 can be derived by equating the flux condition at the flash front, approximated by equation 6.3, to equation D.11 giving:

$$\frac{C_1 T}{\varepsilon^2} = -\frac{T(1-T)}{f_3 f_{10}\delta_m \sqrt{\pi(t+t_e)}} \tag{D.14}$$

$$\implies C_1 = -\frac{\varepsilon^2(1-T)}{f_3 f_{10}\delta_m \sqrt{\pi(t+t_e)}}. \tag{D.15}$$

This calculation only applies if it is accepted that the temperature varies on a slower timescale than the pressure. This allows for the time in the pressure equation to be treated independently of the time in the temperature gradient equation. This dependence on time from the temperature gradient in C_1 and C_2 is what makes this a quasi-steady state equation instead of a steady-state equation, where C_1 and C_2 would both be constant. $C_2 = 1 + 2C_1$ is determined by considering the boundary at the surface of the ejecta is fixed at atmospheric pressure.

D.3.4 Leading term approximation of equation 6.10

The leading term approximation for equation 6.10 after the initial pressure is dropped is:

$$2A\sqrt{\frac{t_m}{t_e}} \approx A\left(\ln\left(2t_m + t_e + 2\sqrt{t_m^2 + t_m t_e}\right) - \ln t_e\right). \tag{D.16}$$

Equation D.16 is derived by considering the Taylor expansions for the square root and log equations The derivation also considers t_m to be approaching zero. First the equation needs to be in a form such that the square root expansion $\sqrt{1+x} = 1 + \frac{1}{2}x...$ where $|x| < 1$ can be used. In this derivation only the leading terms in the Taylor expansion will be considered. The derivation to remove the root is as follows:

$$A\left(\ln\left(2t_m + t_e + 2\sqrt{t_m^2 + t_m t_e}\right) - \ln t_e\right)$$

$$= A\left(\ln\left(2t_m + t_e + 2\sqrt{\frac{t_m}{t_e}}\sqrt{t_m t_e + t_e^2}\right) - \ln t_e\right)$$

$$= A\left(\ln\left(2t_m + t_e + 2t_e\sqrt{\frac{t_m}{t_e}}\sqrt{\frac{t_m}{t_e} + 1}\right) - \ln t_e\right)$$

$$= A\ln\left(2\frac{t_m}{t_e} + 1 + 2\sqrt{\frac{t_m}{t_e}}\sqrt{\frac{t_m}{t_e} + 1}\right)$$

$$\approx A\ln\left(2\frac{t_m}{t_e} + 1 + 2\sqrt{\frac{t_m}{t_e}} \times 1\right). \tag{D.17}$$

The Taylor expansion of the square root can be considered in equation D.17 because t_m is tending to zero and therefore $\frac{t_m}{t_e} \ll 1$.

The next step in the derivation is to expand the natural log using $\ln|1+x| \approx x - \frac{x^2}{2}...$ where $|x| < 1$. This requires some further rearrangement of equation D.17 as follows:

$$A\ln\left(2\frac{t_m}{t_e} + 1 + 2\sqrt{\frac{t_m}{t_e}} \times 1\right) \approx A\ln\left(2\sqrt{\frac{t_m}{t_e}}\left(1 + \sqrt{\frac{t_m}{t_e}}\right) + 1\right)$$

and then by considering $\left(1 + \sqrt{\frac{t_m}{t_e}}\right) \approx 1$ the equation can be reduced to:

$$A\ln\left(2\frac{t_m}{t_e} + 1 + 2\sqrt{\frac{t_m}{t_e}} \times 1\right) \approx A\ln\left(2\sqrt{\frac{t_m}{t_e}} + 1\right). \tag{D.18}$$

Finally equation D.18 is reduced using the log Taylor expansion considering only the leading term to:

$$A \ln \left(2\sqrt{\frac{t_m}{t_e}} + 1 \right) \approx 2A\sqrt{\frac{t_m}{t_e}} \tag{D.19}$$

which gives the leading term approximation for equation 6.10.

Appendix E

Boundary Condition at the flash front

The non-linear solver (fsolve) in MATLAB stops at the first solution it finds to the non-linear equation on the interval. Therefore the interval of temperatures used in the numerics needs to contain a single solution. The boundary condition, equation 4.4, can be rewritten in terms of temperature using equations 4.5 and 4.6. This produces:

$$\frac{f_{10}(1-\varepsilon)}{T(1-s)} e^{H\left[1-\frac{T_0}{T_m T_b}\right]} \frac{\partial}{\partial \xi}\left[e^{H\left[1-\frac{T_0}{T_m T_b}\right]}\right] = \frac{-1}{f_3}\left[\left(\frac{1-\varepsilon}{1-s}\right)\frac{\partial T}{\partial \xi} - \frac{\varepsilon}{s}\frac{\partial T}{\partial \zeta}\right], \quad \text{(E.1)}$$

this equation is discretised to form a quadratic in temperature (on the right-hand side) and a quadratic of an exponential (on the left-hand side). This equation is not guaranteed to have a single solution on the temperature interval.

The right-hand side of the discretised equation E.1 is:

$$\frac{1}{f_3 f_{10}}\left[\left(T_{b+1} + \frac{\varepsilon(1-\varepsilon)\Delta\xi T_{b-1}}{s(1-s)\Delta\zeta}\right)T_b - T_b^2\left(1 + \frac{\varepsilon(1-\varepsilon)\Delta\xi}{s(1-s)\Delta\zeta}\right)\right]$$

where T_b is the temperature at the boundary, T_{b-1} is the temperature one step into the inclusion and T_{b+1} is the temperature one step into the magma. This equation describes a positive parabola with intercepts at $T_b = 0$ and

$T_b = \frac{\left(T_{b+1} + \frac{\varepsilon(1-\varepsilon)\Delta\xi T_{b-1}}{s(1-s)\Delta\zeta}\right)}{\left(1 + \frac{\varepsilon(1-\varepsilon)\Delta\xi}{s(1-s)\Delta\zeta}\right)}$ which is approximately $T_b = 0.6$ at initial time if the

change in mesh in the inclusion is equal to that in the magma.
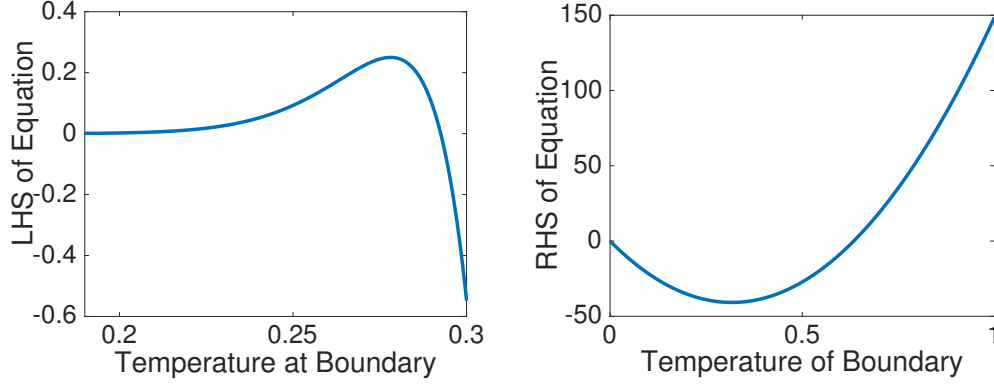
Figure E.1: Left: Left-hand side of the boundary equation at initial time. Right: Right-hand side of the boundary equation at initial time.

The left-hand side of the discretised equation E.1 is:

$$\left(\exp^{H\left[1-\frac{T_0}{T_m T_b}\right]} \right)^2 - p_{b+1} \exp^{H\left[1-\frac{T_0}{T_m T_b}\right]} .$$

It has a local extremum at:

$$T_b = \frac{H T_0}{T_m \left(H - \ln \frac{p_{b+1}}{2} \right)}$$

at initial times is at $T_b \approx 0.20$ and at a non-dimensional pressure of about 20 the extremum is at $T_b \approx 0.25$. This extremum can be categorised as a local maximum because:

$$\frac{d^2 \mathrm{LHS}}{dT_b^{\,2}} (T_b) = \left(\frac{p_{b+1} H T_0}{\sqrt{2} T_m T_b^2} \right)^2$$

and both the high and low pressure cases this maximum is below the initial inclusion temperature. It will therefore not cause multiple solutions to the boundary equation in the interval used in the numerics.

Appendix F

The Method of Lines

F.1   Method of Lines Background

The method of lines, [13], is used to numerically solve partial differential equations by discritising spatial terms to leave a system of ordinary temporal equations. The finite difference method is used to discretise the range which is split into N intervals of size h. The range is now represented by $r = \{r_1, r_2, r_3..., r_N, r_{N+1}\}$. If a point n is considered, it has a temperature T_n and a Taylor expansion can be used to estimate the temperature at neighbouring points:

$$T_{n+1} = T_n + h \left(\frac{\partial T}{\partial r} \right)_n + \frac{1}{2} h^2 \left(\frac{\partial^2 T}{\partial r^2} \right)_n + ... \tag{F.1}$$

$$T_{n-1} = T_n - h \left(\frac{\partial T}{\partial r} \right)_n + \frac{1}{2} h^2 \left(\frac{\partial^2 T}{\partial r^2} \right)_n - ... \tag{F.2}$$

From the Taylor expansions approximations for the first-order partial derivatives can be made. There are three different first-order approximations:

$$\left(\frac{\partial T}{\partial r} \right)_n = \frac{T_{n+1} - T_n}{\Delta r_n} \tag{F.3}$$

$$\left(\frac{\partial T}{\partial r} \right)_n = \frac{T_n - T_{n-1}}{\Delta r_{n-1}} \tag{F.4}$$

$$\left(\frac{\partial T}{\partial r} \right)_n = \frac{T_{n+1} - T_{n-1}}{\Delta r_n + \Delta r_{n-1}}. \tag{F.5}$$

Equation F.3 is the forward, Equation F.4 is the backward and Equation F.5 is the central first-order approximations.

When solving models numerically, the advective terms need to use a derivative that matches the direction of the flow (see Appendix F.2). The second derivative is also approximated using the Taylor expansion by eliminating the first derivative term to give:

$$\left(\frac{\partial^2 T}{\partial r^2}\right)_n = \frac{2T_{n+1}}{\Delta r_n(\Delta r_{n-1} + \Delta r_n)} - \frac{2T_n}{\Delta r_n \Delta r_{n-1}} + \frac{2T_{n-1}}{\Delta r_{n-1}(\Delta r_{n-1} + \Delta r_n)}. \tag{F.6}$$

F.2   Upstream Difference Background

When solving a differential equation using the method of lines the advective term needs to be considered to determine whether the right, left or a central difference is appropriate in each case. This will ensure that if there is a positive velocity in the advective term the finite difference calculations will only consider coordinates already covered by the flow, and similarly for a negative velocity. Using v_T as the advective term, dT^+ and dT^- as the positive and negative difference respectively you can describe the equation for upstream differencing:

$$v_T dT = v_T^+ dT^+ + v_T^- dT^-, \tag{F.7}$$

where $v_T^+ = \mathrm{MAX}(v_T, 0)$ and $v_T^- = \mathrm{MIN}(v_T, 0)$.

F.3   Uniform mesh coordinate transformation

One way to obtain the required mesh size at the boundary is to transform from ζ and ξ to a new coordinate system, χ and ς. This transformation is chosen so that in ζ and ξ there is a finer mesh near the flashing front, but retains a uniform mesh in the χ and ς coordinate system. This is important as this uniform mesh will allow for the use of the second-order accurate spatial derivative formula.

The transformation used to achieve this is:

$$\zeta = \frac{\varepsilon \arctan(a_i \chi)}{\arctan(a_i(m+1))} = \frac{\varepsilon \arctan(a_i \chi)}{B_m}$$

$$\xi = 1 + \frac{(1-\varepsilon)\arctan(a_m(\varsigma - n - 1))}{\arctan(a_m(n+1))} = 1 + \frac{(1-\varepsilon)\arctan(a_m(\varsigma - n - 1))}{B_n}$$

where χ and ς are both unit-spaced meshes varying from 0 to $m+1$ and 0 to $n+1$ respectively. The parameters a_i, a_m, m and n can be varied to study the convergence of the model at the steam generation boundary.

Transforming the first-order spatial derivatives requires the use of the chain rule giving:

$$\frac{\partial f}{\partial \zeta} = \frac{\partial \chi}{\partial \zeta}\frac{\partial f}{\partial \chi} = C_m \frac{\partial f}{\partial \chi}$$

$$\frac{\partial f}{\partial \xi} = \frac{\partial \varsigma}{\partial \xi}\frac{\partial f}{\partial \varsigma} = C_n \frac{\partial f}{\partial \varsigma}$$

with the parameters:

$$C_m = \frac{B_m[1+(a_i\chi)^2]}{\varepsilon a_i}$$

$$C_n = \frac{B_n[1+(a_m(\varsigma - n - 1))^2]}{(1-\varepsilon)a_m}.$$

The second derivative transformation will also require the chain rule and this will create a first-order derivative that will need to be considered in the upstream differencing. This is calculated to be:

$$\frac{\partial^2 f}{\partial \zeta^2} = C_m \frac{\partial}{\partial \chi}\left[C_m \frac{\partial f}{\partial \chi}\right]$$

$$= \frac{2C_m B_m a_i \chi}{\varepsilon}\frac{\partial f}{\partial \chi} + C_m^2 \frac{\partial^2 f}{\partial \chi^2}$$

in the inclusion region and:

$$\frac{\partial^2 f}{\partial \xi^2} = C_n \frac{\partial}{\partial \varsigma}\left[C_n \frac{\partial f}{\partial \varsigma}\right]$$

$$= \frac{2C_n B_n a_m(\varsigma - n - 1)}{(1-\varepsilon)}\frac{\partial f}{\partial \varsigma} + C_n^2 \frac{\partial^2 f}{\partial \varsigma^2}.$$

in the magma region.

Applying the transformation to the model in Chapter 4 gives:

$$\frac{\partial T}{\partial t} = w_{Ti}\frac{\partial T}{\partial \chi} + \frac{f_9 C_m^2 \varepsilon^2}{s^2}\frac{\partial^2 T}{\partial \chi^2}, \qquad \chi = 0,1,2...m+1 \qquad \text{(F.8)}$$

$$\frac{\partial T}{\partial t} = w_{Tm}\frac{\partial T}{\partial \varsigma} + C_n^2 f_{15}\left(\frac{1-\varepsilon}{1-s}\right)^2\frac{\partial^2 T}{\partial \varsigma^2} \quad \varsigma = 0,1,2...n+1 \qquad \text{(F.9)}$$

$$\frac{\partial \rho_v}{\partial t} = W_{\rho_v}\frac{\partial \rho_v}{\partial \varsigma} + W_p\frac{\partial p}{\partial \varsigma}$$

$$+ C_n^2 f_{11}\left(\frac{1-\varepsilon}{1-s}\right)^2\frac{\partial}{\partial \varsigma}\left[\rho_v\frac{\partial p}{\partial \varsigma}\right] \qquad \varsigma = 0,1,2...n+1 \qquad \text{(F.10)}$$

$$\dot{s} = \rho_s f_{10} C_n\left(\frac{1-\varepsilon}{1-s}\right)\frac{\partial p}{\partial \varsigma}$$

$$= -\frac{1}{f_3}\left[C_n\left(\frac{1-\varepsilon}{1-s}\right)\frac{\partial T}{\partial \varsigma} - C_m\frac{\varepsilon}{s}\frac{\partial T}{\partial \chi}\right] \quad \chi = m+1, \varsigma = 0 \qquad \text{(F.11)}$$

$$p = e^{H\left[\frac{T-T_n}{T}\right]}, \qquad \chi = m+1, \varsigma = 0 \qquad \text{(F.12)}$$

$$p = \rho_v T, \qquad \varsigma = 0,1,2...n+1 \qquad \text{(F.13)}$$

with parameters:

$$w_{Ti} = \left[\frac{2f_9\varepsilon^2}{s^2\varsigma} + \frac{\varsigma\dot{s}}{s}\right]C_m + \frac{2C_m B_m a_i \chi f_9 \varepsilon}{s^2}$$

$$w_{Tm} = \left[\frac{2f_{15}}{g(\xi,t)}\left(\frac{1-\varepsilon}{1-s}\right) - \frac{\xi-1}{1-s}\dot{s}\right]C_n + \frac{2C_n B_n a_m f_{15}(\varsigma-n-1)(1-\varepsilon)}{(1-s)^2}$$

$$W_p = \frac{2C_n\rho_v f_{11}}{g(\xi,t)}\left(\frac{1-\varepsilon}{1-s}\right) + \frac{2\rho_v f_{11} C_n B_n a_m(\varsigma-n-1)(1-\varepsilon)}{(1-s)^2}$$

$$W_{\rho_v} = \frac{(1-\xi)C_n}{1-s}\dot{s}$$

$$g(\xi,t) = \frac{(1-s)\xi + (s-\varepsilon)}{1-\varepsilon}.$$

The boundary conditions at the surface of the ejecta $\varsigma = n+1$ are $p = 1$ and $T = T_0$ with the flux condition $\frac{\partial T}{\partial \chi} = 0$, $\chi = 0$; at the centre of the inclusion. The initial conditions in the inclusion $\chi = [0, m+1]$ are $T = T_0$ and in the magma, where $\varsigma = [0, n+1]$, both the temperature and the pressure have an initial condition of 1.

Appendix G

Numerical Code

A sample of some of the code used in the numerical simulations of this thesis is included below. This code is also available at
https://github.com/greenbem/Modelling_Surtseyan_Ejecta_PhD_
Code/blob/main/SursteyEjectaModel.m.

```
function SursteyEjectaModel

% Considering a spherical ejecta with a centred inclusion
% and the model determined in the notes with a coordinate
% transformation to fix the moving boundary and using
% method of lines on the spacial terms to solve.

% The space is split into two sections the inclusion and
% the magma and each section has a different coordinate
% spacing that meet at the boundary between the two. Also
% in each section has an arctan coordinate transform applied
% to it in order to retain the uniformity of the steps but
% allow for small step sizes at the boundary.This allow for
% smooth movement from the smallest to largest mesh sizes

%% Typical Values
format long
M = 18*10^(-3);% Molecular mass of water
```

```
hsl = 2300000 ;% the latent heat of vaporisation
Rg= 8.314 ;% Gas Constant
Tm= 1275 ;% Original magma temperature
T0=373 ;% Original inclusion temperature
R1=0.01 ;% Radius of the inclusion
R2=0.1; % Radius of the magma ball
k=10^(-14); % permeability of magma
muv=3*10^(-5); % viscosity
p0=10^(5); % atmospheric pressure
rhom=2750; % Basalt density Range: 2650-2800
cpm=840; % specific heat Basalt
cps=2000; % specific heat of water vapour
rhol=1000; % Density of water
cpl=4200; % specific heat water
phi=0.4 ; % Porosity
rhol0=rhol; % Water Density ND
rhos0=(p0*M)/(Rg*Tm); % Vapour Density ND
Ke= 2; %thermal conductivity magma and vapour
Kel=3; % Effective thermal conductivity in the inclusion
pc=((1-phi)*rhom*cpm+phi*rhos0*cps); % specific heat and
% density comb magma vapour
pci=((1-phi)*rhom*cpm+phi*rhol*cpl);% specific heat and
% density comb inclusion
t0=(phi*rhol0*hsl*R1^2)/(3*Ke*(Tm-T0));% time scaling
vs0=(R2*rhol0)/(t0*rhos0); % velocity of vapour
epsilon= R1/R2;% Original boundary position(does not move)
p0m=10^(5); % Initial magma pressure
pre=10^(-5); %Size of the pore space;


%% Creating the mesh
% Using an arctan transformation mesh set up
% Setting m and n to give correct spacing
% In the inclusion and magma
n=200;
```

```
m=800;

smallestMesh=pre/R2;
% the smallest desired mesh size is set to twice the
% typical diameter of pores, taken to be 10 microns = 1E-05
% now set aa, given n=m, so that the smallest mesh size
% is roughly smallestMesh:

aa = 2*(1+smallestMesh*n)/( n*(n+1)*smallestMesh*pi);

%constants needed later
Bm = atan(aa*(m+1));
Bn = atan(aa*(n+1));

chi=linspace(0,m+1,m+2); % 0,1,2,3, ... n+1 in value
psi=linspace(0,n+1,n+2); % 0,1,2,3, ... m+1 in value
zeta=epsilon*atan(aa*chi)/atan(aa*(m+1));
% zeta in slurry goes from 0 to epsilon, tightens on epsilon
xi= 1 + (1-epsilon)*atan(aa*(psi-n-1))/atan(aa*(n+1));
% xi in hot magma goes from epsilon to 1,
% and tightens mesh on epsilon
Cn = (Bn./(aa.*(1-epsilon))).*(1+(aa.*(psi-n-1)).^2);
% vector term that arises from chain rule

Cm = (Bm./(aa.*epsilon))*(1+(aa.*chi).^2);
% vector term that arises from chain rule

if (xi(2)-xi(1)) < smallestMesh/2
% possibly n is too large, smallest spacing is too small
    disp('bailing out, smallest mesh size is too small...
    maybe n is too large?')
    display((xi(2)-xi(1)))
    display((zeta(m+2)-zeta(m+1)))
    disp('Magma Step Size Error')
end
```

```
 if (zeta(m+2)-zeta(m+1)) < smallestMesh/2
% possibly m is too large, smallest spacing is too small
    disp('bailing out, smallest mesh size is too small,...
    maybe m is too large?')
    display((xi(2)-xi(1)))
    display((zeta(m+2)-zeta(m+1)))
    disp('Slurry Step Size Error')
 end

%% Parameters from the ND Model
H=(M*hsl)/(Rg*T0);
f9=(Kel*t0)/(R2^2*pci);
f11=(t0*k*p0)/(phi*muv*R2^2);
f15=(Ke*t0)/(R2^2*pc);
f3=(vs0*R2*phi*rhos0*hsl)/(Ke*Tm);
f10=(k*p0)/(muv*R2*phi*vs0);

%% Setting up a time mesh

ts=0 ;% start time
te=0.1; % end time
tsteps=500;% Number of time steps
tspan= [0 logspace(-7, -1,tsteps-1)];

%% Initial Values of y set up

y0= zeros(1,2*n+m+1);
y0(1:m)=375/1275; % Initial Temp in Inclusion
y0(m+1:n+m)=1; % Initial Temp in Magma
y0(n+m+1:2*n+m)=1; % Initial density in magma
y0(2*n+m+1)=R1/R2;% position of flash front
```

```
% Setting up the different temp, density and
% position of the boundary matrices
Tinc=zeros(1,m+2);
Tmagma= zeros(1,n+2);
rhomagma=zeros(1,n+2);
Pmagma=zeros(1,n+2);


%% boundary condition at the surface of the
% magma from fixed end point

Tmagma(n+2)=375/1275;
Pmagma(n+2)=p0m/p0;
rhomagma(n+2)= Pmagma(n+2)/Tmagma(n+2);




%% Setting up to solve
options=odeset('RelTol', 10^(-8), 'AbsTol', 10^(-8), ...
'events', @functionevents, 'OutputFcn', @odeprint);

sol=ode15s(@SurtseyModelODE,[ts te],y0,options);



tspread=tspan;
%provides the solutions for the wanted times
Y=deval(sol,tspread);

% %Splitting Y into different parts
 sval= Y(end,:);
 % svalR=transpose(sval);
%display(sval)
 Tincvals= Y(1:m,:);
%display(Tincvals)
 Tmagmavals= Y(m+1:n+m, :);
%display(Tmagmavals)
```

```
%rhomagmavals=Y(j+m+1:2*j+m, :);
%display(rhomagmavals)
 Pmagmavals=Y(n+m+1:2*n+m, :).*Y(m+1:n+m, :);
%display(Pmagmavals)




%% Boundary
TBvals=zeros(1,tsteps);
PBvals=zeros(1,tsteps);
for i=1:tsteps
    TBvals(i)=functionboundary(Tmagmavals(1,i), ...
    Tincvals(m,i),Pmagmavals(1,i),sval(i));
    PBvals(i)=exp(H*((TBvals(i)-(T0/Tm))/TBvals(i)));
end




 %% Function
function f=SurtseyModelODE(~,y)

% This function generates the right-hand sides of the
% ODEs using the method of lines. This is discretised
% into two sections the inclusion and the magma sections.
% The input is the column vector y and t with is a scalar

% y is a input column vector of solutions. Note f should
% therefore also be a column vector. There are m
% temperature values from inside the inclusion not
% including a boundary condition at either end (as they
% are not calculated with the right hand sides they
% are imputed and n temperature values from the magma
% which also do not include the boundaries. Then there
% are a further n density values from inside the magma,
% boundary not included. So y is a column vector with
% the size m+2n+1
```

```
% Input values
%Values of Tinc not including boundary at ends
Tinc(2:m+1)=y(1:m);
%Values of Tmagma not including boundary at ends
Tmagma(2:n+1)=y((m+1):(n+m));
%Values of density not including boundary at ends
rhomagma(2:n+1)=y(((n+m)+1):(2*n+m));
% position of the flash front
s=y(2*n+m+1);
 %Pressure Ideal Gas Law
Pmagma(2:(n+1))=rhomagma(2:(n+1)).*Tmagma(2:(n+1));

%set up the boundary conditions
% the interior boundary at the centre of the
% inclusion Tinc(1)=y(1) has a temperature flux of zero.

Tinc(1)= Tinc(2);

%boundary condition between inclusion and magma
tau = functionboundary(Tmagma(2),Tinc(m+1),Pmagma(2),s);

Tinc(m+2)=tau;
Tmagma(1)=tau;

% The boundary condition of the density between
% the inclusion and magma

Pmagma(1)= exp(H*(1-T0/(Tm*Tmagma(1))));
rhomagma(1)= Pmagma(1)/Tmagma(1);

%setting up diff
% from 1 to m+1 is a a upstream difference at Tinc(2)
% with the first term of Tinc(2)-Tinc(1) taking 2 to m+2
% this gives a downstream difference of Tinc(3)-Tinc(2)
```

```
% same idea with the others

DTinc=diff(Tinc);
DPmagma= diff(Pmagma);
DTmagma=diff(Tmagma);
Drhomagma=diff(rhomagma);


%derivatives used in right hand sides of equations note
%the differences in chi and psi are all 1

% pressure in magma 1st derivative with i-1 &i
DPN=DPmagma(2:n+1);
DPP=DPmagma(1:n);
% Temp in Inc 1st derivative with i & i-1
DTiP=DTinc(1:m);
DTiN=DTinc(2:m+1);
% Temp in Magma 1st derivative with i & i-1
DTmP=DTmagma(1:n);
DTmN=DTmagma(2:n+1);
% Density in Magma 1st derivative with i &i-1
DrhoP=Drhomagma(1:n);
DrhoN=Drhomagma(2:n+1);



%second derivatives
%Tinc second derivative
DDTi=zeros(1,m);
for i1=2:m+1
  DDTi(i1-1)=(Tinc(i1+1)-2.*Tinc(i1)+Tinc(i1-1));
end
%Tmag second derivative
DDTm=zeros(1,n);
for i2=2:n+1
  DDTm(i2-1)=(Tmagma(i2+1)-2.*Tmagma(i2)+Tmagma(i2-1));
end
```

```
%Pmag second derivative
DDP=zeros(1,n);
for i3=2:n+1
  DDP(i3-1)=(Pmagma(i3+1)-2.*Pmagma(i3)+Pmagma(i3-1));
end


%% Calculating sdot

sdot=functionvelocity(Tmagma(2),Tmagma(1),s, ...
    Tinc(m+2),Tinc(m+1));

%Now to calculate the f function for the Tinc

fTinc=functioninctemp(s,DTiP,DTiN,sdot,DDTi);

%Now calculate the f function for the Tmagma

fTmagma=functionmagma(s,DTmP,DTmN,sdot,DDTm,xi(2:n+1));

%Now Calculate the f function of rhomagma

frhomagma=functionrhomagma(s,rhomagma(1:n+1),DPN, ...
        DrhoN,DrhoP,sdot,DPP,xi(2:n+1),n, DPmagma);


% Now to form the right hand side f
fr=[fTinc,fTmagma,frhomagma,sdot];
f=transpose(fr);
end

%% stop function
function [value,isterminal,direction]= functionevents(~,y)
szero=y(end)-10^(-4)*R1; %value that equals zero
```

```
stop=1; %halt the integration
side=0; % when coming from either direction, +1
        % increasing function -1 decreasing
value=szero;
isterminal=stop;
direction=side;
end



%% boundary function
function [tau]=functionboundary(Th,Ti,Pm,sb)
    function [result]=bfun(tau)
    epsfrac= (1-epsilon)/(1-sb);
    esfrac=epsilon/sb;
    Pb=exp(H*((tau-(T0/Tm))/tau));
    LHS=f10*f3*Pb*Cn(1)*epsfrac*(Pm-Pb);
    RHS=-tau*(epsfrac*Cn(1)*(Th-tau)-Cm(m+1)*esfrac*(tau-Ti));
    result= LHS-RHS;
    end

Min=0.1;
r1=bfun(Min); r2=bfun(0.5);
%T=0.5 is approximately critical temperature
            if r1*r2 > 0   % same sign, not straddling!!
                disp('not straddling zero')
                disp(sb)
                disp(Th)
                disp(Pm)
                disp(Ti)
                % LookAtFlash
                Tflash= fzero(@bfun,Ti);
                % look for a solution near the slurry T
            else % we do have straddle:
            Tflash= fzero(@bfun,[Min 0.5]);
            % solve BC at flash for temperature there
```

```
                end
tau=Tflash;
end
%% s dot function
function [sdot]=functionvelocity(Tm2,Tm1,sp,Tie,Tin)
%Parameters that are needed in the function
epsfrac1= (1-epsilon)./(1-sp);
esfrac1=epsilon./sp;

%Calculate sdot
fluxmagma=(Tm2-Tm1);
fluxinc=(Tie-Tin);
sdot=-(1/f3).*(Cn(1)*epsfrac1.*fluxmagma-Cm(m+1)*esfrac1.*fluxinc);
end


%% T Inc Function
function [fTinc]=functioninctemp(s,DTiP,DTiN,sdot,DDTi)
esfrac=epsilon/s;
VT=(((esfrac.^2)*.2.*f9)./zeta(2:m+1))+((zeta(2:m+1).*sdot)./s);
a43=((esfrac^2)*f9);
A1=VT.*Cm(2:m+1)+a43.*((2.*Cm(2:m+1).*Bm.*aa.*chi(2:m+1))./epsilon);
a44P=min(A1,0);
a44N=max(A1,0);
WDTi=a44P.*DTiP+a44N.*DTiN; %Winding
fTinc= (a43.*Cm(2:m+1).^2).*DDTi+WDTi;

end
%% T magma Function
function [fTmagma]=functionmagma(s,DTmP,DTmN,sdot,DDTm,xi)
epsfrac= (1-epsilon)/(1-s);
gfrac=((1-s).*xi+(s-epsilon))./(1-epsilon);
WT=(((epsfrac)*2*f15)./(gfrac))-(((xi-1).*sdot)./(1-s));
a53=((epsfrac^2)*f15);
A2=WT.*Cn(2:n+1)+a53.*((2.*aa.*Cn(2:n+1).*Bn.*(psi(2:n+1)-n-1)) ...
        ./(1-epsilon));
```

```matlab
a54P=min(A2,0);
a54N=max(A2,0);
WDTm=a54P.*DTmP+a54N.*DTmN; %Winding

fTmagma= (Cn(2:n+1).^2).*a53.*DDTm+WDTm;
end


%% rho magma function
function [frhomagma]=functionrhomagma(s,rhomagma,DPN,DrhoN, ...
                        DrhoP,sdot,DPP,xi,n,DPmagma)
epsfrac= (1-epsilon)/(1-s);
gfrac=((1-s).*xi+(s-epsilon))./(1-epsilon);
Xp=(f11.*2.*rhomagma(2:n+1).*epsfrac./gfrac);
Xrho=-((xi-1)./(1-s))*sdot;
a61=((f11.*(epsfrac).^2));
A3=Xrho.*Cn(2:n+1);
A4=Xp.*Cn(2:n+1)+((a61.*rhomagma(2:n+1).*Cn(2:n+1).*2.*aa.* ...
    Bn.*(psi(2:n+1)-n-1))/(1-epsilon));

a62P=min(A3,0);
a62N=max(A3,0);
WDrhoZ=a62P.*DrhoP+a62N.*DrhoN;

a64P=min(A4,0);
a64N=max(A4,0);
A4WD=a64P.*DPP+a64N.*DPN;

DD=diff(rhomagma.*DPmagma);
frhomagma= (Cn(2:n+1).^2).*a61.*DD+WDrhoZ+A4WD;
end
end
```

Appendix H

Glossary of Terms

Symbol Glossary		
Terms in Chapter 1.2.2		
R_1	Radius of inclusion	m
R_2	Radius of ejecta	m
r	Radius	m
s	Position of the steam generation boundary	m
ρ	effective density	$kg\,m^{-3}$
ρ_l	liquid density	$kg\,m^{-3}$
ρ_v	vapour density	$kg\,m^{-3}$
c_p	effective heat capacity	$J\,kg^{-1}\,K^{-1}$
T	Temperature	K
T_m	Initial magma temperature	K
T_0	Initial Inclusion temperature	K
t	time	s
K	Thermal Conductivity of Magma	$J\,m^{-1}\,K^{-1}\,s^{-1}$
p	Pressure	Pa
$\mathbf{F_v}$	Vapour Density	$kg\,m^{-3}\,s^{-1}$
k	Permeability of magma	m
μ_v	Dynamic Viscosity	Pa s
ϕ	Porosity of Inclusion	
ϕ_m	Porosity of Magma	
p_c	Critical pressure	Pa

h_{vl}	Latent heat of Vaporisation	k J Kg^{-1}
M	Molar mass of water	Kg
R	Gas Constant	J Kg^{-1} K$^-$1
t_c	Critical time	s
Terms in Chapter 1.2.3.1		
Symbol	**Meaning**	**Units**
ϕ	Porosity	
ρ_l	liquid density	kg m^{-3}
ρ_v	vapour density	kg m^{-3}
$\mathbf{u}_v$	Mass flux of vapour	kg s^{-1}
$\mathbf{u}_l$	Mass flux of liquid	kg s^{-1}
S_l	Pore space fraction containing liquid	
S_v	Pore space fraction containing vapour	
R_e	Reynolds Number	
q	flow speed	m s^{-1}
d	pore size	m
γ	kinematic viscosity	m^2 s^{-1}
Terms in Chapter 2		
Symbol	**Meaning**	**Units**
ρ	Density	kg m^{-3}
c_p	Specific heat	J kg^{-1} K^{-1}
T	Temperature	K
t	time	s
$\mathbf{v}$	Local fluid velocity vector	m s^{-1}
β	Coefficient of isothermal compressibility	Pa^{-1}
p	Pressure	Pa
K	Thermal Conductivity	J m^{-3} K^{-1} s^{-1}
ϕ	Porosity	
k	Permeability of magma	m
μ_v	Dynamic Viscosity	Pa s
$\mathbf{u}$	Mass flux	kg s^{-1}
T_R	Reference Temperature	K
h_{vl}	Latent heat of Vaporisation	k J Kg^{-1}
M	Molar mass of water	Kg

R_g	Gas Constant	J Kg^{-1} K^{-1}
R_1	Radius of inclusion	m
R_2	Radius of ejecta	m
r	Radius	m
s	Position of the steam generation boundary	m

Terms in Chapter 3		
Symbol	**Meaning**	**Units**
T	Non-dimensional Temperature	
T_f	Scaled temperature at flash	
T_0	Scaled initial inclusion temperature	
t	Non-dimensional time	
r	Non-dimensional radius	
η	Similarity solution	
ε	$\frac{R_1}{R_2}$	
σ	Co-ordinate transformed r near the boundary	
ψ	Co-ordinate transformed r near the boundary	
p	Non dimensional Pressure	

Terms in Chapter 4		
Symbol	**Meaning**	**Units**
ζ	Frozen boundary inclusion radial coordinate	
ε	$\frac{R_1}{R_2}$	
r	Non-dimensional radius	
s	Non-dimensional steam generation boundary	
t	Non-dimensional time	
ξ	Frozen boundary magma radial coordinate	
T	Non-dimensional temperature	
ρ_v	Non-dimensional vapour density	
p	Non-dimensional pressure	

Terms in Chapter 5		
Symbol	**Meaning**	**Units**
k	permeability of ejecta	m
ϕ	porosity of ejecta	
p_c	critical pressure	Pa

Terms in Chapter 6		
Symbol	**Meaning**	**Units**
t	Non-dimensional time	
r	Non-dimensional radius	
p	Non-dimensional pressure	
ε	$\frac{R_1}{R_2}$	
T	Non-dimensional Temperature	
T_f	Scaled temperature at flash	
T_0	Scaled initial inclusion temperature	
T_m	Initial temperature in magma	K
r_{ramp}	Ramping distance	m
t_e	emplacement time	s
p_e	Non-dimensional early time pressure	
p_u	Non-dimensional upper bound on pressure	
p_{max}	Non-dimensional maximum pressure	
Terms in Appendix A		
Symbol	**Meaning**	**Units**
ρ_x	Density of substance x	kg m^{-3}
h	specific enthalpy	kJ kg^{-1}
$\mathbf{v}$	Local fluid velocity vector	m s^{-1}
$\mathbf{q}$	heat flux	J s^{-1}
τ	Deviatoric stress tensor	N m^2
t	time	s
p	Pressure	Pa
U	Specific internal energy	J
S	Specific entropy	J K^{-1}
c_{px}	Specific heat of x	J kg^{-1} K^{-1}
T	Temperature	K
β_e	Coefficient of isothermal compressibility	Pa^{-1}
K_x	Thermal Conductivity of x	J m^{-1} K^{-1} s^{-1}
Terms in Appendix B		
Symbol	**Meaning**	**Units**
ρ_x	Density of substance x	kg m^{-3}
c_{px}	Specific heat of x	J kg^{-1} K^{-1}

T	Temperature	K
t	time	s
$\mathbf{v}$	Local fluid velocity vector	m s^{-1}
p	Pressure	Pa
K_x	Thermal Conductivity of x	J m^{-1} K^{-1} s^{-1}
ϕ_x	Porosity of x	
h_x	specific enthalpy of x	kJ kg^{-1}
Terms in Appendix C		
Symbol	**Meaning**	**Units**
ρ_x	Density of substance x	kg m^{-3}
c_{px}	Specific heat of x	J kg^{-1} K^{-1}
T	Temperature	K
t	time	s
t_0	Initial time	s
$\mathbf{v}$	Local fluid velocity vector	m s^{-1}
β	Coefficient of isothermal compressibility	Pa^{-1}
p	Pressure	Pa
K_x	Thermal Conductivity of x	J m^{-1} K^{-1} s^{-1}
ϕ_x	Porosity of x	
k	Permeability of magma	m
μ_v	Dynamic Viscosity	Pa s
$\mathbf{u_x}$	Mass flux of x	kg s^{-1}
T_R	Reference Temperature	K
h_{vl}	Latent heat of Vaporisation	k J Kg^{-1}
M	Molar mass of water	Kg
R_g	Gas Constant	J Kg^{-1} K^{-1}
R_1	Radius of inclusion	m
R_2	Radius of ejecta	m
r	Radius	m
s	Position of the steam generation boundary	m
$\tilde{r}$	Non-dimensional radius	
$\tilde{T}$	Non-dimensional temperature	
$\tilde{t}$	Non-dimensional time	
$\tilde{p}$	Non-dimensional pressure	

$\tilde{s}$	Non-dimensional s	
$\tilde{\rho}_x$	Non-dimensional density of substance x	
$\tilde{v}_v$	Non-dimensional vapour velocity	
ρ_{x0}	Initial density of substance x	kg m^{-3}
v_{x0}	Initial velocity of x	m s^{-1}
t_s	Estimate time taken to heat inclusion	s
α	Thermal linear expansion coefficient	K^{-1}
p_0	Initial pressure	Pa
Terms in Appendix D		
Symbol	**Meaning**	**Units**
r	Non-dimensional radius	
T	Non-dimensional Temperature	
T_f	Scaled temperature at flash	
T_0	Scaled initial inclusion temperature	
t	Non dimensional time	
ε	$\frac{R_1}{R_2}$	
σ	Co-ordinate transformed r near the boundary	
ψ	Co-ordinate transformed r near the boundary	
η	Similarity solution $\frac{t}{\sigma^2}$	
T^*	Constant set by outer solution	
A	Constant set by temperature gradients	
T_i^*	Constant set by outer solution	
A_i	Constant set by temperature gradients	
ρ_v	Non-dimensional vapour density	
p	Non-dimensional pressure	
r_{ramp}	Ramping distance	
t_e	emplacement time	
p_e	Non-dimensional early time pressure	
p_q	Non-dimensional quasi steady state pressure	
p_u	Non-dimensional upper bound on pressure	
p_{max}	Non-dimensional maximum pressure	
t_m	Non-dimensional time taken to reach maximum pressure	

Terms in Appendix E		
Symbol	**Meaning**	**Units**
T_x	Non-dimensional temperature at x	
ε	$\frac{R_1}{R_2}$	
s	Non-dimensional steam generation boundary	m
p_x	Non-dimensional pressure at x	
T_m	Initial magma temperature	K
T_0	Initial Inclusion temperature	K
Terms in Appendix F		
Symbol	**Meaning**	**Units**
T_x	Non-dimensional temperature at x	
Δr_x	Change in r at x	
h	Size of interval	
ζ	Frozen boundary inclusion radial coordinate	
ε	$\frac{R_1}{R_2}$	
r	Non-dimensional radius	
s	Non-dimensional steam generation boundary	
t	Non-dimensional time	
ξ	Frozen boundary magma radial coordinate	
T	Non-dimensional temperature	
ρ_v	Non-dimensional vapour density	
p	Non-dimensional pressure	
χ	arctan transformed ζ	
ς	arctan transformed ξ	
n	number of intervals in magma	
m	number of intervals in inclusion	

Bibliography

[1] ALIDIBRIROV, M. A model for viscous magma fragmentation during volcanic blasts. *Bulletin of Volcanology 56* (1994), 459–475.

[2] ALIDIBRIROV, M., AND DINGWELL, D. B. Three fragmentation mechanisms for highly viscous magma under rapid decompression. *Journal of Volcanology and Geothermal Research 100* (2000), 413–422.

[3] ALIDIBRIROV, M., AND PANOV, V. Magma fragmentation dynamics: experiments with analogue porous low-strength material. *Bulletin of Volcanology 59*, 7 (1998), 481–490.

[4] BATCHELOR, G. K. *An Introduction to Fluid Dynamics*. Cambridge University Press, 1967.

[5] BEAR, J. *Modeling Phenomena of Flow and Transport in Porous Media*. Springer International Publishing, 2018.

[6] BEATON, C. F. *Properties of sea water in heat exchanger design handbook*. Hemisphere publishing corporation, 1986.

[7] BENDER, C. M., AND ORSZAG, S. A. *Advanced Mathematical Methods for Scientists and Engineers. Asymptotic Methods and Perturbation Theory*. McGraw-Hill, 1978.

[8] BENNETT, F. D. On volcanic ash formation. *American Journal of Science 274* (1974), 648–661.

[9] CENGEL, Y. A., AND GHAJAR, A. J. *Heat and Mass Transfer: Fundamentals and Applications*, 4 ed. McGraw-Hill Science/Engineering/Math, 2011.

[10] CHEN, S., MERRIMAN, B., OSHER, S., AND SMEREKA, P. A simple level set method for solving Stefan problems. *Journal of Computational Physics 135*, 1 (1997), 8–29.

[11] CHRISHOLM, D. *Two-phase flow in pipelines and heat exchangers*. Pitman Press, Bath, 1983.

[12] COLGATE, S. A., AND SIGURGEIRSSON, T. Dynamic mixing of water and lava. *Nature 244*, 5418 (1973), 552–555.

[13] CRANK, J. *The Mathematics of Diffusion*. Oxford University Press, 1967.

[14] CRANK, J. *Free and Moving Boundary Problems*. Clarendon Press, Oxford, 1984.

[15] DREW, D. A., AND WOOD, R. T. *Overview and taxonomy of models and methods for workshop on two-phase flow fundamentals*. National Bureau of Standards, Gaithersburg, MD, 1985.

[16] FOWLER, A. C. *Mathematical Models in the Applied Sciences*. Cambridge University Press, 1997.

[17] FOWLER, A. C. *Mathematical Geoscience*. Springer, 2011.

[18] FOWLER, A. C., SCHEU, B., LEE, W. T., AND MCGUINNESS, M. J. A theoretical model of the explosive fragmentation of vesicular magma. *Proceedings of the Royal Society A: Mathematical, Physical and Engineering Sciences 466*, 2115 (2010), 731–752.

[19] GRANT, M. A., DONALDSON, I. G., AND BIXLEY, P. F. *Geothermal Reservoir Engineering*. Academic Press, 1982.

[20] GREENBANK, E. Modelling Surtseyan ejecta. Master's thesis, Victoria University of Wellington, 2015.

[21] ICHIHARA, M. Dynamics of a spherical viscoelastic shell: Implications to a criterion for fragmentation/expansion of bubbly magma. *Earth and Planetary Science Letters 265* (2008), 18–32.

[22] ISHII, M., AND HIBIKI, T. *Thermo-Fluid Dynamics of Two Phase Flow*, 2 ed. Springer, 2011.

[23] KOKELAAR, P. The mechanism of Surtseyan volcanism. *Journal of the Geological Society 140*, 6 (1983), 939–944.

[24] KOKELAAR, P. Magma-water interactions in subaqueous and emergent basaltic volcanism. *Bulletin of Volcanology 48* (1986), 275–289.

[25] KOKELAAR, P. Discussion of 'Structure and eruptive mechanisms at Surtsey Volcano, Icelend' by J.G. Moore. *Geological Magazine* (1987).

[26] LANDAU, H. G. Heat conduction in a melting solid. *Quarterly of Applied Mathematics* (1950).

[27] MASTIN, L. G., CHRISTIANSEN, R. L., THORNBER, C., LOWENSTERN, J., AND BEESON, M. What makes hydromagmatic eruptions violent? Some insights from Keanakāko'i Ash, Kīlauea Volcano, Hawai'i. *Journal of Volcanology and Geothermal Reasearch 137* (2004), 15–31.

[28] MASTIN, L. G., AND WITTER, J. B. The hazards of eruptions through lakes and seawater. *Journal of Volcanology and Geothermal Research 97* (2000), 195–214.

[29] MCBIRNEY, A. R. Conductivity variations and terrestrial heat-flow distribution. *Journal of Geophysical Research 68*, 23 (1963), 6323–6329.

[30] MCBIRNEY, A. R., AND MURASE, T. Factors governing the formation of pyroclastic rocks. *Bulletin of Volcanology 34*, 2 (1970), 372–384.

[31] MCGUINNESS, M. J., GREENBANK, E., AND SCHIPPER, C. I. Modelling vapour transport in Surtseyan bombs. *Journal of Volcanology and Geothermal Reasearch* (2016).

[32] OZISIK, M. N. *Heat Conduction*, 2 ed. Wiley-Interscience Publication, 1993.

[33] PRAKASH, A., AND MAHMOOD, S. Modified lumped model for transient heat conduction in spherical shape. *American International Journal of Research in Science, Technology, Engineering and Mathematics 153-176*, 153 (2013), 4.

[34] PRUESS, K., CALORE, C., CELATI, R., AND WU, Y. S. An analytical solution for heat transfer at a boiling front moving through a porous medium. *Pergmon Journals Ltd. 30*, 12 (1987), 2595–2602.

[35] ROBERTSON, E. C. Thermal properties of rocks. Tech. rep., US Geological Survey, Reston, Virginia, USA, 1988.

[36] ROHSENOW, W. M., AND CHOI, H. *Heat, Mass and Momentum Transfer.* Prentice-Hall, Inc., 1961.

[37] SATO, H., UEMATSU, M., WATANABE, K., SAUL, A., AND WAGNER, W. New international skeleton tables for the thermodynamic properties of ordinary water substance. *Journal of Physical Chemistry Reference Data 17*, 4 (1988), 1439–1540.

[38] SCHIPPER, C., BURGISSER, A., AND WHITE, J. Magma permeability and magma-slurry mingling during the 196367 eruption of surtsey, iceland. *Japan Geoscience Union Meeting, Chiba, Japan* (2013).

[39] SCHIPPER, C., AND WHITE, J. Magma-slurry interaction in Surtseyan eruptions. *Geology 44*, 3 (2016), 195–198.

[40] SCHIPPER, C. I. Personal communication, July 2019.

[41] SINGH, H. Dust Eruptions. Master's thesis, Victoria University of Wellington, 2014.

[42] SPARKS, R. S. J. The dynamics of bubble formation and growth in magmas: A review and analysis. *Journal of Volcanology and Geothermal Research 3* (1978), 1–37.

[43] SPIELER, O., DINGWELL, D. B., AND ALIDIBRIROV, M. Magma fragmentation speed: an experimental determination. *Journal of Volcanology and Geothermal Research 129* (2004), 109–124.

[44] SPIELER, O., KENNEDY, B., KUEPPERS, U., DINGWELL, D. B., SCHEU, B., AND TADDEUCCI, J. The fragmentation threshold of pyroclastic rocks. *Earth and Planetary Science Letters 226* (2004), 139–158.

[45] SPIELER, O., KENNEDY, B., KUEPPERS, U., DINGWELL, D. B., SCHEU, B., AND TADDEUCCI, J. The fragmentation threshold of pyroclastic rocks. *Earth an Planetary Science Letters 226* (2004), 139–148.

[46] THORARINSSON, S. *Surtsey: The New Island in the North Atlantic*. Viking, 1967.

[47] VALENTINE, G. A. Stratified flow in pyroclastic surges. *Bulletin of Volcanology 49* (1987), 616–630.

[48] VERHOOGEN, J. Mechanics of ash formation. *American Journal of Science 249* (1951), 729–739.

[49] WHITE, J. D. L., AND HOUGHTON, B. *Encyclopedia of Volcanoes*. Academic Press, 2000.

[50] ZIMANOWSKI, B., BÜTTNER, R., LORENZ, V., AND HÄFELE, H.-G. Fragmentation of basaltic melt in the course of explosive volcanism. *Journal of Geophysical Research 102* (1997), 803–814.